Gene editing of BTK using CRISPR/Cas9 to study drug resistance in acute myeloid leukaemia

Thesis submitted in accordance with the requirements of the University of Liverpool for the Degree of Doctor in Philosophy

by

Melanie Märken

January 2019

Declaration

I declare that this thesis has been composed solely by myself and that it has not been submitted, in whole or in part, in any previous application for a degree. Except where stated otherwise by reference or acknowledgment, the work presented is entirely my own.

Melanie Märken

January 2019

Gene editing of BTK using CRISPR/Cas9 to study drug resistance in acute myeloid leukaemia

By Melanie Märken

Acute myeloid leukaemia (AML) has a current poor 5-year survival rate of only 27%, making the finding of new therapeutic avenues for treatment crucial.

Bruton's tyrosine kinase (BTK) is best known for its role in B-cell receptor signalling but is found to be expressed and constitutively phosphorylated in AML cell lines and patient-derived cells. Targeting BTK in B-cell malignancies with small molecule BTK inhibitor ibrutinib is clinically effective, however a small proportion of CLL and MCL relapse during the therapy and become refractory to ibrutinib. This resistance is mainly due to a cysteine to serine mutation in BTK at position 481 (C481S) that disrupts the irreversible, covalent binding between ibrutinib and the protein. As little is known about the role of BTK and its potential as a therapeutic target in AML, we studied the effects and functional consequences of pharmacological inhibition of BTK using ibrutinib in AML cell lines. Using the CRISPR/Cas9 system we generated the BTK^{C481S} mutation in AML cell lines to explore the functional impact of this mutation on ibrutinib treatment as well as other related protein networks. Whilst no effect of ibrutinib on cell proliferation and viability was observed in a cell culture model using THP-1 cells, we demonstrate that the BTK^{C481S} mutation led to reduced ibrutinib binding affinity as well as reversible binding compared to irreversible binding observed in BTK^{WT} cells. BTK inhibition correlated with a decrease in p-PLCγ2(Y1217) but had no observable effect on p-AKT(S473) or p-p42/44(T202/Y204). Kinase substrate enrichment analysis showed a decrease in NEK2 activity and increased activity in kinases belonging to the RSK family in THP-1 BTK^{WT} and BTK^{C481S} cells. An increase in abundance of PKC family members was also seen in THP-1 BTK^{C481S} cells.

Taken together this data demonstrates the CRISPR/Cas9 system can be utilised to model and study drug resistance mechanisms.

Acknowledgements

“As we express our gratitude, we must never forget that the highest appreciation is not to utter words, but to live by them."
- John F Kennedy

As John F Kennedy has said above showing our gratitude and appreciation is more important than expressing it in words, therefore I want to keep my acknowledgements short.

Thank you, Dave, for giving me the opportunity to do my PhD in your lab, for the regular meetings and teaching me how to become an independent researcher. Thank you, Nick, for reading my thesis and all your help with the CRISPR stuff as well as your time to discuss my work with you whenever I was stuck. Thanks to all the other lab members for making the time during my PhD more enjoyable.

Thank you to my family for always supporting and believing in me. A big thank you to my friend Anita for always being there for me and understanding how challenging a PhD can sometimes be as well as listening to all my moaning. Thanks to my partner George for putting up with my bad moods, being there for me and helping me wherever he could. And finally, I want to thank my two Huskies, Layla and Loki, for managing to always make me smile and cheer me up by just being them and successfully distracting me from writing with their attention seeking nature even when I was not supposed to take a break.

Table of contents

List of Figures

Chapter 1

Chapter 2

Chapter 3

Chapter 4

Chapter 5

Appendix

List of Tables

Chapter 1

Chapter 2

Chapter 5

Abbreviations

AAV	Adeno-associated virus
ABC	Activated B cell-like
ALL	Acute lymphoblastic leukaemia
AML	Acute myeloid leukaemia
APS	Ammonium persulfate
ATCC	American Type Culture Collection
BM	Bone marrow
BMX	Bone marrow-expressed kinase
BSA	Bovine serum albumin
BTK	Bruton's tyrosine kinase
Cbh	Chicken β-Actin
cGVHD	Chronic graft-versus-host disease
CLL	Chronic lymphocytic leukaemia
CML	Chronic myeloid leukaemia
CRISPR	Clustered Regularly Interspaced Palindromic Repeats
crRNA	CRISPR RNA
DLBCL	Diffuse large B-cell lymphoma
DMEM	Dulbecco's Modified Eagle's Medium
DMSO	Dimethyl sulfoxide
DSB	Double strand break
ECL	Enhanced chemiluminescence
EDTA	Ethylenediaminetetraacetic acid
(E)GFP	(Enhanced) green fluorescent protein
EtBr	Ethidium bromide
FAB	French-American-British
FBS	Fetal bovine serum
GCB	Germinal centre B-cell like

HDR	Homology directed repair
HMs	Haematological malignancies
HR	Homologous recombination
HRP	Horseradish peroxidase
HSC	Haematopoietic stem cell
HSCT	Haematopoietic stem cell transplantation
IDLVs	Integrase-defective lentivirus vector
IL	Interleukin
ITK	Interleukin-2-inducible T-cell kinase
LB	Luria broth
MCL	Mantle cell lymphoma
MCS	Multiple cloning site
MIB	Multiplexed inhibitor beads
MM	Multiple myeloma
MOI	Multiplicity of infection
MZL	Marginal zone lymphoma
NaCl	Sodium Chloride
NEAA	Non-essential amino acids
NF-κB	Nuclear factor kappa-light-chain-enhancer of activated B cells
NHEJ	Non-homologous end joining
NRTKs	Non-receptor tyrosine kinases
NSCLC	Non-small-cell lung carcinoma
OBs	Osteoblasts
OCs	Osteoclasts
PAGE	Polyacrylamide gel electrophoresis
PAM	Protospacer adjacent motif
PBS	Phosphate-buffered saline
PCR	Polymerase chain reaction
PEI	Polyethyleneimine

PH domain	Pleckstrin homology domain
PI	Propidium iodide
PI3K	Phosphoinositide-3-kinase
PIP_3	Phosphatidylinositol (3,4,5)-trisphosphate
PLC	Phospholipase-C
PTKs	Protein Tyrosine kinases
RIPA	Radioimmunoprecipitation assay
RPMI	Roswell Park Memorial Institute
RTKs	Receptor tyrosine kinases
RVDs	Repeat-variable diresidues
SDS	Sodium dodecyl sulfate
SFFV	Spleen focus-forming virus
SLL	Small lymphocytic lymphoma
ssODN	Single-stranded oligodeoxynucleotides
TAE	Tris-acetate-EDTA
TALENs	Transcription activator-like effector nucleases
TBST	Tris-buffered saline and Tween 20
TEC	Tyrosine kinase expressed in hepatocellular carcinoma
TEMED	Tetramethylethylenediamine
TH domain	TEC homology domain
TKs	Tyrosine kinases
TLR9	Toll-like receptor 9
TNF	Tumor necrosis factor
tracrRNA	Trans-activating crRNA
UV	Ultraviolet
WHO	World Health Organization
WM	Waldenstrom macroglobulinemia
XLA	X-linked agammaglobulinemia
ZFNs	Zinc finger nucleases

ZFPs	Zinc finger proteins

Chapter 1: Introduction

1.1 Acute myeloid leukaemia

1.1.1 Normal Haematopoiesis

Haematopoiesis describes the process of blood cell formation with the haematopoietic stem cell (HSC) being at the top of the hierarchy. Haematopoiesis occurs in two waves, the primitive wave and the definitive wave (Galloway & Zon, 2003). The primitive wave, also called primitive erythropoiesis, originates in the yolk sac and results in the development of erythrocytes and macrophages (Palis & Yoder, 2001). This wave occurs only once from mesoderm cells during early foetal development for the purpose of tissue oxygenation (Palis, 2014). Even though the primitive wave is transitory, erythroid progenitors are not pluripotent or capable of renewal. Like the primitive wave, the definitive wave originates in the yolk sac but transitions into the liver and finally into the bone marrow, thymus and spleen (Jagannathan-Bogdan & Zon, 2013). The definitive wave involves the production of all haematopoietic lineages and derives from haematopoietic stem cells. HSCs have long-term self-renewal capability and divide into multipotent and lineage-restricted progenitor populations (Kondo et al., 2003; Weissman, 2000).

Common myeloid progenitor cells can differentiate into erythrocytes, granulocytes, macrophages, platelets and dendritic cells. Lymphoid multipotent progenitor cells can differentiate into B-cells, T-cells, natural killer cells and also dendritic cells (Figure 1.1).

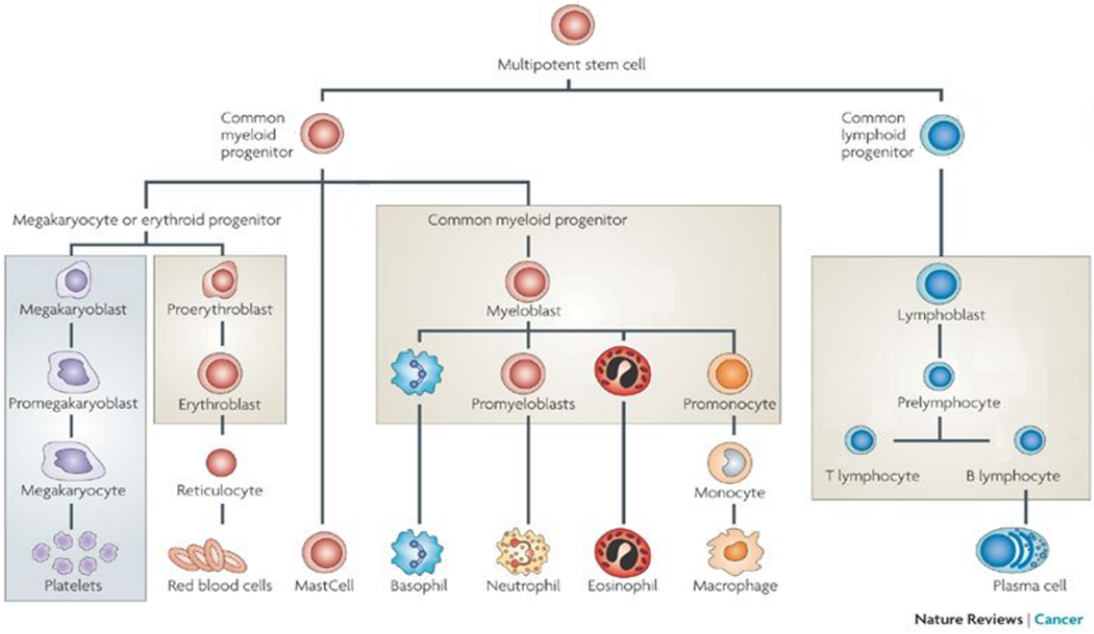

Figure 1.1 Normal haematopoiesis

Diagram of normal haematopoiesis in adults with the multipotent stem cell differentiating into a common myeloid and lymphoid progenitor that gives rise to multiple lineages.

Reprinted by permission from Springer Nature [Nature Reviews Cancer, MYB function in normal and cancer cells, (Ramsay & Gonda, 2008)]

1.1.2 Acute myeloid leukaemia

Haematological malignancies (HMs) are a group of blood cancers that arise from cells originating in the bone marrow. HMs have previously been subdivided into 4 groups: leukaemias, Hodgkin lymphomas, non-Hodgkin lymphomas and myelomas. More recently the World Health Organization (WHO) has further categorized HMs into over 60 disease subtypes according to their cell lineage, genetic abnormalities and clinical features (Swerdlow et al., 2008).

Acute myeloid leukaemia (AML) is a haematological malignancy arising from genetic alterations in normal HSCs (Kumar, 2011). These alterations disrupt the generation of mature blood cells resulting in excessive proliferation of a clonal population of abnormal myeloid progenitors. These immature leukemic cells accumulate in the bone marrow, blood and organs when the disease progresses and affect normal blood cell production resulting in leucocytosis and bone marrow failure (Grove & Vassiliou, 2014). Common symptoms of AML are fatigue, anorexia and weight loss. Patients diagnosed with AML would die within weeks of infections or bleeding if not treated.

1.1.3 Pathogenesis and classification of AML

AML is a heterogeneous disease and most genomes from AML patients contain a series of mutations acquired over time (Grove & Vassiliou, 2014). This explains why the cytogenetic and mutational AML profile in older adults differs from that of younger patients (Rao et al., 2009). Even though AML appears mainly as *de novo* malignancy in previously healthy patients, it can also occur in patients as a result of prior therapy or in patients with an underlying haematological disorder (Sill, Olipitz, Zebisch, Schulz, & Wolfler, 2011). In 97% of AML cases at least one somatic alteration is identified (Patel et al., 2012) but structural abnormalities are absent in many cases and nearly 50% of the patients have a normal karyotype (Cancer Genome Atlas Research et al., 2013).

To explain how the different genetic events associated with AML lead to similar phenotypes, a *two-hit* model for leukaemogenesis is proposed (Kelly & Gilliland, 2002). This model suggests that AML occurs as a consequence of a collaboration of two broad classes of mutations: class I and class II (Gilliland & Griffin, 2002). Class I mutations cause the activation of signal transduction pathways that lead to uncontrolled cellular proliferation and/or confer survival advantage to cells. Examples of such mutations include the tyrosine kinases FLT3 and c-KIT, N/KRAS and TP53. Class II mutations affect transcription factors and impair normal haematopoietic differentiation. Fusion transcripts such as RUNX1/ETO, CBFβ/MYH11 and PML/RARα, which are generated by recurring chromosomal aberrations (t(8; 21), inv(16) and t(15; 17)), all fall into this category (Gilliland & Griffin, 2002; Kelly & Gilliland, 2002; Speck & Gilliland, 2002; Takahashi, 2011) . Whilst the *two-hit* model is supported by the observation that one mutation on its own does not lead to AML development, it has been suggested that the model is an oversimplification due to the fact that other mutations, which do not fall into these categories, may play an important role in the pathogenesis of the disease. This has been supported by data from AML patients carrying additional mutations that modify the epigenetic status (Abdel-Wahab & Levine, 2013; Shih, Abdel-Wahab, Patel, & Levine, 2012). Mutations in genes that are involved in the epigenetic regulation of the genome such as TET2, IDH1/2, EZH2 can cause changes in DNA methylation and histone modification and have been found in a significant portion of AML patients. Based on these recent findings a revised model of leukaemogenesis has been proposed, categorizing mutations into class I, class II and a further two classes of epigenetic modifier genes (Shih et al., 2012).

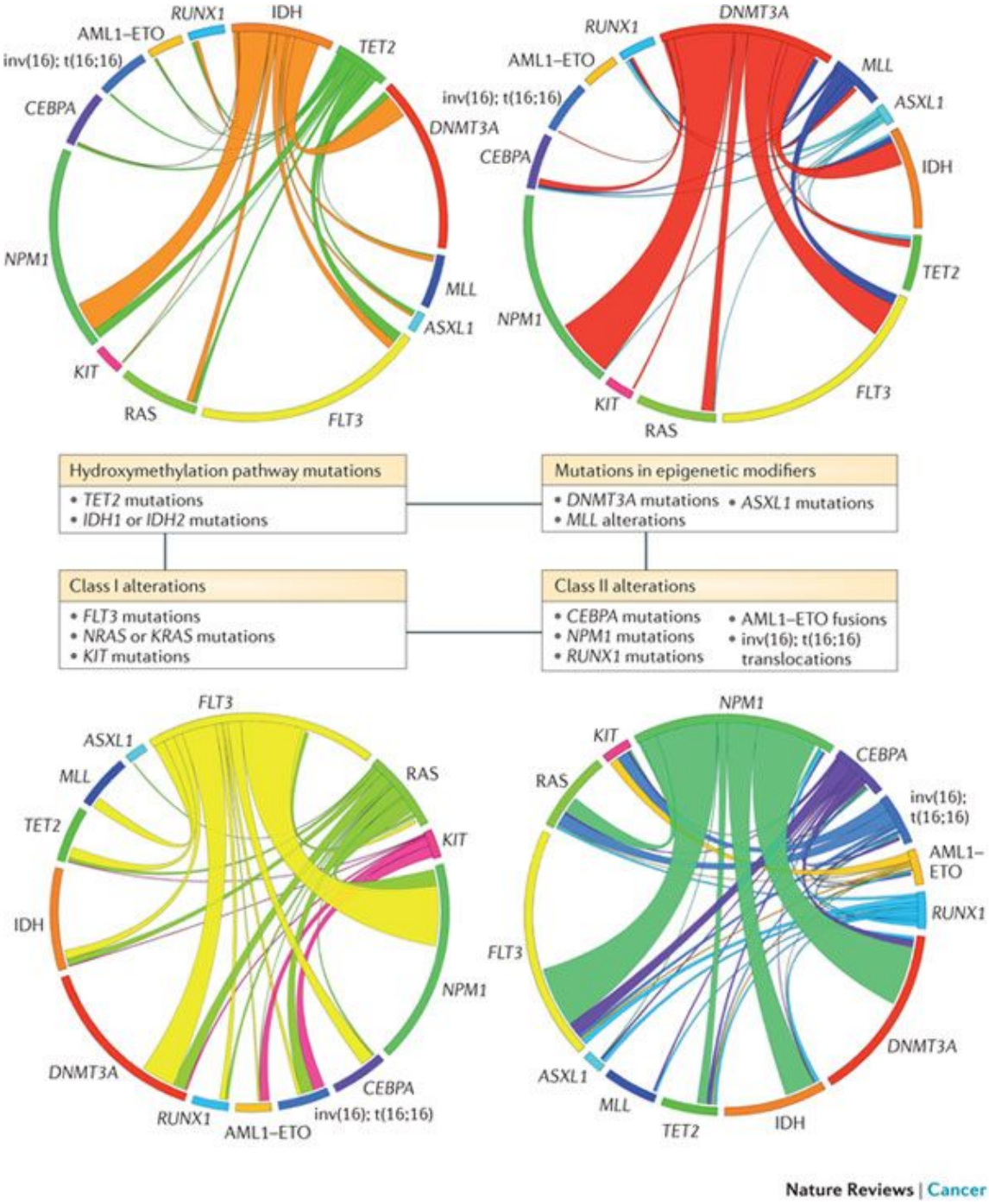

Figure 1.2 Revised model of leukaemogenesis

AML is the consequence of a series of mutations affecting cell proliferation, survival and differentiation. Mutations contributing to the development of the disease have previously been categorized into class I and class II mutations. Mutations modifying the epigenetic status have recently been found in patients with myeloid malignancies. The above Circos diagrams shows the co-occurrence of mutations in AML patients suggesting to classify the mutations as class I, class II and two classes of epigenetic modifier genes.

Reprinted by permission from Springer Nature [Nature Reviews Cancer, The role of mutations in epigenetic regulators in myeloid malignancies, (Shih et al., 2012)]

Knowing the underlying genetic alterations that lead to the development of AML and further defining the subtypes, helps us to better understand the disease and allows the use of targeted treatments based on the individual subtype characteristics.

Established in 1976, the French-American-British (FAB) classification system first attempted to distinguish between different types of AML by defining eight subtypes (M0-M7) based on cyto-chemical characteristics and the morphology of the leukaemic cells (Bennett et al., 1976). The World Health Organization (WHO) introduced a new classification system in 2001 that has been revised twice, last time in 2016. In comparison to the FAB classification system, the WHO incorporated genetic information and distinguished AML into six major categories: AML with recurrent genetic abnormalities, AML with myelodysplasia-related features, therapy-related AML, AML not otherwise specified, myeloid sarcoma, and myeloid proliferation related to Down syndrome (Arber et al., 2016). Further subtypes of these categories as well as genetic abnormalities can be found in Table 1.1.

Table 1.1 World Health Organization Classification of AML

AML with recurrent genetic abnormalities
AML with t(8;21)(q22;q22.1);RUNX1-RUNX1T1
AML with inv(16)(p13.1q22) or t(16;16)(p13.1;q22);CBFB-MYH11
APL with PML-RARA
AML with t(9;11)(p21.3;q23.3);MLLT3-KMT2A
AML with t(6;9)(p23;q34.1);DEK-NUP214
AML with inv(3)(q21.3q26.2) or t(3;3)(q21.3;q26.2); GATA2, MECOM
AML (megakaryoblastic) with t(1;22)(p13.3;q13.3);RBM15-MKL1
Provisional entity: AML with BCR-ABL1
AML with mutated NPM1
AML with biallelic mutations of CEBPA
Provisional entity: AML with mutated RUNX1
AML with myelodysplasia-related changes
Therapy-related myeloid neoplasms
AML, NOS
AML with minimal differentiation
AML without maturation
AML with maturation
Acute myelomonocytic leukaemia
Acute monoblastic/monocytic leukaemia
Pure erythroid leukaemia
Acute megakaryoblastic leukaemia
Acute basophilic leukaemia
Acute panmyelosis with myelofibrosis
Myeloid sarcoma
Myeloid proliferations related to Down syndrome
Transient abnormal myelopoiesis (TAM)
Myeloid leukaemia associated with Down syndrome

1.1.4 AML Epidemiology

AML is the most common acute leukaemia in adults and is responsible for 15-20% of the cases in children (O'Donnell et al., 2012). Even though it is estimated that there will be 19,520 new cases of AML in 2018 in the US, the disease is relatively rare. Based on SEER data from 2011-2015 cases, the National Cancer Institute reported that there were 4.3 new cases of AML per 100,000 men and women and 2.8 deaths per 100,000 men and women per year (https://seer.cancer.gov/statfacts/html/amyl.html). The disease is most commonly found in older individuals (> 60 years) and the incidence generally increases with age from ~1.3 to 12.2 cases per 100,000 men and women comparing patients less than 65 years in age with those over 65 years (De Kouchkovsky & Abdul-Hay, 2016). AML is also more common in men than women and the number of new cases and deaths is not only dependent on age and sex but also on race/ethnicity. Whilst Caucasians have the highest percentage of new cases and deaths, Native Americans / Alaska Natives have the lowest incidence as reported by the National Cancer Institute.

1.1.5 Treatment and Prognosis for AML

Even though an improved survival rate has been reported over the past years with a current 5-year survival rate of ~ 27%, the prognosis of AML in older patients is still poor due to comorbidities, a reduced treatment response and treatment-related suffering (Dohner et al., 2010). Stratifying patients according to prognostic factors helps to decide which treatment is most beneficial for the patient (De Kouchkovsky & Abdul-Hay, 2016). Although clinical factors play an important role in therapy-related decisions, cytogenetic changes are the strongest prognostic indicator for overall survival and remission rates. Based on the cytogenetic changes, cases of AML can be divided into three prognostic risk groups: favourable, intermediate or adverse (Mrozek et al., 2012). Patients that fall into the favourable and intermediate prognostic risk group are treated according to the '*7+3'* regime ('10+3' in the UK), which combines

7 days (10 days) of cytarabine treatment (100-200 mg/m^2 daily) with 3 days of anthracycline (O'Donnell et al., 2017).

Daunorubicin is the most commonly used anthracycline and is given at doses of 45-60 mg/m^2 daily. Using this standard for induction therapy to treat patients aged 50 years or younger shows a complete response rate between 60% and 80% (De Kouchkovsky & Abdul-Hay, 2016). Unfortunately, these rates are not observed in older patients or patients that fall into the adverse prognostic risk group. Intensive chemotherapy has not proven to increase the overall survival in elderly patients and early mortality as well as short-lasting responses are often the consequences of a less intensive therapy in those patients (Kantarjian et al., 2006). As a post-remission therapy, repetitive cycles of high-dose cytarabine are used in favourable- and intermediate risk AML. Alternatively, allogenic haematopoietic stem cell transplantation (HSCT) is a good post-remission option for patients with intermediate risk cytogenetics. HSCT is also recommended for elderly patients as well as patients with high risk cytogenetics (Almeida & Ramos, 2016).

1.2 Protein tyrosine kinases

Protein kinases represent one of the largest protein families in humans containing 538 members that constitute about 1.7% of all human genes (Bhullar et al., 2018). Protein kinases regulate other proteins by post-translational phosphorylation of serine, threonine and tyrosine residues (Manning, Plowman, Hunter, & Sudarsanam, 2002).

Protein tyrosine kinases (PTKs) were first discovered in 1979 (Eckhart, Hutchinson, & Hunter, 1979) and play a role in cell fate decisions through their involvement in cell differentiation, proliferation, survival and motility pathways (Hubbard & Till, 2000). PTKs themselves are controlled by post-translational modifications, such as phosphorylation and ubiquitination, and by changes in their abundance (Blume-Jensen

& Hunter, 2001). PTKs can be divided into receptor tyrosine kinases (RTKs) and non-receptor tyrosine kinases (NRTKs).

Whilst RTKs are transmembrane proteins consisting of an extracellular and intracellular domain, non-receptor tyrosine kinases do not have a transmembrane domain and are generally found in the nucleus, cytosol and inner surface of the plasma membrane (Krause & Van Etten, 2005). Non-receptor tyrosine kinases can be divided into 10 subfamilies with the SRC family being the largest (Figure 1.3).

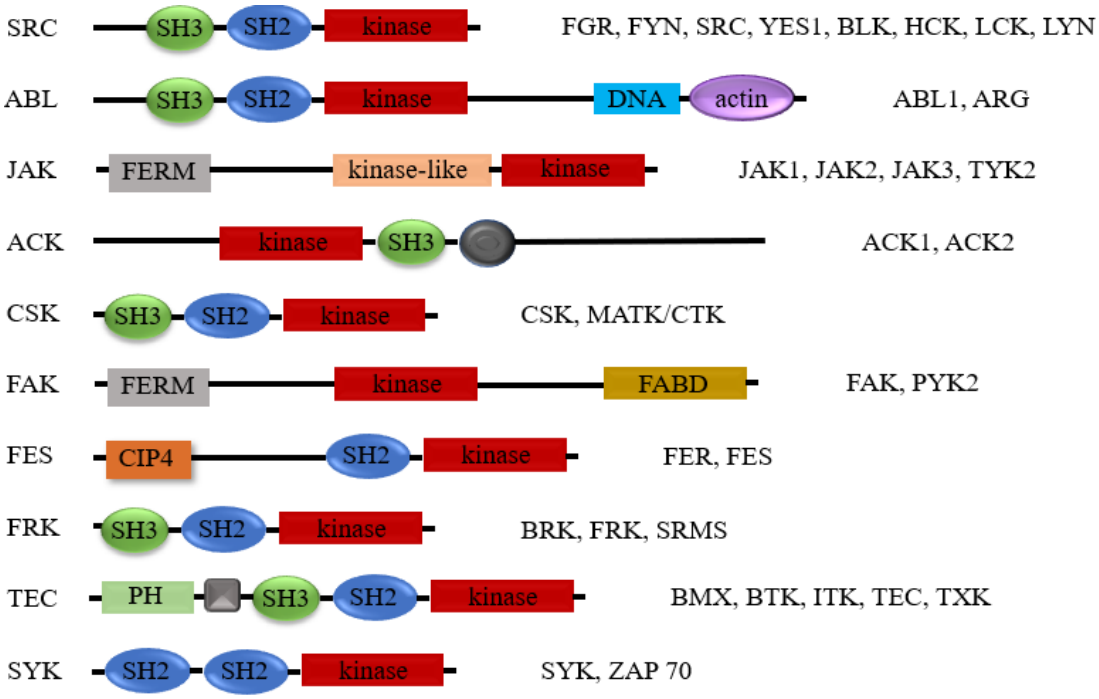

Figure 1.3 Non-receptor tyrosine kinase subfamilies

The figure depicts the 10 subfamilies (left) of non-receptor tyrosine kinases indicating their domain structure and members listed on the right.

Adapted from [Nature, Oncogenic kinase signalling, (Blume-Jensen & Hunter, 2001)]

1.2.1 TEC protein family of non-receptor tyrosine kinases

The TEC family is the second largest non-receptor protein tyrosine kinase (NRTK) family and consists of 5 members: bone marrow-expressed kinase (BMX), Bruton's tyrosine kinase (BTK), IL2-inducible T-cell kinase (ITK), tyrosine kinase expressed in hepatocellular carcinoma (TEC) and TXK. Unlike other NRTKs, TEC family kinases contain a pleckstrin homology domain and a conserved TEC homology domain that contains a Btk motif and a proline-rich region (Figure 1.3) (Tsukada et al., 1993). The Btk motif contains a His and three Cys residues that form a zinc finger whilst the proline-rich region is involved in protein-protein interactions. Besides being involved in the activation of phospholipase-C γ and Ca^{2+} mobilization it has been shown that TEC family kinases also play a role in multiple signalling pathways including cell adhesion, actin remodelling and transcriptional regulation (Figure 1.4) (Fluckiger et al., 1998; Lin & Weiss, 2001).

Mutations in TEC family kinases that lead to a loss-of-function mainly affect the haematopoietic system but also the liver and endothelial cells (Hussain et al., 2011; C. I. Smith et al., 2001).

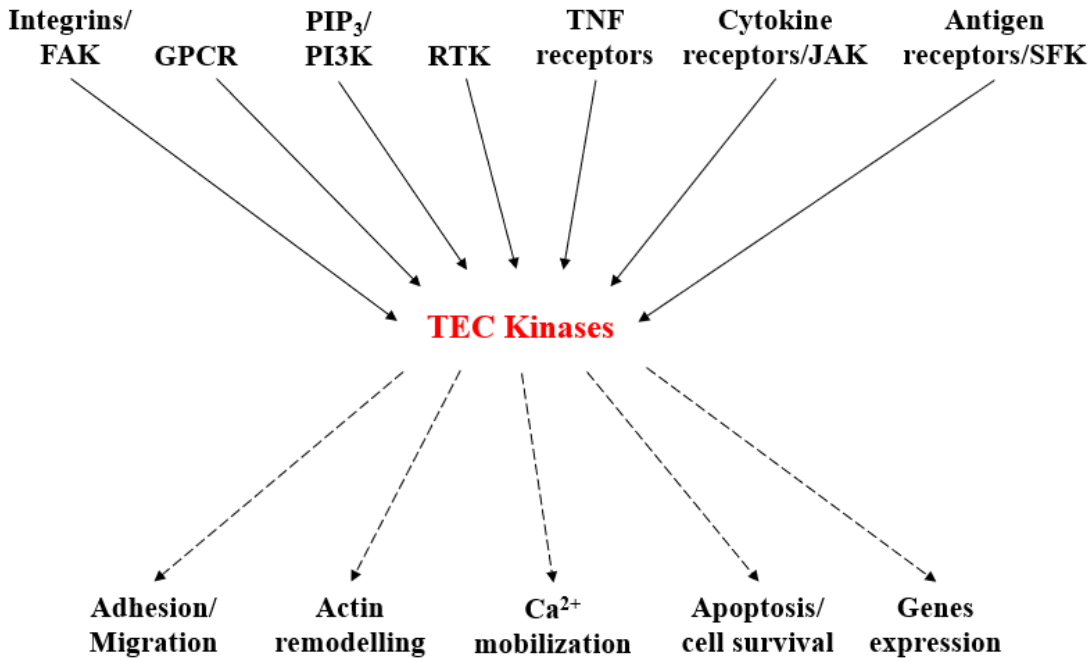

Figure 1.4 Signals transmitted through TEC family Kinases

TEC kinases are activated by membrane receptors such as GPCR, TNF and Cytokine receptors and are involved in different downstream pathways including apoptosis, adhesion and actin remodelling.

Adapted from [Critical Reviews in Clinical Laboratory Sciences, Non-receptor protein tyrosine kinases signaling pathways in normal and cancer cells, (Gocek, Moulas, & Studzinski, 2014)]

1.3.2 Bruton's tyrosine kinase (BTK)

BTK was the third member of TEC family kinases identified and revealed the importance of the family with the discovery that the human disease X-linked agammaglobulinemia (XLA) was caused by mutations in BTK. Due to BTK's involvement in the disease it was named after Ogden Bruton who reported the first case of XLA (Ponader & Burger, 2014). Of all tyrosine kinases in humans, BTK is the kinase for which most mutations have been identified (Hussain et al., 2011). The database documenting mutations in the BTK gene contains over 1700 entries with over 800 unique DNA variants reported (https://databases.lovd.nl/shared/genes/BTK).

1.2.3 BTK structure and regulation

BTK is located on the X chromosome (Xq22.1) and is a 659 amino-acid protein containing 5 signalling domains (Figure 1.5). The amino-terminal pleckstrin homology (PH) domain is required for membrane localization. Unlike other non-receptor tyrosine kinases, BTK is mainly found in the cytoplasm and is only transiently recruited to the membrane (Hendriks, Yuvaraj, & Kil, 2014). The PH domain is followed by a proline-rich TEC homology (TH) domain, which contains a highly conserved zinc-finger motif required for optimal activity and stability (Hyvonen & Saraste, 1997). BTK also contains the SRC homology domains SH3 and SH2, as well as a catalytic domain. SH3 and SH2 have binding functions and SH3 contains the autophosphorylation site tyrosine Y223 whilst the primary phosphorylation site, Y551, is located within the catalytic domain (Mohamed, Nore, Christensson, & Smith, 1999).

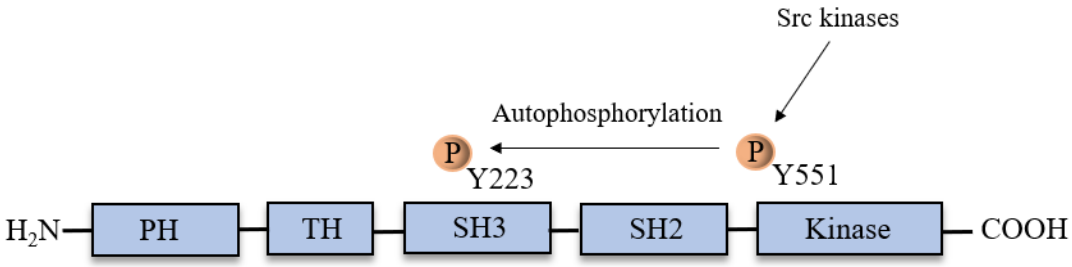

Figure 1.5 Domain structure of BTK

Schematic domain structure or BTK. PH, Pleckstrin homology domain; TH, TEC homology domain; SH3 and SH2, Src homology domains. Following phosphorylation by Src kinases on Y551 the protein undergoes autophosphorylation at Y223.

Adapted from [Journal of Clinical Oncology, Bruton's Tyrosine Kinase: From X-Linked Agammaglobulinemia Toward Targeted Therapy for B-Cell Malignancies, (Ponader & Burger, 2014)]

BTK is activated by SRC and SYK family kinases following stimulation of cell surface receptors including growth factor and cytokine receptors, G protein-coupled receptors, integrins and antigen receptors (Ponader & Burger, 2014). After BTK is recruited to the plasma membrane by phosphatidylinositol (3,4,5)-trisphosphate (PIP_3) via its PH domain it can undergo activating phosphorylation at Y551 by SYK and LYN (Rawlings et al., 1996). This results in autophosphorylation at Y223 within the SH3 domain (Park et al., 1996). BTK is expressed in all haematopoietic cells except T-cells and although it is mainly found in the cytoplasm a small proportion is also detected in the nucleus (Gustafsson et al., 2012). BTK is involved in many major pathways including phospholipase-C (PLC), nuclear factor kappa B (NF-κB), protein kinase C and phosphoinositol-3 kinase (PI3K)-AKT pathway (Lindvall et al., 2005).

1.2.4 The role of BTK in AML

Whilst BTKs role in B-cells is well studied and has been linked to several B-cell malignancies including Chronic Lymphocytic Leukaemia (CLL), Mantle Cell Lymphoma (MCL) and Diffuse Large B-Cell Lymphoma (DLBCL) (D'Cruz & Uckun, 2013), little is known about BTKs role in myelopoiesis. BTK inhibition/deficiency affects collagen-induced platelet aggregation (Quek, Bolen, & Watson, 1998), neutrophil development (Fiedler et al., 2011), macrophage lipopolysaccharide/TLR-induced tumour necrosis factor (TNF) production (Horwood et al., 2006) and dendritic cell function via interleukin (IL)-10 and Stat3 (Kawakami et al., 2006). BTK mutations are absent in AML (Ritis et al., 1998) and BTKs role in the disease is not fully understood yet but its relevance has been reported quite recently. Several groups have studied the role of BTK in AML and it has been found that BTK protein expression levels are elevated in newly diagnosed patients compared to patients in complete remission (Tao et al., 2013) and that BTK promotes AML cell proliferation and survival via pathways downstream of Toll-like receptor 9 (TLR9) and FLT3-ITD in FLT3-ITD negative and FLT3-ITD positive cells respectively (Oellerich et al., 2015).

Furthermore, pharmacological inhibition of BTK using ibrutinib (a covalent BTK inhibitor) leads to reduced AML blast adhesion to bone marrow stromal cells and inhibits SDF1/CXCR4-mediated AML migration (Rushworth et al., 2014). Therefore, pharmacological inhibition of BTK may not only have a direct anti-proliferative effect but may also disrupt the protection of AML cells by the bone marrow microenvironment. These findings suggest a role for BTK as a therapeutic target in AML, however, further studies are needed to better understand the signalling pathways of BTK in myeloid cells and its mechanism of activation in AML.

1.3 Ibrutinib

1.3.1 Targeting protein tyrosine kinases in cancer

Given the involvement of tyrosine kinases (TKs) in multiple pathways that control fundamental cellular functions it is not surprising that TKs have been found to be dysregulated in cancer cells. Out of the 90 TKs identified, 90% have been implicated in oncogenesis (Wilson et al., 2018). Genetically altered but also wild type TKs can act as "drivers" through different mechanisms including DNA-translocations, activating mutations and DNA amplifications (Figure 1.6). This generally results in constitutively active kinases that contribute to pathway signalling resulting in increased tumour cell proliferation and survival.

The involvement of TKs in carcinogenesis explains why they are such attractive druggable targets in cancer therapy. By designing drugs to bind to the ATP or substrate binding domain of TKs, their catalytic activity can be inhibited. Drugs have also been designed to block dimerization of RTKs preventing ligand binding and receptor internalization. One of the most successful developed TK inhibitors is Imatinib which inhibits BCR-ABL TK activity, a fusion protein that is present in almost all chronic myelogenous leukaemia (CML) patients and 15% to 30% of adult acute lymphoblastic

leukaemia (ALL) patients but absent in normal blood cells (Faderl et al., 1999; Shawver, Slamon, & Ullrich, 2002). The development of Imatinib has increased the survival rate of CML patients in chronic and accelerated phase (Kantarjian et al., 2012) and demonstrated that targeting TKs is a promising approach in cancer therapy.

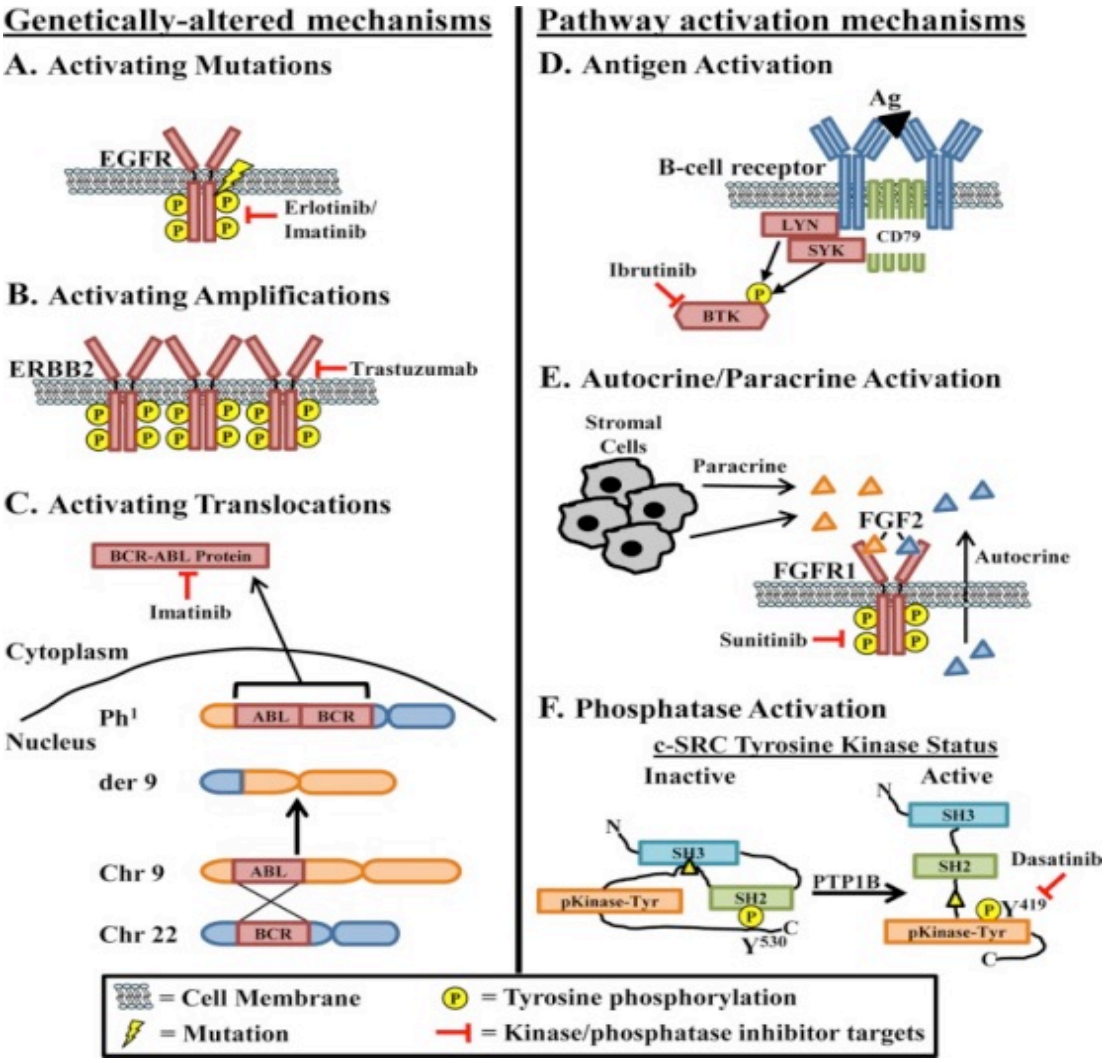

Figure 1.6 Tyrosine Kinase activation in cancer

Mechanisms of wild type and mutated tyrosine kinase activation together with compounds that have been developed to inhibit their activation. Mechanisms include genetical alterations (A-C) or pathway activations (D-F) that all contribute to increased tumour cell proliferation and survival.

Reprinted by Permission from American Society of Microbiology [Molecular and Cellular Biology, Clinical Targeting of Mutated and Wild-Type Protein Tyrosine Kinases in Cancer, (Drake, Lee & Witte, 2014)]

1.3.2 Ibrutinib - a BTK inhibitor

Ibrutinib is a first-in-class, oral, irreversible inhibitor of the TEC family kinase BTK. It belongs to a class of drugs called 'targeted covalent drugs' and is indicated for the treatment of adult patients with Mantle cell lymphoma (MCL), who have at least received one prior therapy, Chronic lymphocytic leukaemia (CLL) / Small lymphocytic leukaemia (SLL), CLL and SLL with 17p deletion, Waldenström's macroglobulinemia (WM), Marginal zone lymphoma (MZL) who require systemic therapy and have received at least one prior anti-CD20-based therapy and Chronic graft versus host disease (cGVHD) after failure of one or more lines of systemic therapy (JanssenMD®). Ibrutinib inactivates BTK by binding to Cysteine 481 in the ATP binding pocket of the protein (Pan et al., 2007). Despite being highly selective for BTK (IC_{50} 0.381 nmol/L) it also binds to other kinases with equivalent cysteine residues in the ATP binding pocket such as BLK, BMX, ErbB2, EGFR, JAK3, ITK and TEC (Singh, Petter, & Kluge, 2010). Comparing ibrutinib's activity against those off-target effects, IC_{50} values for the same kinase found in the literature seem to differ but a high activity is observed against BLK (IC_{50} 0.5 nmol/L), BMX (IC_{50} 0.8 nmol/L), EGFR (IC_{50} 1.81 nmol/L), ErbB2 (IC_{50} 9.4 nmol/L) and ITK (IC_{50} 10.7 nmol/L) (Bose, Gandhi, & Keating, 2016; Chen, Kinoshita, Sukbuntherng, Chang, & Elias, 2016). Whilst off-target binding can offer a therapeutic benefit in other diseases, it can also add a limitation due to off-target toxicity such as atrial fibrillation and bleeding observed for ibrutinib (Caldeira et al., 2019; Dreyling et al., 2016).

1.3.3 Clinical effects of ibrutinib in B-cell malignancies

Ibrutinib has demonstrated to benefit the duration and quality of life of patients with B cell malignancies. It took only 4.5 years from the clinical development and first in-human treatment to the first regulatory approval in 2013 (Gayko et al., 2015).

In a study of CLL patients comparing Ofatumumab, an anti-CD20 antibody that inhibits early stage B lymphocyte activation, with ibrutinib, ibrutinib displayed a 78% lower progression risk and 57% lower death risk in previously treated patients (Byrd et al., 2014). In previously untreated patients aged 65 years and older, ibrutinib even achieved an overall response rate of 84% and an overall survival rate of 97% at 30 months (Byrd et al., 2015).

In a phase 1/2 clinical trial of patients with the diffuse large B cell lymphoma (DLBCL) subtype activated B cell like (ABC), 37% of patients receiving ibrutinib treatment showed a complete or partial response whilst only 5% of patients with the germinal centre B cell like (GCB) subtype responded to the treatment (Wilson et al., 2015). As the current cure rate for the ABC subtype is worse than for the GCB subtype, new ABC subtype specific treatment strategies are very important. Patients with the ABC subtype have chronic active B cell receptor signalling which therefore makes targeting the BCR signalling with ibrutinib a promising treatment strategy (Shaffer, Young, & Staudt, 2012).

Ibrutinib has also shown good clinical effects in previously treated patients with Waldenström's Macroglobulinemia. An overall response rate of 90.5% was determined with an estimated 2-year overall survival rate of 95.2%. Ibrutinib showed the highest efficacy in patients with $MYD88^{L265P}$ $CXCR4^{WT}$ (100% overall response rate) and the lowest efficacy in patients with $MYD88^{WT}$ $CXCR4^{WT}$ (71.4%) (Treon et al., 2015).

Similar good outcomes were observed in a phase II clinical trial in patients with relapsed/refractory Mantle cell lymphoma (MCL). Ibrutinib demonstrated a 67% overall response rate at 24 months and a complete remission of 23% (M. L. Wang et al., 2015).

1.3.4 Targeting BTK beyond B-cell malignancies

BTK is expressed in all haematopoietic cells except T-cells but as mutations in BTK do not seem to affect the myeloid phenotype or myeloid cell activity it was long assumed that BTK is not important for the development and function of these cells. This assumption was proven to be wrong when several groups demonstrated the importance of BTK in normal as well as malignant myeloid cells.

BTKs role in myeloid cells as well as the increasing knowledge of ibrutinib's off-target effects has led to the exploration of targeting BTK beyond B-cell malignancies including non-haematological malignancies.

One example is the targeting of BTK in Multiple myeloma (MM). MM develops when malignant plasma cells accumulate in the bone marrow (BM). Overactive osteoclasts (OCs) and inactive osteoblasts (OBs) result in bone resorption and minimal bone regeneration, a clinical key feature of the disease (Raje & Roodman, 2011). BTK was identified to play a role in osteoclast (OC) differentiation (Shinohara et al., 2008) and was found to be expressed in cell lines and >85% of malignant plasma cells in Multiple myeloma (MM) patients (Rushworth et al., 2013; Tai et al., 2012). BTK inhibition using ibrutinib resulted in decreased bone resorption, decreased SDF-1-induced migration of MM cells and it also blocked MM cell growth and survival in vitro. In mice, ibrutinib inhibits MM cell growth and MM-induced osteolysis (Tai et al., 2012). These findings provided the preclinical results for clinical evaluation of ibrutinib as a therapeutic in MM.

Ibrutinib activity has also been studied in several other tumour types including lung, breast, gastro-oesophageal, pancreatic, ovarian, prostata, glioma and renal cell carcinomas (Campbell, Chong, & Hawkes, 2018). Those studies led to the evaluation of ibrutinib in a phase I/II trial in patients with previously treated EGFR-mutant non-small cell lung cancer (NSCLC) (Clinical Trials.gov ID NCT02321540), a phase II trial recruitment for MYC and/or HER2 amplified oesophageal cancer patients

(ClinicalTrials.gov ID NCT02884453), a phase II/III trial in patients with previously untreated metastatic pancreatic cancer (Tempero et al., 2016) (ClinicalTrials.gov ID NCT 02436668), a phase I/II study as initial curative treatment in men with prostate cancer undergoing prostatectomy (ClinicalTrials.gov ID 02643667) and a phase Ib/II trial in previously treated metastatic kidney cancer (ClinicalTrials.gov ID NCT02899078).

Those studies show that a specifically targeted compound can be less restrictive than originally thought and that knowing off-target activities is useful for finding new indications and broadening the clinical application of the drug.

1.3.5 Resistance mechanisms for the BTK inhibitor ibrutinib

Ibrutinib has been approved by the US Food and Drug Administration (FDA) for the treatment of several diseases including CLL and MCL and has shown clinical effectiveness and tolerability. However, it was found that some of the patients who received ibrutinib treatment had exhibited a primary resistance while others developed an acquired resistance to the drug.

In phase I and II studies of CLL, 14 out of 246 patients (5.3%) have disease progression (Furman et al., 2014). RNA-Seq or whole-exome sequencing was performed on 7 of the patients and revealed a cysteine to serine mutation at residue 481 in BTK (C481S) in 6 of the patients and mutations in PLCγ2 (L845F, R665W, S707Y) in two of the patients (Cheng et al., 2015; Woyach et al., 2014). In another clinical trial of 308 patients, acquired mutations of BTK or PLCγ2 were detected in 85% of relapsed CLL patients and mutations in samples before relapse were detected at a median of 9.3 months before clinical relapse (Woyach et al., 2017). The BTK C481S mutation was also found in relapsed MCL patients but was not present in MCL patients with a primary ibrutinib resistance (Chiron et al., 2014).

The S707Y mutation in PLCγ2 has previously been characterized and was identified to have a gain-of-function effect by disrupting the autoinhibitory SH2 domain leading to enhanced PLCγ2 activity (Zhou et al., 2012). The L845F and R665W mutations in PLCγ2 are less characterized but in vitro models demonstrated that these mutants appear to bypass BTK upon BCR activation, as indicated by higher cytosolic Ca^{2+} levels (T. M. Liu et al., 2015).

Functional analysis of the BTK C481S mutation revealed reversible binding of Ibrutinib to the protein together with a reduced binding affinity (Woyach et al., 2014). In addition to the C481S mutation other mutations within the protein have been identified including C481F/Y/R, T474I/S, T316A and L528W (Sharma et al., 2016). As some of these mutations are only present at 4-8% variant allele frequencies their effects have not yet been assessed (Maddocks et al., 2015). Even though BTK mutations are only present in patients who have received ibrutinib treatment, it is possible that these mutations are present at a low frequency in patients prior to therapy, expanding with the pressure of the drug (Komarova, Burger, & Wodarz, 2014). The cysteine to serine mutation in BTK (C481S) seems to be the most common mutation leading to ibrutinib resistance, but further investigation is required to understand the mechanisms behind the other identified mutations and whether they cause or coexist with ibrutinib resistance.

1.3.6 Second generation BTK inhibitors

Resistance to ibrutinib as well as the drugs off target effects have led to the development of more specific second generation BTK inhibitors such as ONO/GS-4059, ACP-196 and GDC-0853. GDC-0853 is the most specific BTK inhibitor developed so far but ONO/GS-4059 and ACP-196 are also more potent than ibrutinib (Wu, Liu, Tsui, & Liu, 2016). Like ibrutinib, both ONO/GS-4059 and ACP-196 are irreversible inhibitors whilst GDC-0853 is a reversible, noncovalent inhibitor.

In comparison with ibrutinib, other more selective irreversible BTK inhibitors have the advantage of less off target effects, thereby reducing the side effects in patients. Studies with ibrutinib have shown that toxicities related to off target binding are common and can include gastrointestinal toxicity, haematological toxicity as well as bleeding.

Clinical studies in different B-cell malignancy subsets with ONO/GS-4059 and ACP-196 have shown a lower incidence of associated toxicities (Byrd et al., 2016; Walter et al., 2016) but due to a similar electrophilic warhead to ibrutinib, these compounds are likely not efficient in patients carrying Cys481 mutations. GDC-0853 on the other hand binds the hinge region of BTK but does not interact with the Cys481 residue and would be expected to obtain its activity against BTK C481S (Crawford et al., 2018). GDC-0853 is currently being used in a first-in-human Phase I study of patients with relapsed or refractory B-cell NHL and CLL that relapsed on ibrutinib, particularly those carrying the BTK C481S mutation (ClinicalTrials.gov Identifier: NCT01991184). Results of this study will show if GDC-0853 can overcome ibrutinib resistance.

1.4 Genome editing

1.4.1 Development and mechanism of targeted genome editing

Genome editing describes the process of manipulating the DNA of a cell or organism. Genome editing technologies have advanced immensely over the past few years enabling researchers now to precisely modify a specific locus within the genome. Conventional gene targeting is achieved by providing cells with a donor DNA template containing a gene of interest or mutation that would recombine at a target site by homologous recombination (HR) (Capecchi, 1989, 2005).

This technique is utilised extensively to generate "knock-out" mice but unfortunately the levels of HR in most other cell types are orders of magnitude lower than the murine embryonic stem cells.

The foundation for targeted genome editing was set with the discovery in 1988 that the poor efficiency of HR could be boosted in yeast by the introduction of double-strand breaks (DSBs) and this was later demonstrated to also be applicable to mammalian cells (Figure 1.7) (Rouet, Smih, & Jasin, 1994; Rudin & Haber, 1988).

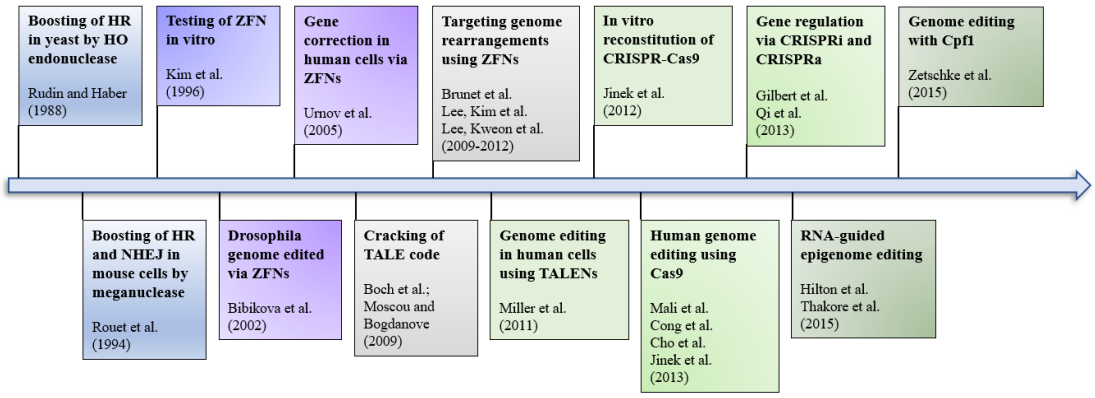

Figure 1.7 Timeline of nuclease-dependent gene editing methods

Timeline from 1988 to 2015 of landmark discoveries in the genome editing field.
Adapted from [Nature Protocols, Genome editing comes of Age, (J. S. Kim, 2016)]

Genome editing development was further boosted with the discovery that DSBs are repaired via non-homologous end joining (NHEJ) in the absence of a donor DNA template leading to a potential mechanism of gene disruption (Wake, Gudewicz, Porter, White, & Wilson, 1984).

Zinc finger nucleases (ZFNs) were the first to be used to make precise genomic modifications followed by transcription activator-like effector nucleases (TALENs) and most recently clustered regularly interspaced short palindromic repeats (CRISPR) – associated Cas9 (CRISPR/Cas9). The nucleases and their individual characteristics

are described below in the next few sections. Regardless of their differences, all three systems use the same mechanism of action – targeted delivery of a nuclease leading to cleavage of DNA that triggers the cells natural repair mechanism resulting in specific genome modifications.

A DSB is repaired through one of two major pathways: Non-homologous end joining (NHEJ) and Homology directed repair (HDR). NHEJ is an error-prone mechanism that religates the broken DNA directly, does not require a homologous template and is active throughout the cell cycle (Weterings & Chen, 2008). During NHEJ, the DSB is detected by the Ku 70/80 heterodimer which has a high affinity for DSBs (Walker, Corpina, & Goldberg, 2001) and consequently forms a complex with DNA-dependent protein kinase catalytic subunit (DNA-PKcs) (Weterings, Verkaik, Bruggenwirth, Hoeijmakers, & van Gent, 2003). The exposed DNA termini are then processed by DNA polymerases μ and λ (Nick McElhinny et al., 2005) and the Ligase IV/X-Ray Cross-Complementation group 4 protein (XRCC4) complex ligates the DSB ends (Mahaney, Meek, & Lees-Miller, 2009).

HDR, by comparison, is an error-free process that requires a homologous template and is only active in late S and G2 phases of the cell cycle (Kakarougkas & Jeggo, 2014). The MRN complex consisting of Mre11, Rad50 and NbsI detects the DSB and removes nucleotides to create 3' DNA single stranded overhangs (Kobayashi, Antoccia, Tauchi, Matsuura, & Komatsu, 2004). The Rad51 family of proteins and other HR proteins are then recruited to the overhangs coated with replication protein A (RPA) and the overhangs invade the complementary sister chromatid. The single strand base pairs with the complementary strand, forms a D-Loop and DNA-Polymerases extend the invading strand from the 3' end. The cross-over structure formed is then reversed and the adjacent ends ligated by Ligase I completing the repair of the DSB (San Filippo, Sung, & Klein, 2008).

1.4.2 Zinc finger nucleases

Zinc finger nucleases (ZNFs) are endonucleases containing a DNA-binding motif fused to a separate DNA-cleavage domain (Carroll, 2011). The binding domain, a class of eukaryotic transcription factors called zinc finger proteins (ZFPs), can be customized to target any user-defined sequence providing DNA binding specificity. The most common binding domain in humans is the Cys2His2 zinc finger (Chou, Leng, & Mixson, 2012) with each zinc finger domain recognizing around three base pairs of DNA (Pavletich & Pabo, 1991). The cleavage domain is non-specific and is mediated by the restriction enzyme FokI (Bibikova et al., 2001; J. Smith et al., 2000). FokI is only active as a dimer, therefore two sets of fingers must bind to neighbouring sequences on opposite strands to enable the FokI to dimerize and cleave the DNA (Figure 1.8). The requirement of dimerization has two advantages; the first is that binding of a single ZNF does not lead to cleavage because the monomer is not active. The second advantage is that two ZNFs provide a higher target specificity therefore reducing off-target cleavage as they have to bind within a certain distance from one another to enable the FokI to dimerize.

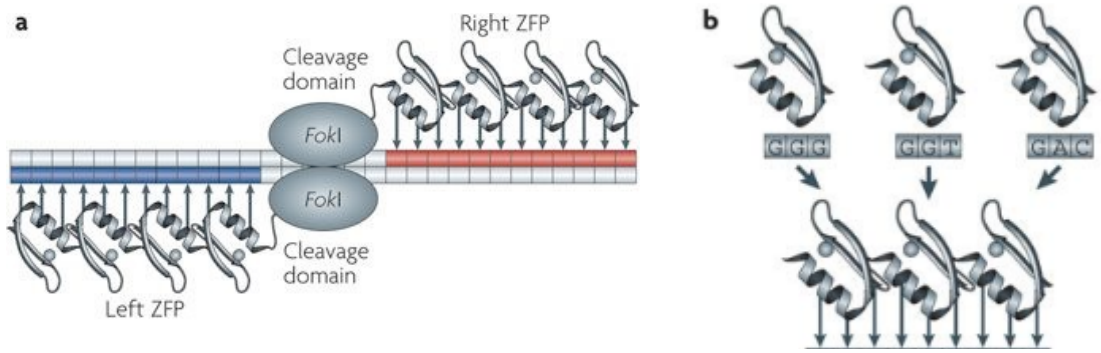

Figure 1.8 Structure and design of Zinc finger nucleases

a Zinc finger nuclease dimer bound to its target with each ZFP containing a FokI cleavage domain and an array of zinc fingers that recognize the target site flanking the cleavage site. **b** An example of a three finger protein with specificity for the sequence GGGGGTGAC.

Reprinted by Permission from Springer Nature [Nature Reviews genetics, Genome editing with engineered zinc finger nucleases, (Urnov, Rebar, Holmes, Zhang, & Gregory, 2010)]

ZNF pairs have been developed and successfully been used in a variety of organisms and cell types including Drosophila, Zebrafish, Rat, Mouse, Human, Tobacco and Maize (Carroll, 2011).

1.4.3 Transcription activator-like effector nucleases

Transcription activator-like effector nucleases (TALENs) are similar to ZFNs, containing two user-defined DNA binding domains linked to the FokI endonuclease domain (Figure 1.9) (Joung & Sander, 2013). The DNA binding domains, TALEs, are repeats of 33-35 amino acids each that recognize a single nucleotide in the target sequence (Pellagatti, Dolatshad, Yip, Valletta, & Boultwood, 2016). TALEs are proteins found in the protobacteria of the *Xanthomonas* species (Boch & Bonas, 2010). Within each alpha-sheet repeat there are two amino acids at positions 12 and 13 known as repeat variable diresidues (RVDs) (Boch et al., 2009) that can be modified to target a specific base. The four RVDs; NI (Asn-Ile) , NN (Asn-Asn), HD (His-Asp) and NG (Asn-Gly) are most widely used and recognize the DNA nucleotides A, G, C and T respectively (Deng et al., 2012). One advantage of TALENs over other nucleases is that almost any DNA sequence can be targeted, and the simple protein-DNA recognition code makes it easy to design TALENs. Construction and delivery into cells however can be challenging due to the large size of TALENs that can often consist of up to 20 almost identical RVD-containing motifs, precluding them for use in viral delivery methods.

Despite this TALENs have successfully been used in a variety of species including plants, frogs, fish, mice and mammalian cells (H. Kim & Kim, 2014).

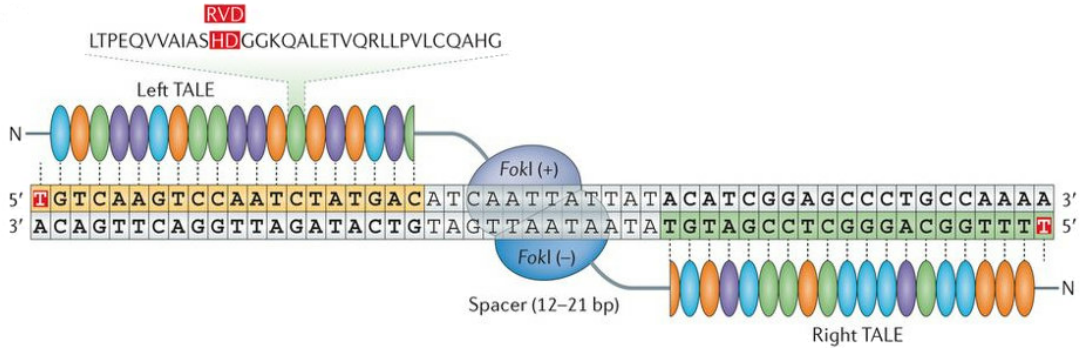

Figure 1.9 Schematic diagram of a TALEN pair

A schematic of a TALEN pair with each composed of TALE repeats and a Fok I domain. Each TALE recognizes a single base through the amino acids at position 12 and 13 (RVD, shown in red).

Reprinted by Permission from Springer Nature [Nature Reviews Genetics, A Guide to genome engineering with programmable nucleases, (H.Kim & Kim, 2014)]

1.4.4 Clustered regularly interspaced short palindromic repeats

The most recently developed programmable nuclease is the CRISPR/Cas9 endonuclease. CRISPR is a natural system used by bacteria and archaea to protect themselves from infections by viruses and invading plasmids (Wiedenheft, Sternberg, & Doudna, 2012). The CRISPR/Cas systems can be divided into two classes with each class including 3 types and several subtypes. Class 2 systems (type II, V, VI) act as monomers whilst Class 1 systems (type I, III, IV) act as multi subunit effector complexes. Type I, II and V systems target DNA whilst the type VI system targets RNA and the type III system can target both (Koonin, Makarova, & Zhang, 2017). The most commonly used Cas enzyme in genome editing is SpCas9 derived from *Streptococcus pyogenes* which belongs to the Class 2, type II system.

The Cas9 endonuclease contains a RuvC and HNH nuclease domain responsible for cleavage of the non-complimentary and complimentary strand, respectively (Figure 1.10) (Sternberg, LaFrance, Kaplan, & Doudna, 2015). Unlike ZNFs and TALENs that contain a modifiable DNA-binding domain, CRISPR/Cas9 can target a user-defined sequence by replacing guide RNAs making it easily re-taskable (J. S. Kim, 2016). As well as Cas9, two other components are required: the CRISPR RNA (crRNA) and the trans-activating crRNA (tracrRNA) (Deltcheva et al., 2011). The crRNA, also known as protospacer, is the sequence that can be modified to target a specific location within the genome. The tracrRNA hybridizes with the crRNA and provides a scaffold for Cas9 binding (Pellagatti et al., 2016). It was discovered that the tracrRNA and crRNA can be fused together to create a single guide RNA (sgRNA) simplifying its use in plasmid-based delivery systems (Jinek et al., 2012).

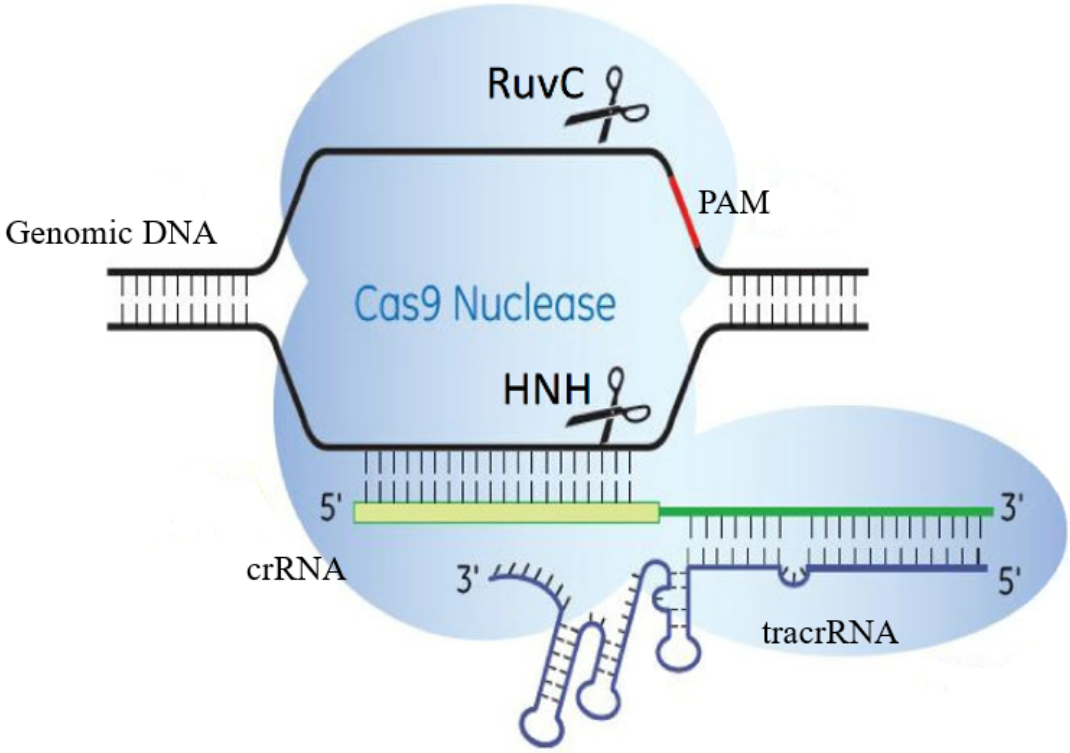

The Cas9 nuclease is recruited to the DNA by the tracrRNA:crRNA (trans-activating crRNA:CRISPR RNA) duplex and after binding upstream of the PAM (Protospacer adjacent motif) sequence a double strand break is induced by the RuvC and HNH domain.

Adapted from the Cell culture dish [CRISPR/Cas9 system and its applications, Debbie King]

The Cas9 endonuclease also requires a species-dependent Protospacer Adjacent Motif (PAM) for DNA binding immediately 3' to the target sequence which can limit guide placement depending on the genomic location. The PAM site of SpCas9 5' NGG occurs approximately every 8 bps (Graham & Root, 2015), which is frequent enough for gene knock-out/knock-ins but can be a limitation for targeting specific nucleotides. Recognition of the PAM by Cas9 triggers a conformational transformation and enables cleavage of the DNA (Sternberg, Redding, Jinek, Greene, & Doudna, 2014).

The induced DSB is then repaired via NHEJ or HDR, as described previously, resulting in sequence insertions, nucleotide changes or corrections via the HDR pathway, in the presence of a suitable homologous template, or small insertions and deletions (indels) via the NHEJ pathway (Figure 1.11).

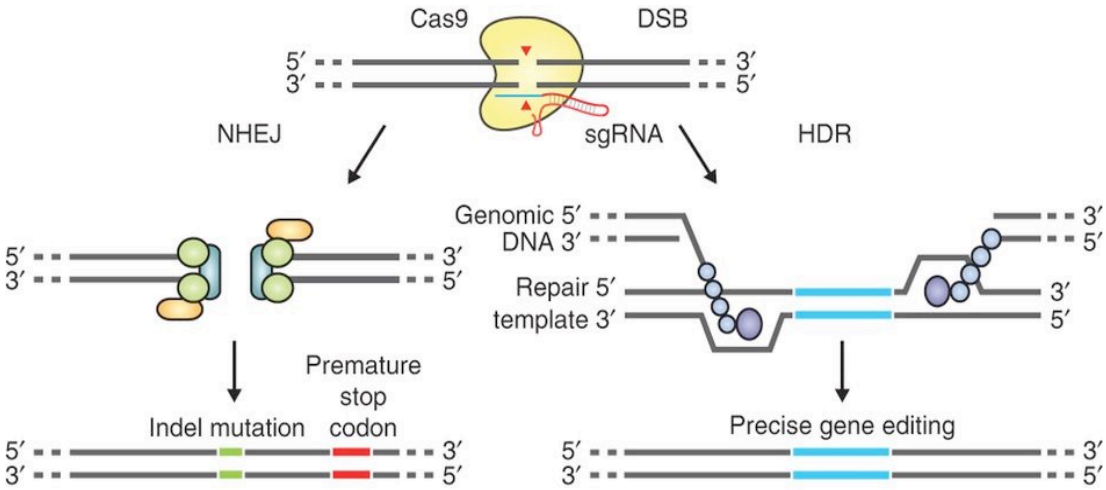

Figure 1.11 Double strand break repair promotes gene editing

A Cas9 induced DSB is repaired via the error prone NHEJ pathway resulting in random small insertions and deletions or via HDR in the presence of a suitable repair template allowing precise gene editing.

Reprinted by Permission from Springer nature [Nature protocols, Genome engineering using the CRISPR-Cas9 system, Ran et al., 2013]

Several Cas9 variants and orthologues have been identified, characterized and adapted for genome editing. As different orthologues recognize different PAM sites and require a different lengths of target sequence, their use can overcome the SpCas9 PAM limitation and widen the range of available sequences that can be targeted (Cebrian-Serrano & Davies, 2017). Two Cas9 orthologues (SaCas9 and AsCas12a) and their characteristics are described below.

SaCas9 belongs, like SpCas9, to the Class 2 type II CRISPR system but is derived from *Staphylococcus aureus.* SaCas9 targets sequences of 21 to 24 bps and requires a 5' NNGRRT PAM for DNA binding. One advantage of SaCas9 over SpCas9 is its smaller size (1053 vs 1368 amino acids) which allows packaging into adeno-associated virus vectors and therefore makes delivery, especially in vivo, much easier (Ran et al., 2015).

Another Cas9 orthologue from *Acidaminococcus* sp., AsCas12a, belongs to the class 2 type V CRISPR systems and has unique features distinct to SpCas9 (Jeon et al., 2018). Unlike SpCas9, AsCas12a only requires a crRNA and has the ability to process its own pre-crRNA into crRNA allowing multiplex genome editing (Fonfara, Richter, Bratovic, Le Rhun, & Charpentier, 2016; Zetsche et al., 2017). Furthermore, AsCas12a creates a DSB by inducing a staggered cut downstream of the PAM site 5' TTN containing only a single active site in the RuvC domain and missing the HNH nuclease domain (Yamano et al., 2016).

1.4.5 Applications of the CRISPR/Cas system in cancer biology

Genome editing technologies have nearly endless applications from basic biology to biotechnology and medicine. In 2015, a one year old girl with leukaemia was successfully treated with CAR T-cells, generated using TALENs (Reardon, 2015). Another in human application of targeted nucleases (ZNFs) was used to disrupt CCR5 gene expression, a receptor used by most HIV strains to enter and infect cells (Wang & Cannon, 2016). Since then, targeted nucleases have been used to better understand molecular mechanisms of several diseases, including cancer, and genome editing has been applied to multiple stages of drug discovery and development.

The CRISPR/Cas system has not yet been used for in human applications but is a breakthrough in the study of cancer genes in mouse models. Tumour suppressor genes p53 and PTEN were successfully targeted in the liver using CRISPR/Cas9 allowing the development of liver cancer models and functional genomics (Xue et al., 2014). To study lung adenocarcinoma, loss of function mutations in p53 and Lkb1 as well as the $KRAS_{G12D}$ mutation were generated using CRISPR/Cas9, leading to the formation of tumours with adenocarcinoma pathology (Platt et al., 2014). Chromosomal rearrangements are common in the pathogenesis of human cancers but have proven to be challenging to model in mice. The CRISPR/Cas system can effectively model chromosomal rearrangements such as inversions and duplications. The Eml4-Alk inversion expressing the Eml4-Alk fusion gene was generated in a mouse model using CRISPR/Cas9 to study lung cancer (Maddalo et al., 2014). The list of applications of the CRISPR/Cas system in cancer biology is endless with its ability to target any gene and either inhibit, repress, activate, translocate, invert or duplicate them. Most importantly, the CRISPR/Cas system offers a replacement for nearly all long experimental procedures for cancer gene therapies (Sachdeva et al., 2015). Newly identified mutations in oncogenes and tumour suppressor genes can rapidly be modelled and functionally analysed and help to choose the optimal targeted therapy in individual cancer patients (Kannan & Ventura, 2015).

1.5 Thesis aims

Manipulating the genome of normal and cancer cells is an important approach to model the disease and study the many genes that are involved in the pathogenesis. The CRISPR/Cas system is a rapidly evolving tool for genome editing allowing easy alteration of the genomes of a huge variety of organisms. This not only helps to better understand the cancer biology but also contributes to the development of novel anti-cancer drugs and the study of drug resistance.

Acute myeloid leukaemia (AML), a malignant disease of the bone marrow and blood, is associated with a poor prognosis in general. Despite an improved understanding of pathogenesis, AML treatment has changed little over the past years. Due to the heterogeneity of the disease, treatment response as well as drug resistance and disease relapse varies, and personalized therapeutic regimes pose a challenge.

Our first aim was to establish and validate a CRISPR-based gene knock-out as well as knock-in strategy in HEK-293T cells targeting Bruton's tyrosine kinase (BTK), a potential therapeutic target in AML.

We next wanted to use CRISPR to generate the C481S mutation of BTK in the AML cell lines HL-60, MV4-11, U937, THP-1 and OCI-AML3. The C481S mutation causes secondary drug resistance in some patients treated with the BTK inhibitor ibrutinib.

Our third aim was to study the functional consequences of the BTK C481S mutation in AML cell lines using ibrutinib.

Chapter 2: Materials and Methods

2.1 Materials

2.1.1 Purchased Reagents and Kits

A list of reagents and kits used in this thesis can be found in Table 2.1. The majority of reagents were purchased from either Sigma-Aldrich (Poole, UK) or Thermo Fisher Scientific (Loughborough, UK).

Table 2.1 Purchased Reagents and Kits

Name	Supplier
4 x Laemmli Buffer	Bio-Rad
Acrylamide	Geneflow
Agarose	Invitrogen
Ammonium persulfate (APS)	Thermo Fisher Scientific
Annexin V APC	Biolegend
Bovine Serum Albumin (BSA)	Sigma-Aldrich
DC Protein Assay kit	Bio-Rad
Dimethylsulphoxide (DMSO)	Sigma-Aldrich
DNA Ladder 100 bp / 1 kb	NEB
Dulbecco's Modified Eagle's Medium (DMEM)	Invitrogen
Ethidium bromide (EtBr)	Promega
Foetal bovine serum (FBS)	Invitrogen
GDC-0853	MedChemExpress
Hexadimethrine bromide (polybrene)	Sigma-Aldrich
Hybond C Nitrocellulose membrane	Amersham
Ibrutinib	Selleckchem
Immobilon Western Chemiluminescent HRP substrate	Millipore
KiNET-1 CTx-0294885	SYNkinase
Luria Bertani (LB)	Sigma-Aldrich
Methylcellulose	Sigma-Aldrich

Milk powder	Tesco
Mix and go E.Coli transformation kit	Zymo Research
Non-essential Amino Acids (NEAA)	Invitrogen
OneTaq Quick-Load 2 x Master Mix with Standard Buffer	NEB
Opti-MEM	Invitrogen
Penicillin, Streptomycin (10 mg/ mL)	Invitrogen
Phosphate buffered saline (PBS)	Sigma-Aldrich
PhosSTOP™ Phosphatase Inhibitor	Roche
Precision Plus Protein Kaleidoscope Prestained Protein Standard	Bio-Rad
Propidium Iodide (PI)	Sigma-Aldrich
Protease Inhibitor Cocktail	Roche
PureLink™ HiPure Maxiprep Kit	Invitrogen
PureLink™ Quick Plasmid miniprep Kit	Invitrogen
Puromycin	Invivogen
RNeasy™ mini kit	Qiagen
Roswell Park Memorial Institute (RPMI)	Invitrogen
SuperScript III Reverse Transcriptase	Invitrogen
Tetramethylethylenediamine (TEMED)	Sigma-Aldrich
TransIT-mRNA Transfection Kit	Mirus
TransIT-Oligo Transfection Reagent	Mirus
Trypsin/EDTA (0.25%)	Sigma-Aldrich
Tween 20	Fisher Bio Reagents
Wizard SV™ Gel and PCR Clean-Up System	Promega
β-Mercaptoethanol	Sigma-Aldrich

2.1.2 Buffers

Table 2.2 Buffers

Name	Constituents
1 x Annexin V binding buffer	10 mM HEPES/NaOH (pH 7.4), 140 mM NaCl, 2.5 mM $CaCl_2$
1 x TAE buffer	40 mM TRIS, 20 mM acetic acid and 1 mM EDTA
10 x Running buffer	1% (w/v) SDS, 1.92 M glycine, 0.25 M Tris
10 x TBS	10 mM Tris-HCl, 150 mM NaCl, pH 8.0
10 x Transfer buffer	0.25 M Tris, 1.92 M glycine
High salt MIB wash buffer	50 mM HEPES (pH 7.5), 1 M NaCl, 0.5% Triton X-100, 1 mM EDTA, 1 mM EGTA
Low salt MIB wash buffer	50 mM HEPES (pH 7.5), 150 mM NaCl, 0.5% Triton X-100, 1 mM EDTA, 1 mM EGTA
MIB elution buffer	0.5% (w/v) SDS, 1% (v/v) β-Mercaptoethanol, 0.1 M Tris-HCl (pH 6.8), LC-MS grade water
MIB lysis buffer	50 mM HEPES (pH 7.5), 150 mM NaCl, 0.5% Triton X-100, 1 mM EDTA, 1 mM EGTA, 10 mM NaF, 2.5 mM $NaVO_4$
Resolving gel buffer	1.5 M Tris-HCl, 0.4% (w/v) SDS, pH 8.8
RIPA buffer	150 mM sodium chloride, 1% Triton X-100, 0.5% sodium deoxycholate, 0.1% sodium dodecyl sulfate, 50 mM Tris pH 8.0
SDS wash buffer	0.1% (w/v) SDS in low salt MIB wash buffer
Stacking gel buffer	0.5 M Tris-HCl, 0.4% (w/v) SDS, pH 6.8

Tail lysis buffer	50 mM Tris/HCL (pH 7.5), 150 mM NaCl, 1 mM EDTA
TBST	1 x TBS, 0.1% tween 20

2.1.3 Antibodies

All primary and secondary antibodies were purchased from Cell Signalling Technology. A table of antibodies used in this thesis is found in Table 2.3.

Table 2.3 Primary and secondary antibodies

Antibody	Type	Species	MW (kDa)	Dilution
β-Actin	Polyclonal	Mouse	42	1:10000
Cas-9	Monoclonal (7A9-3A3)	Mouse	160	1:1500
Btk	Monoclonal (D3H5)	Rabbit	77	1:1000
p-Btk (Tyr223)	Monoclonal (D9T6H)	Rabbit	77	1:1000
PLCγ2	Polyclonal	Rabbit	150	1:1000
p-PLCγ2 (Tyr1217)	Polyclonal	Rabbit	150	1:1000
Akt (pan)	Monoclonal (40D4)	Mouse	60	1:1000
p-Akt (Ser473)	Monoclonal (D9E)	Rabbit	60	1:1000
p42/44 MAPK	Polyclonal	Rabbit	42,44	1:1000
p-p42/44 MAPK (Thr202/Tyr204)	Monoclonal (197G2)	Rabbit	42,44	1:1000
Anti-rabbit IgG		Goat		1:3000

Anti–mouse IgG	Horse	1:5000

2.1.4 Primers, guides and ssODN

Primers and guide oligonucleotides were purchased from Integrated DNA technologies (IDT, Leuven, Belgium). Single-stranded oligodeoxynucleotides (ssODN) used as homology directed repair (HDR) template was purchased from Sigma. A full list of primers, guide oligonucleotides and the ssODN used in this thesis can be found below in Table 2.4.

Table 2.4 Primers, guides and ssODN sequences

Primers	Sequence 5' to 3'
ex15F	ATCTATTTGCTGGAGTCTAGG
Ex15F EcoRI	AGGAATTCACACAACAACCCACT GAGG
ex15R	AGGCTGGAGATATTTGATGGG
Ex15R NheI	GCAAACCCTTAAAAAGAAACATT TCGCTTGCTAGCTCTAG
ex15R2	CCACATTCTCACGAACCGCC
ex2F	GGAACCAAGAGGGATGAGG
ex2R	GGTAGTCATAGATTTATAGATC
ex3F	GCCCTCCATTTGGTAGTCATAG
ex3R	CCCTCAGTTCTCTCAGGATC
mutF	ATGGCGAACGGTAGTCTTC
mutR	TAAGAAGACTACCGTTCGC
sgRNA reverse	GGCACCGAGTCGGTGCTTTT
T7-sgRNA forward	TAATACGACTCACTATAGGGCTG CCTCCTGAACTACC

Template R	CCCATCTTCATCATCACTGAGTACAT

SpCas9 guides	**Sequence 5’ to 3’**
Guide #1 (exon 15)	CCTGAACTACCTGAGGGAGAT
Guide #2 (exon 15)	ATGGCTGCCTCCTGAACTA
Guide #3 (exon 15)	CTGCCTCCTGAACTACCTG
Guide #4 (exon 15)	AGCAGCGCCCCATCTTCAT
Guide #5 (exon 15)	CTGCCTCCTGAACTACCTGA
Guide #7 (exon 2)	AGCTATGGCCGCAGTGATTC
Guide #8 (exon 2)	GTTTCTCTTGACCGTGCACA
Guide #9 (exon 3)	GATCACTTGTGTTGAAACAG
Guide #10 (exon 3)	GAAAGACAGATTCCGGTAAG

SaCas9 guide	**Sequence 5’ to 3’**
Guide #6 (exon 15)	GCGCCCCATCTTCATCATCA

Cas12a guides	**Sequence 5’ to 3’**
Cas12a #1 (exon 2)	ATTATCAACAGCACACAGGTGAA
Cas12a #2 (exon 2)	CAACAGCACACAGGTGAACTCCA
Cas12a #3 (exon 2)	TGAAGCGATCCCAACAGAAAAAG
Cas12a #4 (exon 2)	TCTTGACCGTGCACAAACTCTCCT

HDR template	**Sequence 5’ to 3’**
HDR template binding to bases 38 to 148 within exon 15 of BTK (equal to bases 19154 to 19265 of the whole gene sequence)	GTCTGCACCAAGCAGCGCCCCATCTTCATCATCACTGAGTACATGGCGAACGGTAGTCTTCTTAATTATCTTAGAGAGATGCGCCACCGCTTCCAGACTCAGCAGCTGCTA

2.1.5 Plasmids

Plasmids were purchased from Addgene or were a kind gift from Dr. Nicholas Harper. Plasmid maps can be found in the Appendix.

Table 2.5 Plasmids

Name	Details
LentiCRISPR v2	Lentiviral plasmid expressing SpCas9
pCW-Cas9	Doxycycline-inducible SpCas9 expressing lentiviral plasmid
pLeGO	EGFP expressing lentiviral plasmid
pX459	Nonviral SpCas9 expressing plasmid
pX601	Adeno-associated viral plasmid expressing SaCas9
pcDNA6	Mammalian expression vector

2.1.6 Cell lines

All AML cell lines (HL-60, MV4-11, OCI-AML3, THP-1 and U937) were obtained from the American Type Culture Collection (ATCC). Cell identity was verified by the supplier via STR analysis. The human embryonic kidney cell line HEK-293T was a kind gift from Dr. John Quinn.

2.2 Maintenance of cell lines

2.2.1 Cell culture

All cell lines were cultured in T75 tissue culture flasks at 37°C in a humidified atmosphere containing 5% CO_2 and tested for mycoplasma contamination twice using PCR.

AML cell lines were cultured in Roswell Park Memorial Institute (RPMI) 1640 supplemented with 1% GlutaMax, 20% heat-inactivated foetal bovine serum (FBS) and 10 U/mL Penicillin/Streptomycin.

HEK-293T cells were cultured in Dulbecco's Modified Eagle Medium (DMEM), both supplemented with 10% FBS and 10 U/mL Penicillin/Streptomycin.

All cells were passaged 2-3 times a week to maintain a density appropriate for each cell line. Suspension cells were diluted in their culture flask either by adding growth medium until the maximal culture volume was reached or by withdrawing a portion of cells and adding medium to the remaining cells.

The adherent cell line HEK-293T had to be enzymatically treated to detach the cells from the culture flask surface prior to passaging. When cells were confluent, the growth medium was removed and 5 mL of trypsin ethylenediaminetetraacetic (EDTA) solution was added to the cells. After incubation for 5 min at 37°C / 5% CO_2 an equal volume of growth medium was added to the cells to inactivate trypsin. Cells were then transferred to a 15 mL conical tube and pelleted at 113 x g for 3 min. The supernatant was removed, and cells were resuspended in 5 mL of growth medium. Part of the media containing cells was transferred to the culture flask and cells were further diluted with growth medium.

2.2.2 Cryopreservation and Thawing cells

For Cryopreservation cells were centrifuged at 113 x g for 5 min, growth medium was removed, and cells were resuspended in freezing medium consisting of 90% FBS and 10% Dimethyl sulfoxide (DMSO). Cells were then transferred into 2 mL cryogenic vials and placed into a Mr. Frosty Freezing Container for storage at -80°C overnight. The freezing container is filled with isopropanol to allow the samples to achieve a slow cooling rate of -1°C / minute which is the optimal rate for cell preservation. Following

overnight storage, cryogenic vials were transferred into liquid nitrogen for long-term storage.

To defrost cells, cryogenic vials were taken out of the liquid nitrogen tank and left at room temperature for several minutes to thaw. Warm cell culture medium was added, and cells transferred into a 15 mL conical tube for centrifugation at 113 x g for 5 min. Cells were then resuspended in 7 mL culture medium and placed into a T25 tissue culture flask.

2.2.3 Single cell clone Isolation

Single cell clones were isolated by growing cells in methylcellulose. 2.4 g of sterilised methylcellulose 1500 cP dry powder was added to 50 mL of sterile water and gently simmered for several hours with constant stirring. The solution was then cooled to 50°C and diluted 1:1 with 2 x RPMI medium. To allow the methylcellulose to fully solubilise the solution was stirred overnight at 4°C. The following day the solution was transferred to a 50 mL conical tube and centrifuged at 920 x g for 60 min to clear any particles that had not solubilised. The methylcellulose solution was stored at -20°C in 10 mL aliquots until used.

50 µL of non-essential amino acids (NEAA), 50 µL of 10 U/mL Penicillin/Streptomycin and 1 mL FBS were added to 2 mL of media containing 3000 cells. 3 mL of Methylcellulose / RPMI was added to the cells and mixed with a 5 mL syringe and 12-gauge needle. This was then left to stand for the bubbles to disperse before the cells were seeded in either a 6 well or 12 well plate (2.5 mL / 1 mL). Plates were left for 10-14 days after which colonies were picked under a microscope using a 10 µL pipette and transferred to a 96 well plate for expansion.

2.2.4 Ibrutinib treatment and wash-out experiment

1.5 x 10^6 THP-1 and OCI-AML3 wild type cells as well as selected BTK^{C481S} positive clones were seeded in a 12 well plate in 1.5 mL of media. Cells were treated with 1, 3,

10, 30, 100, 300, 1000 nM ibrutinib for 2.5 h. Untreated cells and vehicle treated cells were used as a control. Cells were then either harvested or washed with PBS 3 times and incubated for another hour (wash out experiment).

2.3 Protein analysis

2.3.1 Protein Isolation and quantification

To extract cellular proteins, at least 1 x 10^6 cells were harvested on ice, washed in ice-cold Phosphate buffered saline (PBS) and pelleted at 500 x g for 1 min at 4°C. The cell pellet was resuspended in 100 µL Radioimmunoprecipitation buffer (RIPA buffer) supplemented with proteinase inhibitors (Aprotinin, Leupeptin, Pepstatin A, Pefabloc, E64 all at 1 µg / mL) and PhosSTOP phosphatase inhibitor cocktail tablets. Cells were left on ice for 30 min before clearing the lysate by centrifugation at 16000 x g for 10 min. The supernatant containing the proteins was transferred into a clean 1.5 mL tube and protein concentration was determined using the DC protein Assay kit before samples were stored at -20°C. The DC protein Assay is a colorimetric assay and was performed according to the manufacturer's instructions. Bovine serum albumin (BSA) was diluted in RIPA buffer to create a standard curve of concentrations ranging from 0.125 mg / mL to 2 mg / mL.

2.3.2 Protein separation by SDS-PAGE

Sodium dodecyl sulfate polyacrylamide gel electrophoresis (SDS-PAGE) was performed to separate extracted cellular proteins by their molecular weight. Protein lysates were mixed with 4 x Laemmli buffer containing 1% freshly added β-mercaptoethanol for reduction and samples denatured by heating at 95°C for 5 min. Between 10 - 15 µg of total protein and 4 µL of Precision Plus Protein Kaleidoscope Prestained Protein Standard were then loaded on a Tris-glycine PAGE gel and electrophoresis was carried out in 1 x running buffer at 30 mA per gel for 75 min. Tris-glycine PAGE gel recipes can be found in Table 2.6.

Table 2.6 Resolving and Stacking gel recipes for 2 gels

	Resolving gel		Stacking gel
	7%	10%	5%
ddH_2O	8.8 mL	7.05 mL	1.24 mL
Acrylamide (30% w/v)	3.9 mL	5.7 mL	4.36 mL
5 x Gel buffer	4.25 mL	4.25 mL	1.9 mL
10% APS	75 µL	75 µL	75 µL
TEMED	22.5 µL	22.5 µL	22.5 µL

2.3.3 Western blotting

Following SDS-PAGE, proteins were transferred onto a nitrocellulose membrane in 1 x transfer buffer at 400 mA for 1 h. The membrane was washed three times for 10 min in Tris-buffered saline containing 0.1% Tween 20 (TBST) and blocked at room temperature for 1 h in TBST containing 5% milk. After blocking, the membrane was washed again three times for 10 min in TBST before being incubated with primary antibodies at 4°C overnight on a rocker platform. Phospho-specific antibodies were diluted in TBST containing 5% BSA and all other antibodies used were diluted in TBST containing 5% milk.

Following overnight incubation with primary antibodies the membrane was washed three times for 10 min in TBST and incubated with a horseradish peroxidase (HRP) conjugated secondary antibody for 1 h at room temperature. The membrane was developed after three further washes in TBST for 10 min using enhanced chemiluminescence (ECL) and a ChemiDoc Imaging system (Bio-rad).

All antibodies and their dilutions used in this thesis can be found in Table 2.3 (page 38).

2.4 Lentivirus

2.4.1 Virus production in HEK-293T cells

For increased safety a 3rd generation lentiviral system was used (Dull et al., 1998). The 4 plasmids necessary for virus production are 2 packaging plasmids, one encoding Rev (pRSV-REV) and one encoding Gag and Pol (pMDLg/pRRE), an envelope plasmid encoding VSV-G (pCMV-VSV-G) and a lentiviral transfer plasmid encoding the insert of interest.

3.5 x 10^6 HEK-293T cells were seeded in 100 mM cell culture dishes and grown until they reached 80% confluency. Culture medium was changed 4 h prior to transient transfection. Transfection mixture was prepared by combining 150 µL of 150 mM NaCl with 20 µL of 1 mg/mL Polyethylenimine (PEI) in one tube and 150 µL of 150 mM NaCl with 4 µg of transfer plasmid and 2 µg of each of the packaging and envelope plasmids in a second tube. The NaCl/PEI mix was added to the NaCl/plasmid mix, vortexed and left for 20 min at room temperature before it was added dropwise to the HEK-293T cells. Medium was changed the next morning and the supernatant containing viral particles harvested 48 h and 72 h post transfection. Viral particles were concentrated on the day of harvesting by Ultracentrifugation at 4°C for 1.5 h at 25000 rpm using an SW41Ti rotor in a Beckman Ultracentrifuge. Concentrated viral particles were resuspended in PBS and stored at -80°C after the second harvest.

2.4.2 Determining viral titre

To measure how many of the produced Lentiviral particles are infectious, viral titre was determined using HEK-293T cells. 4 x 10^5 HEK-293T cells were seeded in a 6 well plate and left overnight before transduction with different amounts of the viral prep. The number of HEK-293T cells that were positive for vector encoded transgene expression (green fluorescent protein) were measured by flow cytometry 48 h after transduction.

The viral titre in transducing units (TU) per mL was calculated using the following formula:

$$\boldsymbol{Viral\ titre}\ [\boldsymbol{TU/mL}] = \frac{\boldsymbol{number\ of\ seeded\ cells\ x\ GFP\ positive\ cells}\ [\%]}{\boldsymbol{Volume\ of\ virus}\ [\boldsymbol{mL}]}$$

2.4.3 Transduction of mammalian cells

For Lentiviral transduction of mammalian cells, a multiplicity of infection (MOI) ratio of 10 was used and the amount of virus needed for transduction was calculated according to the following formula:

$$\boldsymbol{Volume\ of\ virus}\ [\boldsymbol{mL}] = \frac{\boldsymbol{MOI\ x\ number\ of\ seeded\ cells}}{\boldsymbol{viral\ titre}\ [\boldsymbol{TU/mL}]}$$

Medium of target cells was changed 24 h before transduction. 0.5 x 10^6 cells were seeded in a 24 well plate in 0.5 mL of medium or 0.2 x 10^6 cells in a 12 well plate in 1 mL of medium for HEK-293T cells. Virus was mixed with polybrene (8 µg/ mL final concentration) and added onto the cells. Cells were transduced via spinoculation at 450 x g for 45 min at 37°C and incubated overnight. Fresh medium was added to each well the next morning to reduce the polybrene concentration to 4 µg/ mL. Virus containing medium was removed 48 h post transduction and cells were pooled and transferred into a T25 tissue culture flask for selection/expansion or used immediately for experiments.

2.5 Molecular biology techniques

2.5.1 Preparation of competent cells

Competent NEB stable E.coli cells needed for transformations were generated using the 'Mix and Go' E.coli transformation kit. Cells were prepared according to the manufacturer's protocol.

2.5.2 Transformation of competent E.coli cells

Plasmid DNA was added to 30 µL of competent cells in a 1.5 mL tube and incubated for 30 min on ice. Bacteria were then heat shocked at 42°C for 45 sec and placed on ice for 2 min to recover before 500 µL of Luria Broth (LB) medium was added and bacteria were grown in a shaking incubator at 37°C for 45 min. Bacteria were then plated on a LB-Agar plate containing the appropriate antibiotic for selection and plates were incubated at 37°C overnight.

2.5.3 Isolation of Plasmid DNA

Plasmid DNA was isolated from E.coli after transformation and propagation. Depending on the starting E.coli culture volume, which was either 5 mL or 200 mL, a mini or maxi prep was performed using the Invitrogen PureLink™ Quick Plasmid miniprep Kit/ Invitrogen PureLink™ HiPure Plasmid Maxiprep Kit. The plasmid DNA isolation is based on the alkaline lysis method and was performed according to manufacturers instructions. Isolated plasmid DNA was resuspended in water and quantified by Nanodrop.

2.5.4 Transfection of HEK-293T cells

4 x 10^5 HEK-293T cells were seeded in a 6 well plate in 1.5 mL of medium and left overnight to adhere.

For plasmid transfections 50 µL of 150 mM NaCl was mixed with 1 µg plasmid (750 ng if more than 1 plasmid was used) and in a separate tube 50 µL of 150 mM NaCl was mixed with 3 µL PEI.

The NaCl/PEI mix was added to the NaCl/Plasmid mix, vortexed and left for 20 min at room temperature before it was added dropwise to the HEK-293T cells.
For transfection of the ssODN HDR template the TransIT-Oligo Transfection Reagent was used. 250 µL Opti-MEM, 15 µL TransIT-Oligo transfection Reagent and 3 µL of 100 µM ssODN was added to a tube, mixed by pipetting and incubated for 20 min before being added dropwise to HEK-293T cells.

For transfection of sgRNA the Trans-IT mRNA Transfection kit was used. 250 µL Opti-MEM, 2.5 µg RNA, 5 µL mRNA boost reagent and 5 µL Trans-IT mRNA reagent were added to a tube and incubated for 4 min before being added dropwise to HEK-293T cells.

Cells were harvested 48 h post transfection for protein or DNA isolation.

2.5.5 Isolation of genomic DNA

At least 1 x 10^6 cells were pelleted in a 1.5 mL tube, washed in PBS and resuspended in 240 µL of tail lysis buffer. 60 µL of 1% SDS and 6 µL Proteinase K (20 mg/ mL) were added and cells were incubated at 55°C in a heat block overnight. After the addition of 2 µL RNAse A (50 mg/ mL) and a further incubation for 30 min at 55°C, Proteinase K was inactivated at 95°C for 10 min. Tubes were cooled on ice and DNA was precipitated by adding 400 µL isopropanol. Genomic DNA was then pelleted by centrifugation at 17000 x g for 10 min, washed in 70% ethanol and resuspended in water before quantification by Nanodrop.

2.5.6 Polymerase chain reaction (PCR)

DNA was amplified by PCR for several different experiments including genotyping, colony screening, T7 endonuclease assays and cloning. PCR conditions varied depending on the DNA template, primer sequence, DNA Polymerase and length of target DNA. For the majority of PCRs, OneTaq Quick-Load 2 x Master Mix with Standard Buffer was used which only required the addition of a DNA template and primers. In a typical genomic PCR reaction 8 µL of OneTaq mix, 300 ng of genomic DNA and 1 µL of each primer were used. DNA was initially denatured for 2 min at 95°C followed by 35 cycles consisting of a 30 sec denaturation step, primer annealing at 58°C for 30 sec and extension at 72°C for 1 min. Following a final 5 min extension step at 72°C the samples were cooled down to 4°C.

For bacterial colony screens, bacteria were picked using a 10 µL pipette, transferred into 30 µL H_2O and incubated for 10 min at 95°C. This was then used as a template in a PCR reaction.

2.5.7 DNA electrophoresis

To separate DNA fragments according to their size, agarose or polyacrylamide gel electrophoresis was performed.

For agarose gels, agarose was weighed out and added to 1 x Tris-acetate-EDTA (TAE) buffer. The percentage of agarose is dependent on the DNA fragment size but in most cases a 1% (w/v) gel was used. The agarose was dissolved in 1 x TAE using a microwave and ethidium bromide (EtBr) was added before pouring into the gel tray. EtBr is a fluorescent dye that intercalates DNA and RNA. DNA was separated at 80 V and visualized under ultraviolet (UV) light.

Polyacrylamide gel electrophoresis (PAGE) was performed following a T7 endonuclease assay (see 2.5.10) as this assay creates small DNA fragments that require a high resolving power and a thin gel for separation. A 12.5% PAGE gel was cast by

mixing 10 mL 30% acrylamide, 12.5 mL 2 x TAE, 2.5 mL H_20, 150 µL APS, and 30 µL TEMED together, pipetted between two plates and left to polymerize once the comb had been inserted. DNA was separated at 135 V for 90 min, stained with EtBr and visualized under UV light.

2.5.8 DNA Restriction digest

To digest DNA using restriction endonucleases, restriction sites were either added to DNA fragments by PCR or determined using a plasmid map when plasmid DNA was digested.

Restriction digests were performed for 4 h using the appropriate endonuclease, recommended buffer and incubation temperature according to manufacturer's instructions. Digested fragments were either gel extracted, or PCR purified using the Wizard SV gel and PCR clean up system.

2.5.9 DNA Ligation

Digested and purified DNA fragments or annealed and phosphorylated oligos were used as inserts in ligation reactions. To prevent self-ligation, digested plasmid DNA was dephosphorylated prior to ligation using Antarctic Phosphatase. For ligation a molar ratio of 1:3 of plasmid to insert was used and added to a tube with 1 µL T4 DNA Ligase, 1 µL 10 x T4 DNA Ligase buffer and H_2O (up to 10 µL). The reaction was incubated either at 4°C overnight or 2 h at room temperature. After heat inactivation of T4 DNA Ligase at 65°C for 10 min followed by cooling down on ice, the reaction was used for transformation.

2.5.10 T7 endonuclease I assay

To determine gene targeting efficiency of the CRISPR guides a T7 endonuclease I (T7E1) assay was performed. T7E1 recognizes and cleaves mismatched dsDNA. Whilst homoduplex DNA is perfectly paired, heteroduplex DNA normally contains 'bubbles' formed by extra helical loops from unpaired regions. The T7E1 assay can be used as a mutation detection assay based on the ability of T7E1 to determine between homo- and heteroduplex DNA.

When Cas9 causes a double strand break (DSB) in the targeted region this is repaired by non-homologous end joining (NHEJ) if a suitable template is not present. This repair process is error-prone and therefore leads to small insertions or deletions (indels) that can be recognized and cleaved by T7E1.

For the T7 endonuclease I assay the CRISPR targeted region was amplified by PCR. The PCR product was then denatured at 95°C for 10 min in a hot-block and left to cool down to room temperature to allow for re-annealing. This leads to wild-type and modified homoduplexes as well as wild-type and modified heteroduplexes as shown in Figure 2.1

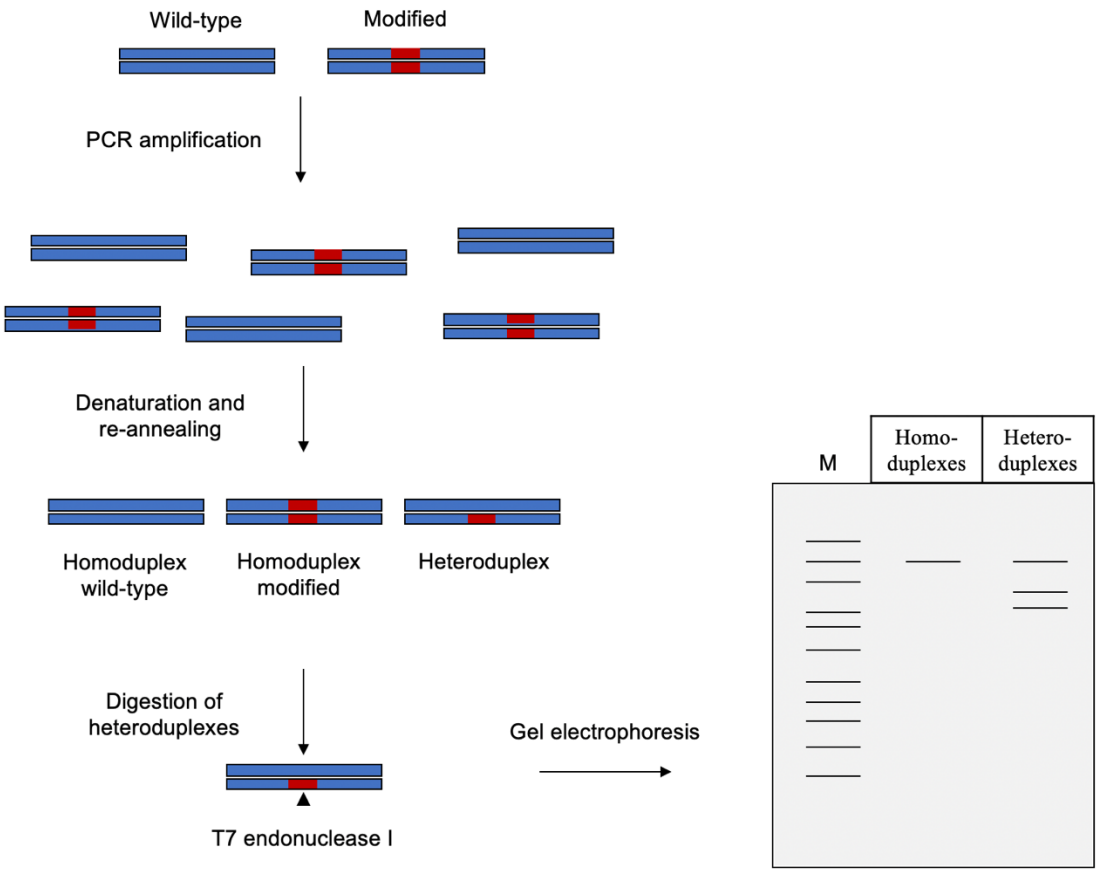

Figure 2.1 T7 endonuclease I assay

Amplified DNA from edited and wild-type cells forms homoduplex wild type, homoduplex modified and heteroduplex fragments after denaturing and re-annealing. T7 endonuclease I recognises the mismatched DNA and cleaves the heteroduplex fragments resulting in smaller fragments. DNA incubated with T7 endonuclease I is separated on a polyacrylamide gel and gives an estimate of gene targeting efficiency.

1 µL of NEB buffer 2 was added to 5 µL of the re-annealed PCR products, and reactions were incubated with or without the addition of T7E1 for 40 min at 37°C. The T7E1 will cleave heteroduplex DNA if present with different efficiency depending on the number of mismatched nucleotides and the flanking sequence as this affects the heteroduplex structure. Deletions are cleaved more efficiently than single base mutations.

After incubation of the DNA with or without T7E1, DNA was separated on polyacrylamide gel for 130 min at 80 V and analysed for the presence or absence of cleaved products. The presence of cleaved products after digestion with T7E1 indicates the efficiency of editing.

2.6 Functional Assays

2.6.1 Flow cytometry / Cell-sorting

Flow cytometry is a technique that measures a cells characteristic including cell size and volume but can also be used to measure for example the expression of cell surface or intracellular molecules using fluorescent labelled antibodies or ligands for their detection. The technique is based on the presence or absence of fluorescence and light scattering signals that are measured when cells pass one or more laser beams. The direction of light scattered when cells pass the laser beam(s) correlates with the size of the cell (forward scatter) and granularity (side scatter). To separate a population from a heterogenous sample (cell sorting) a vibration is introduced generating waves that break the fluid stream into regular droplets allowing to select individual cells and divert them into a collection tube.

Flow cytometry was used to determine the viral titre and measure cell viability using an Attune NxT flow cytometer whilst cell sorting was performed using a BD Aria and was used to isolate GFP-transduced cells from untransduced cells. Cell debris were excluded in a FSC-A versus SSC-A dot plot, duplets were discriminated in a FSC-W vs FSC-A dot plot and the remaining cell population was analysed depending on the application.

2.6.2 Apoptosis assay

Between 0.5 and 1 x 10^6 cells were transferred to a 1.5 mL tube, pelleted at 100 x g for 5 min and washed with PBS. Cells were then washed in 300 µL 1 x Annexin V binding buffer before being pelleted again and resuspended in 100 µL 1 x Annexin V binding buffer containing 5 µL Annexin V conjugated to FITC. Following incubation for 15 min at room temperature in the dark cells were washed again in 300 µL 1 x Annexin V buffer. After a final spin at 100 x g for 5 min the cell pellet was resuspended in 400 µL 1 x Annexin V binding buffer containing 7 µL of 1 µg/ mL propidium iodide (PI) and analysed via flow cytometry.

2.6.3 Cell Proliferation assay

CellTiter-Glo Luminescent Cell Viability Assay was used to measure cell proliferation. The assay determines the number of viable cells based on quantitation of the ATP present. The amount of ATP is proportional to the number of cells which allows using the assay to measure cell proliferation.

100 µL of cultured cells (1 x 10^6 cells / mL seeding density) as well as 100 µL RPMI medium on its own as a control were pipetted in duplicates into a white 96 well plate and incubated with 100 µL of CellTiter-Glo reagent for 10 min on an orbital shaker to mix contents, induce lysis and stabilize luminescent signal. Luminescent signal was measured at a wavelength of 560 nm.

2.7 Mass spectrometric analysis

2.7.1 Phosphoproteomics

Phosphoproteomics were performed by Vinothini Rajeeve from the lab of Pedro Cutillas, Barts Cancer Institute, Queen Mary University of London.

Phosphoproteomics experiments were performed using mass spectrometry as reported (Casado et al., 2013; Rajeeve, Vendrell, Wilkes, Torbett, & Cutillas, 2014).

In brief, frozen cell pellets were lysed in 8 M urea buffer and supplemented with phosphatase inhibitors (10 mM Na_3VO_4, 100 mM β-glycerol phosphate and 25 mM $Na_2H_2P_2O_7$ (Sigma)). Proteins were digested into peptides using trypsin and phosphopeptides enriched from total peptides by TiO_2 chromatography (Larsen, Thingholm, Jensen, Roepstorff, & Jorgensen, 2005)). Dried phosphopeptides were dissolved in 0.1% TFA and analysed using a Nanoflow UltiMate 3000 RSLCnano instrument coupled to a Q Exactive Plus mass spectrometer (Thermo Fisher Scientific). Gradient elution was from 3% to 35% with 0.1% formic acid in acetonitrile in 120 min at a flow rate of 300 nL/min with 0.1% formic acid in water used to balance the mobile phase. The spray voltage was 1.95 kV and the capillary temperature was set to 255 ºC. The Q Exactive Plus was operated in data dependent mode with one survey MS scan followed by 15 MS/MS scans. The full scans were acquired in the mass analyser at 375- 1500m/z with the resolution of 70 000, and the MS/MS scans were obtained with a resolution of 17 500. MS raw files were converted into Mascot Generic Format using Mascot Distiller (version 2.5.1) and searched against the SwissProt database (release December 2015) restricted to human entries using the Mascot search daemon (version 2.5.0).

Allowed mass windows were 10 ppm and 25 mmu for parent and fragment mass to charge values, respectively. Variable modifications included in searches were oxidation of methionine, pyro-glu (N-term) and phosphorylation of serine, threonine and tyrosine. Phosphopeptide quantification was performed using in-house software Pescal as described (Alcolea, Casado, Rodriguez-Prados, Vanhaesebroeck, & Cutillas, 2012). The resulting quantitative data was parsed into excel files for further normalisation and statistical analysis.

2.7.2 Multiplexed Inhibitor Bead (MIB) Assay

Protein lysates were prepared as described in 2.3.1 using MIB lysis buffer supplemented with Protease Inhibitor Cocktail and Phosphatase Inhibitor Cocktail 2+3. Samples were lysed on ice in MIB lysis buffer, sonicated 3 x 10 sec and lysates clarified by centrifugation at 17000 x g for 10 min at 4°C.

Following protein determination assay, 2 mg of protein was further diluted in MIB buffer to a total volume of 3.5 mL per sample and 743 µL of 5 M NaCl was added to the samples giving a final concentration of 1 M NaCl. 350 µL of MIB was added onto each MIB column and 200 µL ECH-Sepharose slurry was added onto each block column before being washed with 2 mL of high salt MIB wash buffer. The block columns were then placed over the MIB columns and lysates were pipetted onto block columns. MIB columns were washed with 5 mL high salt MIB wash buffer followed by a wash with 5 mL low salt MIB wash buffer and a final wash with 500 µL 0.1% (w/v) SDS in low salt MIB wash buffer. Columns were secured with a yellow cap and proteins were eluted by adding 500 µL MIB elution buffer onto the columns. After incubating the columns for 15 min at 95°C the eluate was collected in a 1.5 mL low-retention tube. The elution and collection using 500 µL MIB elution buffer was then repeated collecting the eluate in the same tube.

Samples were then treated with Dithiothreitol and Iodoacetamide for reduction and alkylation before being concentrated. Methanol/Chloroform Precipitation was performed to remove the detergent before samples were trypsin digested overnight. The next day, ethyl acetate extraction was performed to remove Triton from the digested peptides and digested peptides were cleaned using C-18 PepClean spin columns. Samples were then analysed by Mass Spectrometry (University of Warwick).

Chapter 3: Validation of BTK^{C481S} knock-in and BTK knock-out strategy in HEK-293T cells

3.1 Introduction

Genome editing using programmable nucleases is a rapidly evolving field enabling targeted gene disruption both in vitro and in vivo. While editing has been performed with nucleases such as Zinc fingers (ZFNs) and Transcription activator like effectors (TALENs), the clustered regularly interspaced short palindromic repeats (CRISPR) - associated nuclease 9 (Cas9) system has become the most popular technique and has found its use in a variety of applications in biotechnology and medicine. When the Cas9 nuclease induces a double strand break (DSB) at a user-defined target sequence, it triggers the cells natural repair system which will attempt to repair the break either by non-homologous end joining (NHEJ) or homology directed repair (HDR) (Zaboikin, Zaboikina, Freter, & Srinivasakumar, 2017). NHEJ is an error-prone process that results in small insertions and/or deletions (indels) and disrupts the gene (Rodgers & McVey, 2016). By contrast, HDR is a more specific process which allows custom modifications in the presence of a suitable homologous donor template.

Several CRISPR/Cas systems have been developed and characterized from different bacteria with each of them having their own application-dependent advantages. The first Cas endonuclease used successfully in human cells, which is also the best characterized and most commonly used Cas nuclease, is SpCas9 derived from *Streptococcus pyogenes* (Jinek et al., 2013). One advantage of SpCas9 is that its required Protospacer adjacent motif (PAM) for DNA binding, 3' NGG, occurs relatively frequent in most genomes, resulting in many available target sites (Cong et al., 2013). On the other hand, the large size of the endonuclease is a major disadvantage, restricting some in vivo applications. Other Cas9 orthologues, including SaCas9, are smaller in size but require more restrictive PAMs (Komor, Badran, & Liu, 2017).

Comparing the efficiency of different Cas nucleases in engineering mammalian genomes appears to be difficult due to differences in target size, cellular context and protein expression levels of performed studies. It is therefore necessary to validate and optimize experimental designs to achieve the best result.

To date, Bruton's tyrosine kinase (BTK), known for its role in B-cell receptor signalling, has not been targeted using the CRISPR/Cas system. The CRISPR/Cas system was chosen as the preferred method over other genome editing technologies due to its simplicity and efficiency. Comparing CRISPR/Cas with RNA interference to disrupt gene expression, CRISPR/Cas seems to be more consistent and robust and allows to completely block protein expression, eliminating low level protein expressions that can remain using RNA interference (Gilbert et al., 2014; Gilbert et al., 2013). We therefore aimed to establish and validate a CRISPR/Cas strategy to knock-out BTK but also generate a cysteine to serine mutation in BTK at position 481 via "knock-in". The mutation appears in some patients treated with the BTK inhibitor ibrutinib and causes a secondary resistance. Establishing a strategy to knock out BTK and create the BTK^{C481S} mutation will allow us to analyse the role of the protein but also the effects of the mutation in different cellular contexts.

3.2 Establishing a CRISPR-based BTK^{C481S} knock-in strategy

3.2.1 Design of BTK^{C481S} knock-in guides, HDR template and genotyping primers

The BTK gene, located on the X chromosome, consists of 19 exons (659 amino acids) with the Cys481 residing in exon 15. To mutate C481 we designed 5 different guides targeting exon 15. The guides recognize a specific DNA sequence and direct the Cas9 endonuclease to this location for binding and cleavage. The cDNA sequence for *BTK* was obtained from the NCBI Unigene database (https://www.ncbi.nlm.nih.gov/unigene) and guides were designed using the CRISPR design tool at the Broad Institute (https://portals.broadinstitute.org/gpp/public/analysis-tools/sgrna-design). Guide sequences and their binding location can be found in Figure 3.1. All guides are immediately 5' to the *Streptococcus pyogenes* Cas9 (SpCas9) PAM sequence 5' NGG 3' (highlighted in red). Guides were chosen both for their proximity to the target site C481 and low off-target score according to the Broad Institute tool. The PAM sequence serves as a Cas9 binding site and the double-strand break (DSB) will occur 3 nucleotides 5' to the PAM site.

Figure 3.1 Schematic of guides targeting exon 15 of BTK

5 different guides targeting exon 15 of BTK were designed using the CRISPR design tool at the Broad institute. All guides are immediately adjacent to the SpCas9 PAM sequence 5' NGG 3'. The PAM sequences are highlighted in red.

A Cas9-induced DSB is either repaired by non-homologous end joining (NHEJ) or homology directed repair (HDR). The NHEJ repair mechanism is prone to error and often results in insertion or deletion (indels) of bases. The HDR mechanism is more accurate and occurs when a homologous piece of DNA is present to act as a template. The HDR pathway can therefore be utilized to create specific insertions or modifications into the genome.

For the homology directed repair of the Cas9-introduced double strand break a 111 bp single-stranded oligodeoxynucleotide (ssODN), containing the desired mutations, was synthesised and used as a template. The template was designed by changing bases of the BTK wild type sequence leading to a change in the amino acid at position 481 from Cysteine to Serine (Figure 3.2). We also introduced a number of silent mutations in the HDR template that would disrupt the SpCas9 PAM sequence and therefore prevent further editing once a successful knock-in has occurred. Because single base changes are difficult to detect the introduction of these additional silent mutations also allowed us to screen for a knock-in via PCR.

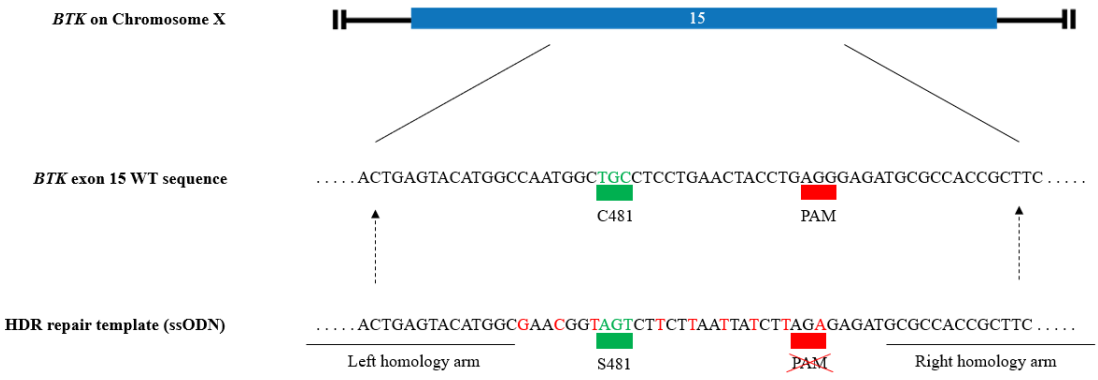

Figure 3.2 BTK^{C481S} knock-in HDR template design

A ssODN containing silent mutations as well as necessary base changes to change the amino acid at position 481 of BTK from Cysteine to Serine was designed as a HDR template. Silent mutations are highlighted in red showing the destruction of the 5' NGG 3' PAM sequence.

To genotype cells for a successful knock-in of the designed HDR template, PCR genotyping primers were designed and checked for specificity using the NCBI Blast algorithm. Figure 3.3 shows the primer binding location and expected PCR product sizes. Primers ex15F and ex15R span exon 15 and are outside of the targeted region giving an 884 bp product for wild type (WT) as well as mutated cells. MutF and mutR are 481S specific primers and do not bind to the WT sequence. Using these primers in combination with primers ex15F and ex15R will result in a 588 bp or 315 bp product only when the HDR template was successfully knocked in.

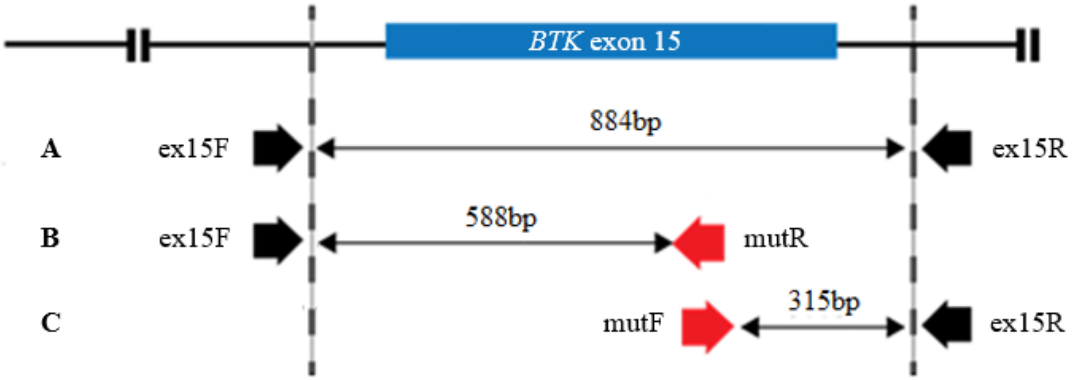

Primer pair	ex15F/ex15R (**A**)	ex15F/mutR (**B**)	mutF/ex15R (**C**)
PCR product size	884bp	588bp	315bp

Figure 3.3 BTK^{C481S} genotyping primer design

2 primers flanking exon 15 (ex15F, ex15R) as well as 2 BTK^{481S} mutant specific primers (mutF, mutR) were designed using the NCBI Blast algorithm and used for genotyping.

3.2.2 BTK^{C481S} knock-in using pX459 and a ssODN repair template

To validate the gene targeting efficiency of the guides designed in 3.2.1, all 5 guide sequences were cloned individually into the SpCas9 endonuclease and tracrRNA-expressing plasmid pX459. This plasmid contains a puromycin selection marker and the SpCas9 endonuclease is under the control of a chicken β-actin (Cbh) promoter. The guide oligonucleotides were phosphorylated using T4 Polynucleotide Kinase, annealed and ligated into the plasmid digested with BbsI. Following transformation and colony screening for correctly inserted clones, plasmids were extracted and sequenced before being used for transfections.

HEK-293T cells were then transfected with the pX459 plasmids containing the different guides as well as with the ssODN serving as an HDR template for the Cas9-induced DSB. Genomic DNA was isolated 48 h post transfection and a genotyping PCR was performed using the primers shown in Figure 3.3. The PCR reaction was separated on a 1% agarose gel and compared to the expected product sizes.

Figure 3.4 top panel shows the predicted agarose gel of PCR products expected from cells containing the BTK^{C481S} mutation. Figure 3.4 bottom panel shows the results in untransfected (first 3 lanes on the left) and transfected HEK-293T cells. As predicted the exon-spanning primer set A gives an 884 bp product in all cells acting as a control for the genotyping PCR. The 588 bp and 315 bp products only occur in transfected cells as primer pairs B and C contain mutation-specific primers. This result confirmed that all 5 guides tested are able to target exon 15 of BTK and that the HDR template was successfully incorporated into some cells to enable detection via PCR.

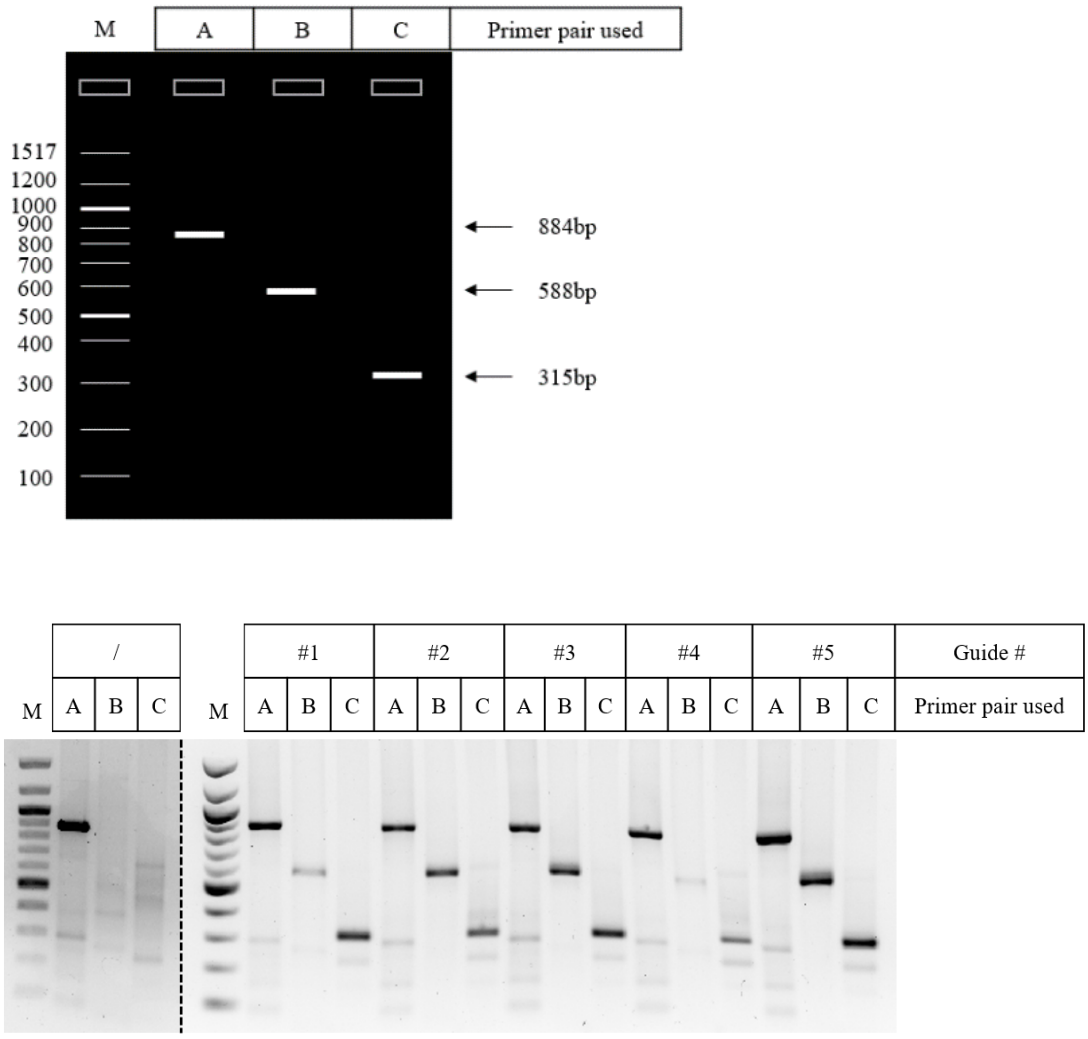

Figure 3.4 Validation of HDR using pX459-SpCas9 and a ssODN BTK^{C481S} HDR template

HEK-293T cells were transfected for 48 h with the SpCas9 and guide expressing plasmid pX459 together with a ssODN HDR template to generate the BTK^{C481S} mutation. Genomic DNA was isolated from untransfected and transfected cells and a genotyping PCR was performed using an exon 15 spanning primer set (A) as well as mutation-specific primers (B and C).

3.2.3 sgRNA delivery as in vitro transcripts

The two CRISPR components, Cas9 endonuclease and small guide RNA (sgRNA), can be delivered into cells in various formats. The sgRNA can be delivered either via a plasmid under the control of an RNA polymerase III promoter as described in 3.2.2 or as in vitro- transcribed/synthetic RNA. sgRNA delivery as RNA has two advantages over plasmid delivery. The first is the higher transfection efficiency of small RNA molecules in some cell lines. The second advantage is that RNAs are short-lived meaning that they get degraded quickly and therefore will not be passed on to daughter cells. This reduces the risk of unwanted mutations due to off-target binding of the guides.

For in vitro transcription the sgRNA was amplified from the pX459 plasmid using a forward primer containing of a T7 promoter fused to the guide sequence and a reverse primer which binds to the sgRNA backbone and contains the Polymerase III stop signal (TTTT). The resulting PCR product has the sgRNA sequence fused to a T7 promoter which can then be transcribed to RNA using a T7 RNA polymerase.

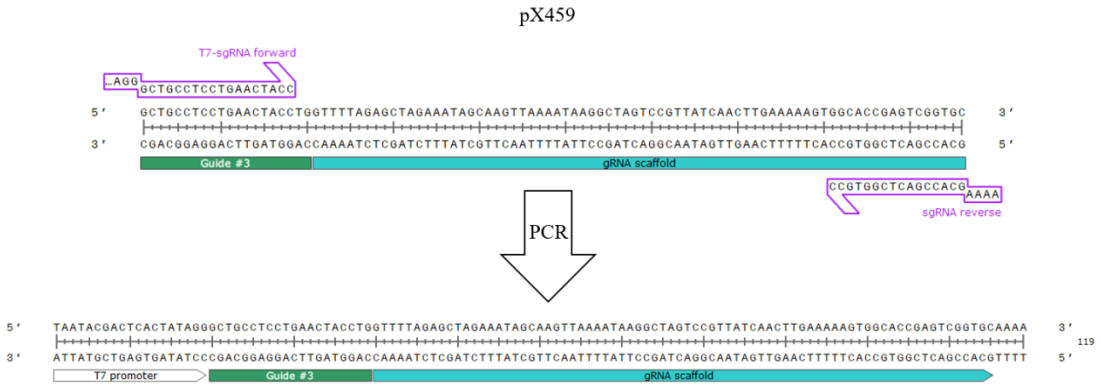

Figure 3.5 Schematic of sgRNA amplification

Plasmid pX459 containing the 5 different guides targeting exon 15 of BTK was used as a template to amplify the sgRNA. A T7 promoter was added 5' to the guide sequence to allow for in vitro RNA transcription.

The amplified PCR product was purified using the Wizard SV Gel and PCR clean-up system and the DNA was used as a template for in vitro sgRNA synthesis using a T7 RNA Polymerase. After RNA purification and quantification by Nanodrop, a small amount of the sgRNA was separated on a 1% agarose gel to ensure the PCR had worked and was of the correct size.

To supply cells with the Cas9 endonuclease, empty pX459 was then transfected into HEK-293T cells together with the ssODN HDR template and the 5 different transcribed sgRNAs. Genomic DNA was isolated 48 h post transfection and a genotyping PCR was performed using the primers shown in Figure 3.3. The PCR reaction was separated on a 1% agarose gel and compared to the expected products from the predicted agarose gel (Figure 3.4 top panel). Delivery of all 5 sgRNAs as in vitro transcripts as well as their ability to mutate the C481 residue together with the HDR template was successful as determined by a 588 bp and 315 bp product in transfected cells when using mutation-specific primers (B,C).

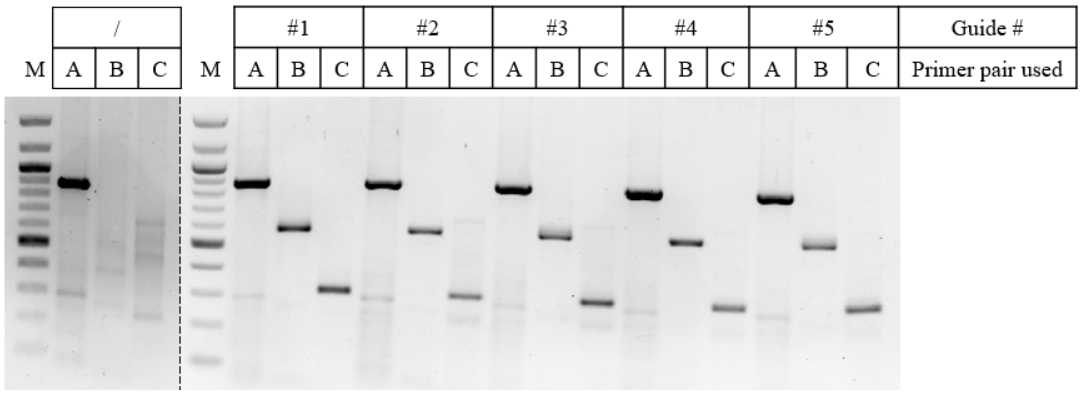

Figure 3.6 Validation of HDR to generate BTK^{C481S} knock-in cells using in vitro transcribed sgRNAs

HEK-293T cells were transfected with the SpCas9 expressing plasmid pX459, a ssODN HDR template and in vitro transcribed sgRNAs to generate the *BTK*^{C481S} mutation. Genomic DNA was isolated from untransfected (first 3 lanes on the left) and transfected cells and a genotyping PCR was performed using exon 15 spanning primers (A) as well as mutation-specific primers (B and C).

3.2.4 Exploring the use of Staphylococcus aureus Cas9 (SaCas9) to generate BTK^{C481S} knock-in cells

Though SpCas9 is the most commonly used CRISPR endonuclease it may not be the best for all applications mainly due to its size. Over 20 Cas9 orthologs have been isolated from other species so far and these orthologs may have characteristics that make them more suitable for certain applications. Cas9 from *Staphylococcus aureus* for example requires a more restrictive PAM sequence 5' NGGRRT/NGRRN '3 but is around 1 kb smaller than SpCas9. The smaller size enables efficient packaging into adeno-associated virus (AAV) which have limitations on their packaging capacity. As viruses are commonly used as a delivery system for hard to transfect cells such as AML cell lines, we wanted to explore the possibility of using SaCas9 to generate the BTK^{C481S} mutation.

SaCas9 requires a different PAM sequence and tracrRNA than SpCas9 and therefore we had to design new guide oligonucleotides targeting exon 15. The SaCas9 PAM sequence 5' NGGRRT '3 is more restrictive and only appeared once within exon 15 of BTK and therefore we only designed one guide sequence (Figure 3.7).

Figure 3.7 Schematic of SaCas9 guide targeting exon 15 of BTK

Guide targeting exon 15 of BTK was designed using the CRISPR design tool at the Broad institute. The guide sequence is immediately adjacent to the SaCas9 PAM 5' NGGRRT 3' (highlighted in red).

The guide was then cloned into the SaCas9-containing plasmid pX601which contains a puromycin selection marker with SaCas9 expression under the control of a cytomegalovirus (CMV) promoter. The guide was phosphorylated using T4 Polynucleotide Kinase, annealed and ligated into the plasmid digested with BsaI. Following transformation and plasmid extraction, the plasmid was sequenced before being used for transfections. HEK-293T cells were then transfected with the SaCas9 expressing plasmid pX601 containing the guide sequence together with the ssODN serving as an HDR template. Genomic DNA was isolated 48 h post transfection and a genotyping PCR performed using the primers shown in Figure 3.3. The PCR reaction was separated on a 1% agarose gel and compared to the expected products from the simulated agarose gel (Figure 3.8 left panel).

As seen in Figure 3.8 (right panel) the SaCas9 and designed guide are able to target exon 15 of BTK. The mutations were successfully introduced as determined by the 588 bp and 315 bp products in the transfected cells when using mutation-specific primers (primer pair B and C).

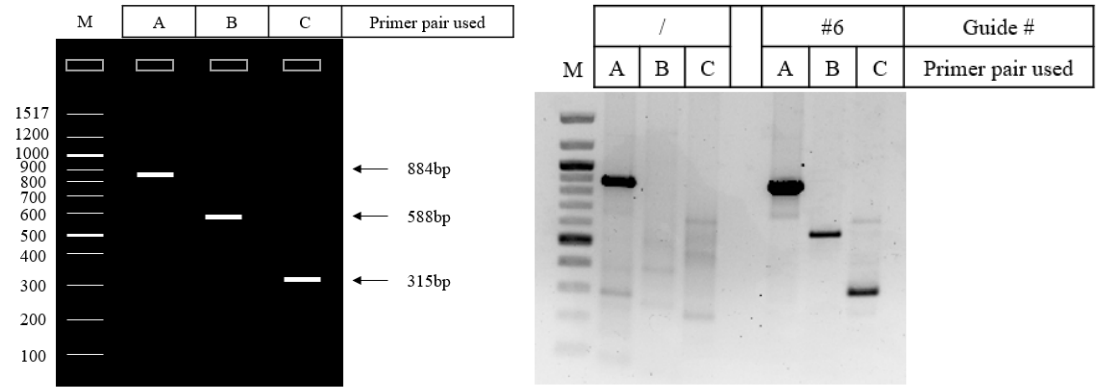

Figure 3.8 BTK^{C481S} HDR template knock-in using SaCas9 and a ssODN HDR template

HEK-293T cells were transfected with the SaCas9 expressing adenoviral plasmid pX601 and ssODN HDR template to generate the BTK^{C481S} mutation. Genomic DNA was isolated, and a genotyping PCR was performed using exon 15 spanning primers (A) as well as mutant specific primers (B and C).

3.2.5 Generation of an HDR template for delivery using lentivirus

The efficiency of polymer and liposome-based transfection reagents is very low in haematopoietic cells. Given that the efficiency of CRISPR-mediated HDR is also extremely low we had to utilise a more efficient transfection method for the AML cell lines. A 3rd generation lentiviral system was therefore chosen for delivery of the CRISPR components. Thus far, the guides are cloned in the same plasmid as the Cas9 endonuclease or delivered as in vitro transcripts with a Cas9-containing plasmid and the HDR template delivered separately as a ssODN. To deliver these components using lentivirus we required a system where the guide and HDR template are located within the same plasmid to ensure packaging together in the virus. Having the Cas9 nuclease in the same plasmid would cause issues with packaging and it would be more efficient if it was already stably integrated into the cells.

A plasmid, pLeGO, was obtained from Addgene and modified, removing the Eu enhancer and replacing it with a multiple cloning site (LH MCS). A second multiple cloning site was added downstream of the WPRE element (RH MCS). These modifications would allow us to clone the HDR template and the guide RNA cassette (U6 promoter and tracrRNA) into the LH-MCS. The plasmid also encodes EGFP under the control of an SFFV promoter enabling us to monitor and select transfected cells using a cell sorter.

The previously designed HDR template contains the necessary base changes to mutate the amino acid at position 481 from Cysteine to Serine but requires longer homology arms for use in plasmid form than needed for a ssODN delivery. To generate a bigger dsODN HDR template we amplified two overlapping regions from genomic DNA by PCR using the ssODN HDR template as primer to introduce the required mutations, a BTK exon 15 primer as well as two outside primers containing restriction sides (EcoRI and NheI) for plasmid cloning. The primer sequences and the binding sites are shown in Figure 3.9.

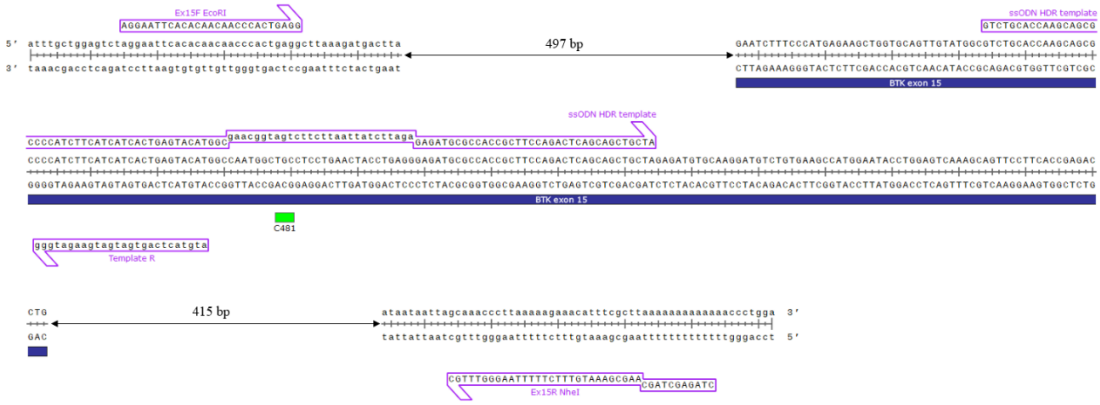

Figure 3.9 Primer design to generate a plasmid-based BTK^{C481S} HDR template

Two primers spanning exon 15, the previously designed ssODN HDR template and a primer binding to exon 15 were used to amplify two products with an overlapping sequence of 44 bp. Ex15F EcoRI and Ex15R NheI primers contain 5' restriction sites enabling cloning of the amplified PCR products.

The two amplified overlapping PCR products were gel extracted, mixed together and denatured for 10 min at 95°C. The sample was slowly cooled down, allowing the DNA to re-anneal and then subjected to overlap PCR. This resulted in the fusion of the two products to form the full-length HDR template which could then be cloned into a plasmid for delivery. The two amplified PCR products as well as the annealed product are shown in Figure 3.10.

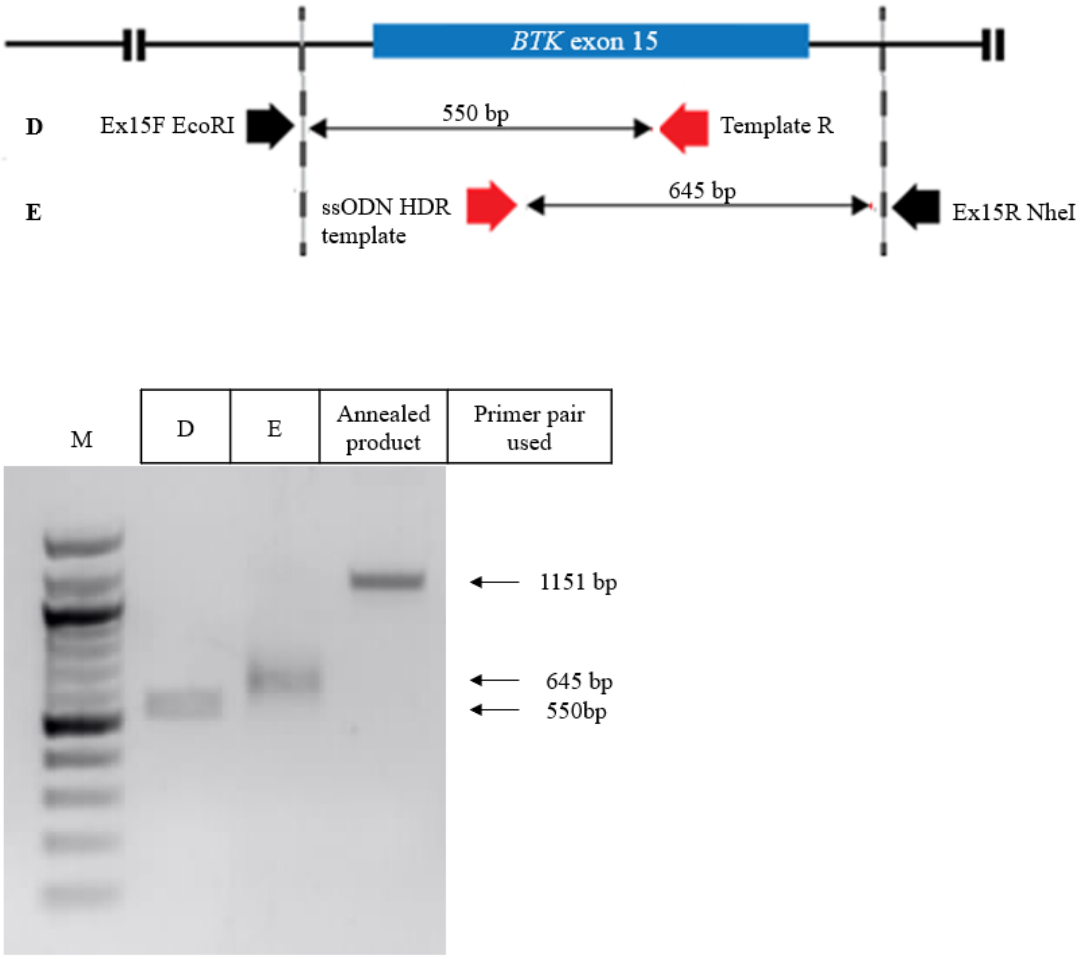

Figure 3.10 Overlap PCR for amplification of a plasmid-based BTK^{C481S} HDR template

To generate a dsODN HDR template, primers amplifying exon 15 and its surrounding sequence were used, adding restriction sites as well as inserting the C481S mutation. The two overlapping amplified products D and E were denatured and re-annealed resulting in one DNA fragment (dsODN HDR template).

3.2.6 Validating the BTK^{C481S} knock-in strategy using lentiviral constructs in HEK-293T cells

The annealed 1151 bp product described in the previous section was used as a dsODN HDR template that could be delivered via plasmid. The dsODN was digested with EcoRI and NheI for cloning into the modified lentiviral plasmid pLeGO. Modified pLeGO contains an ampicillin resistance and an enhanced green fluorescent protein (EGFP) cassette flanked by two multiple cloning sites (MCS).

All 5 previously tested SpCas9 guides were efficient in targeting exon 15 of BTK however, we decided to only clone one guide (guide #3) into the left-hand MCS in pLeGO together with the HDR template. Guide #3 was chosen due to its close location to the target site, its efficiency and because the designed HDR template destroys the PAM for guide#3 once successfully inserted, preventing further editing to occur. pLeGO containing the HDR template as well as guide #3 was sequenced before being used for experiments.

For SpCas9 endonuclease delivery we tested two different lentiviral plasmids: a modified lentiCRISPR v2 plasmid and pCW-Cas9. LentiCRISPR v2 contains a puromycin selection marker and SpCas9 endonuclease expression is under the control of a spleen focus forming virus (SFFV) promoter. pCW-Cas9 contains a puromycin selection marker and SpCas9 endonuclease expression is under the control of the doxycycline-inducible Tet ON promoter.

The modified pLeGO plasmid containing the HDR template and guide #3 was transfected with either lentiCRISPR v2 or pCW-Cas9 into HEK-293T cells. Transfection efficiency was checked 24 h post transfection under the microscope.

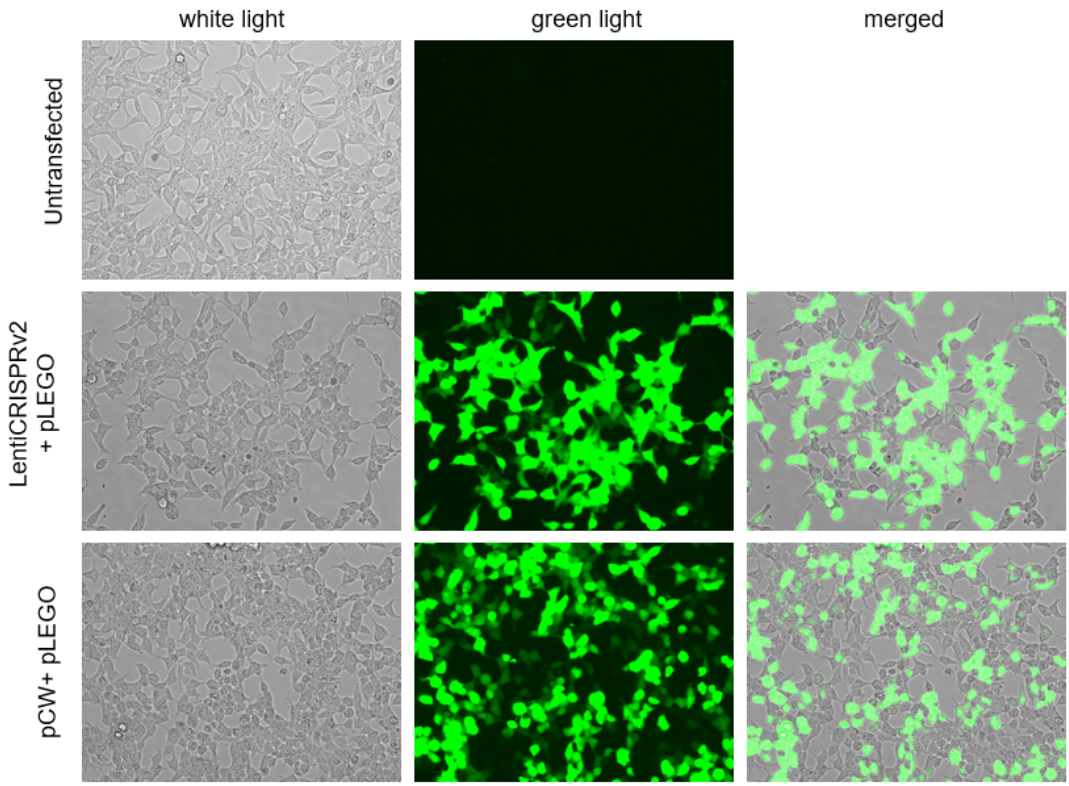

Figure 3.11 Reporter EGFP expression in pLeGO transfected HEK-293T cells
HEK-293T cells were transfected with the SpCas9 expressing plasmid lentiCRISPR v2 or pCW-Cas9 and the EGFP expressing plasmid pLeGO containing the guide targeting exon 15 of BTK and the HDR template. Transfection efficiency was analysed 24 h post transfection by examining EGFP positive cells.

As seen in Figure 3.11, HEK-293T cells transfected with the lentiviral plasmid pLeGO express EGFP with no expression detected in untransfected cells.

SpCas9 endonuclease expression is under the control of a Tet ON promoter in the pCW-Cas9 plasmid. To induce SpCas9 expression in pCW-Cas9 transfected cells we added 4 µg/mL Doxycycline 24 h post transfection. Untransfected and transfected cells were harvested 48 h post transfection and genomic DNA as well as proteins extracted. A Western blot was performed to determine SpCas9 and β-Actin protein expression.

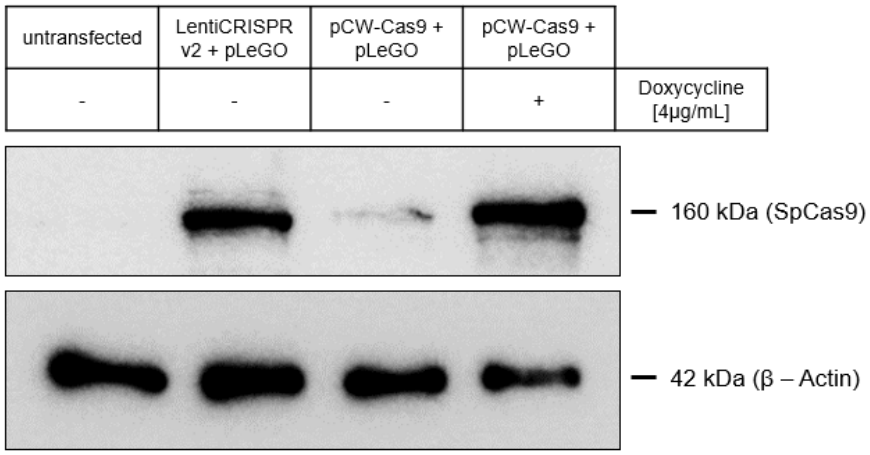

Figure 3.12 SpCas9 expression in lentiCRISPR v2 and pCW-Cas9 transfected HEK-293T cells

Cells were transfected with SpCas9 expressing plasmids lentiCRISPR v2 and pCW-Cas9. In pCW-Cas9 transfected cells, SpCas9 expression was induced by the addition of 4 µg/mL doxycycline. SpCas9 and β-Actin expression was determined 48 h post transfection.

The western blot results show that cells transfected with either lentiCRISPR v2 or pCW-Cas9 express the SpCas9 endonuclease. A weak SpCas9 expression was seen in cells transfected with pCW-Cas9 before the addition of doxycycline but higher protein levels were observed after the induction by doxycycline.

To check for a successful knock-in of the HDR template, genomic DNA was isolated from transfected cells and used for genotyping. Due to the extended homology arms, which were necessary to present the HDR template in a plasmid, a new genotyping reverse primer (Ex15R2) was designed to screen for a knock-in. Ex15R2 binds outside of the extended HDR template to confirm that the HDR template was inserted at the correct location within the gene. Using the newly designed reverse primer ex15R2 in combination with the previously designed forward primer ex15F will amplify a 1244 bp product in wild type as well as BTK^{C481S} mutant cells. Using these two primers in combination with the 481S mutant specific primers mutF and mutR will only amplify a 678 bp and 588 bp product when the HDR template was successfully knocked in.

Amplified PCR products from untransfected and transfected cells were separated on a 1% agarose gel and compared to the predicted agarose gel shown in Figure 3.13 (bottom left panel). All three predicted products were seen in transfected cells but as expected only one product was seen in untransfected cells as the mutant specific primers (mutF and mutR) do not bind to the wild type BTK sequence (Figure 3.13 bottom right panel).

These results showed that both SpCas9 expressing lentiviral plasmids are functional and that delivery of the HDR template via plasmid was successful. All lentiviral constructs tested could therefore be used to produce lentiviral particles to introduce the BTK^{C481S} mutation in AML cell lines.

Primer pair	ex15F/ex15R2 (**F**)	mutF/ex15R2 (**G**)	ex15F/mutR (**B**)
PCR product size	1244 bp	678 bp	588 bp

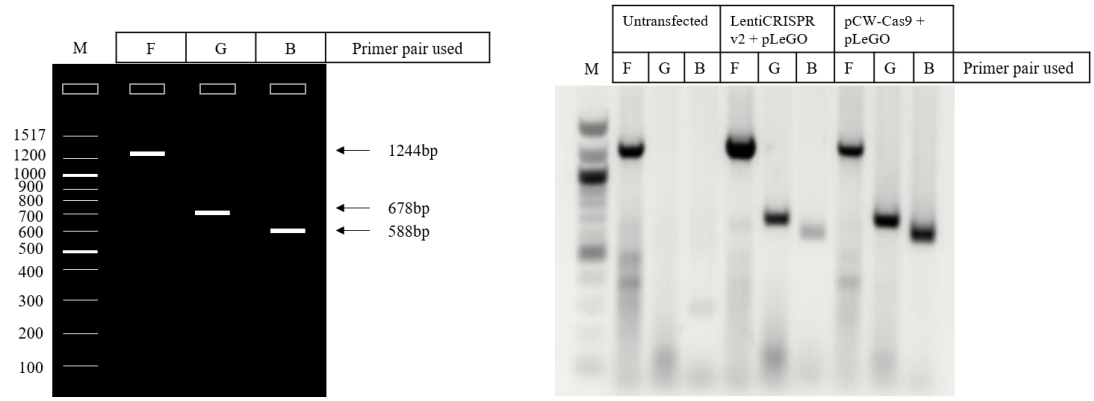

Figure 3.13 BTK^{C481S} HDR template knock-in using lentiviral constructs

HEK-293T cells were transfected with the stable SpCas9 expressing plasmid lentiCRISPR v2 or the inducible SpCas9 expressing plasmid pCW-Cas9 followed by transfection with the guide #3 and HDR template expressing plasmid pLeGO. Genomic DNA was isolated, and a genotyping PCR was performed using exon 15 spanning primers (F) as well as mutant specific primers (G and B).

3.3 Establishing a CRISPR-based BTK knock-out strategy

3.3.1 SpCas9 and Cas12a guide design to target exon 2 and exon 3 of BTK

Besides generating and validating a strategy to knock-in BTK^{C481S} we also wanted to design a BTK knock-out strategy to further study the role of BTK in AML.

As mentioned previously, over 20 Cas9 orthologs have been characterized thus far. It has previously been shown that using multiple guides to knock-out genes is an effective strategy. The Cas9 ortholog AsCas12a which is derived from the *Acidaminococcus sp BV3L6*, is a class 2/type V CRISPR/Cas DNA endonuclease that has several advantages over SpCas9, particularly when it comes to multiplexing guides. AsCas12a recognizes a 5' TTTV 3' PAM sequence and creates a staggered overhang ~20 nt downstream of the protospacer sequence. Cleaving further away from the PAM sequence can prevent the PAM sequence from being destroyed during the NHEJ repair process allowing further editing to occur. Additionally, whilst SpCas9 requires a crRNA and tracrRNA, AsCas12a only requires a crRNA as it processes its own pre-crRNA arrays. Multiplexing guides therefore becomes easier as only one promoter is needed to drive expression. Due to the smaller size of the AsCas12a, multiple guides can be cloned in the same plasmid as the endonuclease, therefore avoiding co-transfections of multiple plasmids which can lead to a lower transfection efficiency and is difficult when using lentivirus.

To establish a BTK knock-out strategy we designed SpCas9 as well as AsCas12a guides using the CRISPR design tool at the Broad institute (https://portals.broadinstitute.org/gpp/public/analysis-tools/sgrna-design) or the design tool at Benchling (https://benchling.com/). Translation of the BTK transcript starts at the ATG site within exon 2. We therefore designed 6 guides targeting exon 2 (2 SpCas9 guides, 4 AsCas12a guides) and 2 additional SpCas9 guides targeting exon 3. The guides and their target binding location can be found in Figure 3.14. SpCas9 and AsCas12a PAM sequences are highlighted in red.

Figure 3.14 Schematic of guides targeting exon 2 and 3 of BTK

6 different guides targeting exon 2 of BTK and 2 guides targeting exon 3 of BTK were designed using the CRISPR design tool at the Broad institute. SpCas9 guides are immediately adjacent to the SpCas9 PAM sequence 5' NGG 3' and AsCas12a guides are immediately 3' of the 5' TTTV 3' AsCas12a PAM sequence. The PAM sequences are highlighted in red.

We also designed 2 primer pairs which would amplify either exon 2 or exon 3 or exon 2-3 when used in combination to screen for successful gene editing following transfection with the endonucleases and guides. The primer pairs and their predicted amplified product sizes are shown in the figure on the next page (Figure 3.15).

Primer pair	ex2F/ex2R (**H**)	ex3F/ex3R (**I**)	ex2F/ex3R (**J**)
PCR product size	596 bp	570 bp	1133 bp

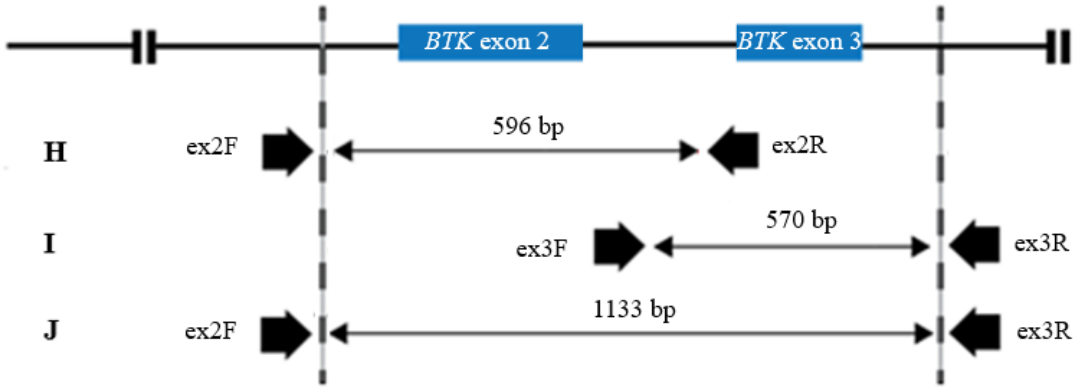

Figure 3.15 BTK exon 2 and 3 genotyping primer design

2 primers flanking exon 2 (ex2F, ex2R) as well as 2 primers flanking exon 3 (ex3F, ex3R) were designed using the NCBI Blast algorithm and used for genotyping.

3.3.2 Determining guide targeting efficiency using the T7 endonuclease I DNA mismatch assay

When a Cas9-induced double strand break (DSB) is repaired through non-homologous end joining (NHEJ) it often leads to small insertions and deletions (indels) which will lead to gene disruption. These indels are too small to be resolved on an agarose gel but can be detected via T7 endonuclease I (T7EI) assay.

Guides designed in 3.14 were either cloned in the previously described lentiviral plasmid lentiCRISPR v2 or in the lentiviral plasmid pY108. pY108 expresses AsCas12a, has a puromycin selection marker and AsCas12a expression is under the control of a CMV promoter. Plasmids containing the guides were then transfected as singles or doubles in HEK-293T cells.

Genomic DNA was isolated 48 h post transfection and the genotyping PCR used as a template for a T7EI assay. After digestion with T7EI, PCR products were separated on a polyacrylamide gel and compared to undigested products for additional bands.

All guides tested were able to target exons 2 or 3 of BTK. Expected cut products and their sizes are shown in Figure 3.16 and were compared to the products seen on the polyacrylamide gels.

Guide#	#7	#8	#7+8	Cas12a #1	Cas12a #2	Cas12a #3	Cas12a #4
PCR product size	596 bp	596 bp	596 bp, 521 bp	596 bp	596 bp	596 bp	596 bp
Expected cut size	102 bp, 494 bp	178 bp, 418 bp		67 bp, 529 bp	57 bp, 539 bp	139 bp, 457 bp	199 bp, 397 bp

Guide #	#9	#10	#9+10
PCR product size	570 bp	570 bp	570 bp, 538 bp
Expected cut size	263 bp, 307 bp	231 bp, 339 bp	

A

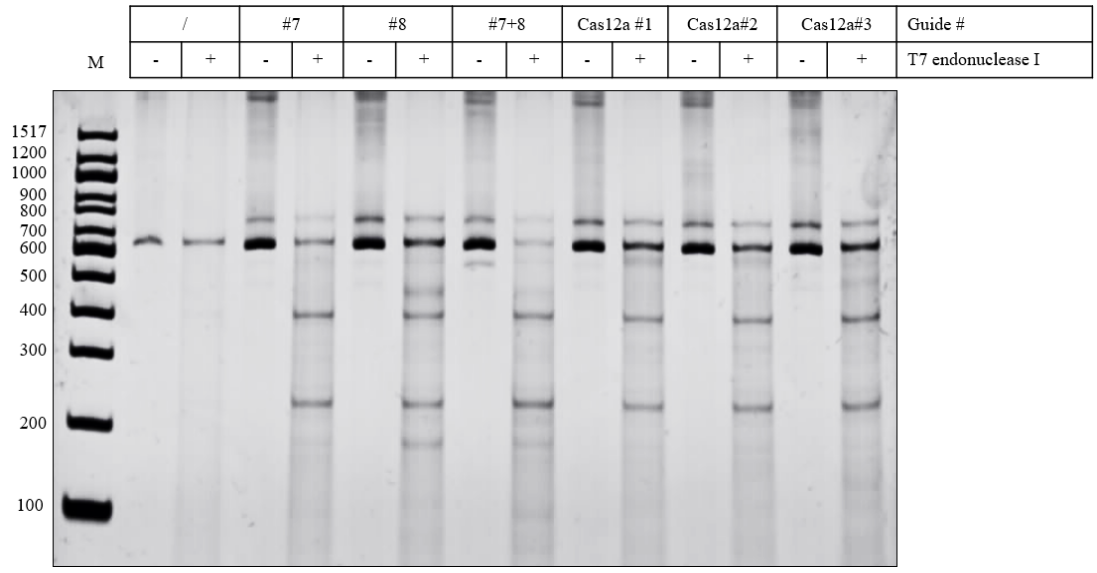

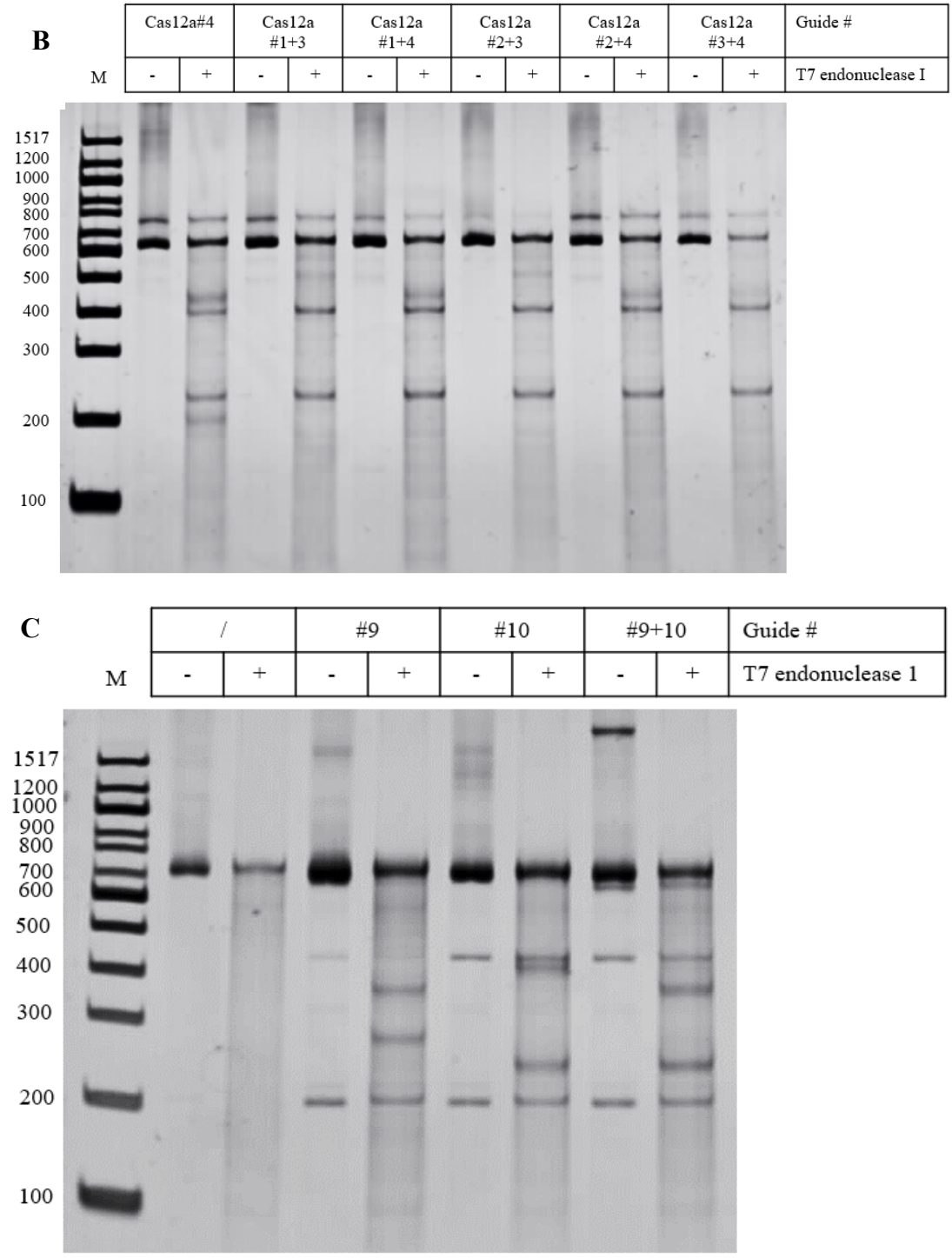

Figure 3.16 T7 endonuclease assay for exon 2 and 3 of BTK

Gene editing of Exon 2 and 3 was confirmed by T7 endonuclease assay after HEK-293 cells were transfected with either one guide or a combination of 2 guides. **A** and **B** show DNA PAGE gel results for guides used to target exon 2 of BTK and **C** shows the result for guides used to target exon 3. Cleaved fragments can be seen for all guides tested after the incubation with T7 endonuclease compared to uncleaved products in samples without incubation of T7 endonuclease.

3.3.3 Guide multiplexing to knock-out BTK in HEK-293T cells

Gene targeting using a single guide to generate a knock-out often results in small indels that are difficult to resolve from a non-modified locus and therefore additional assays such as the T7E1 have to be performed to assess editing efficiency. By using multiple guides, targeting the same gene can result in bigger deletions when the sequences between two induced DSBs are removed (Figure 3.17). Larger deletions can then easily be detected on an agarose gel after amplification of the targeted region. We therefore used multiple guides and picked guides #7+8 targeting exon 2 as well as guides #9+10 targeting exon 3 of BTK to generate BTK knock-out cells. Though multiplexing is easier with Cas12a the required PAM sequence was absent in exon 3 of BTK and we had to use SpCas9.

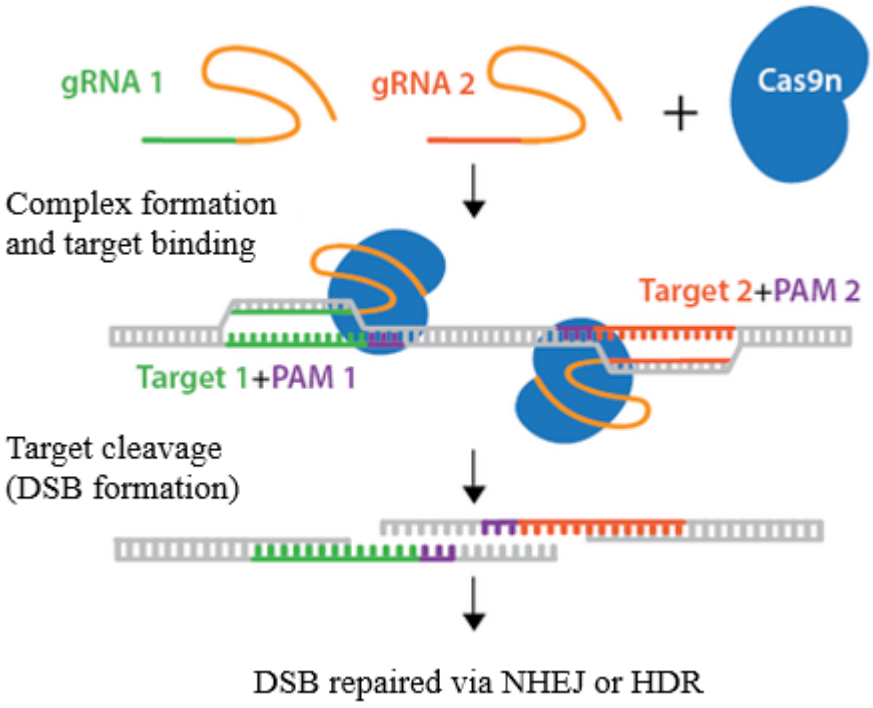

Figure 3.17 Guide multiplexing to knock-out genes

Schematic showing multiple guides targeting the same gene resulting in a big deletion when the sequence between the induced DSBs is removed therefore enhancing the knock-out efficiency and allowing for an easy screen via PCR.

Adapted from Addgene.org/CRISPR/guide/

To avoid large expression constructs by cloning the guides into the SpCas9-containing plasmid, we cloned the 4 selected guides into a modified form of pLeGO which has had multiple cloning sites added 5' and 3' to the EGFP selection cassette.

HEK-293T cells were then transfected with the SpCas9 expressing plasmid lentiCRISPR v2 as well as the guide expressing plasmid pLeGO. Genomic DNA was isolated 48 h post transfection and used as a template for a genotyping PCR. Exon 2, exon 3 and exon 2-3 were amplified using DNA from untransfected as well as transfected cells and separated on a 1% agarose gel. Additional smaller PCR products were detected in transfected cells (highlighted on the agarose gel in figure 3.18). These smaller products appear because of deletions within the amplified region showing that gene editing in exon 2 as well as exon 3 has occurred.

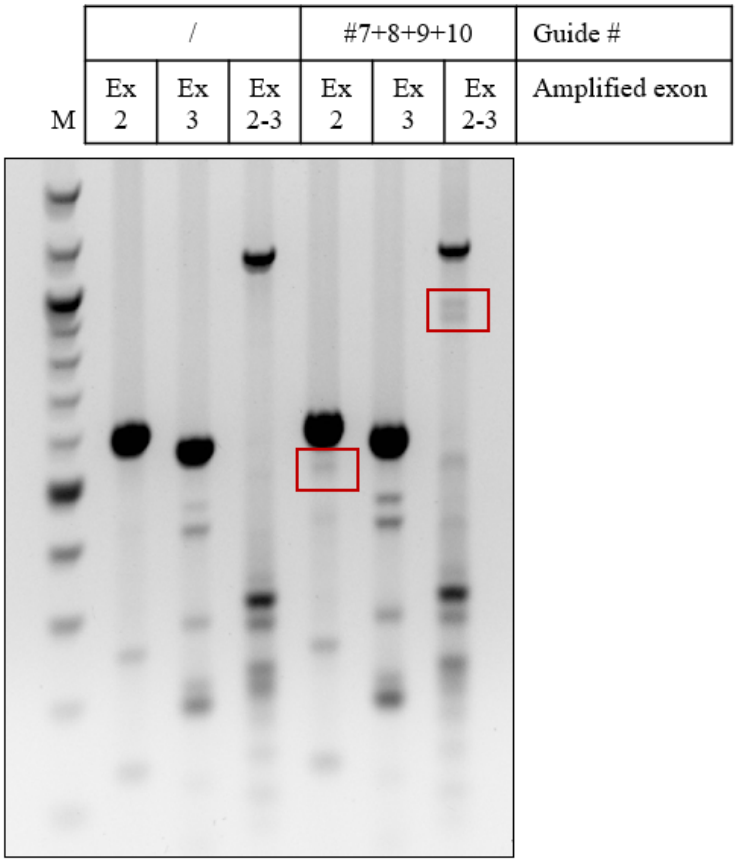

Figure 3.18 Validating BTK exon 2 and 3 multiplex editing efficiency

Cells were transfected with 4 guides targeting Exon 2 and 3 (2 guides targeting each exon). DNA was isolated 12 h post transfection. Exon 2, exon 3 and exon 2-3 were amplified via PCR followed by separation on an agarose gel.

3.3.4 Determining BTK knock-out efficiency in HEK-293T cells using Western Blot

Besides determining the BTK gene targeting efficiency on a genomic level we also wanted to assess BTK knock-out efficiency on the protein level. As HEK-293T cells do not express BTK we instead used cells transfected with a BTK expressing plasmid. A spleen cDNA library was used as a template to amplify the BTK gene. Restriction sites were included at the 5' site of designed primers to allow cloning into pcDNA6.1 Hygro. The plasmid was sequenced before being used for transfections to ensure it contains the correct sequence of the BTK cDNA.

HEK-293T cells were then transfected with either the BTK expressing plasmid pcDNA6 and lentiCRISPR v2 alone or in combination with the guide expressing plasmid pLeGO. Proteins were extracted 48 h post transfection and Cas9, BTK and β-Actin expression levels were determined via Western blot. As seen in Figure 3.19 cells transfected with the pcDNA6-BTK plasmid express BTK. A reduction in BTK protein level was seen in cells transfected with the guides targeting exon 2 and 3 of BTK indicating that using these 4 guides in combination is an efficient strategy to knock-out BTK.

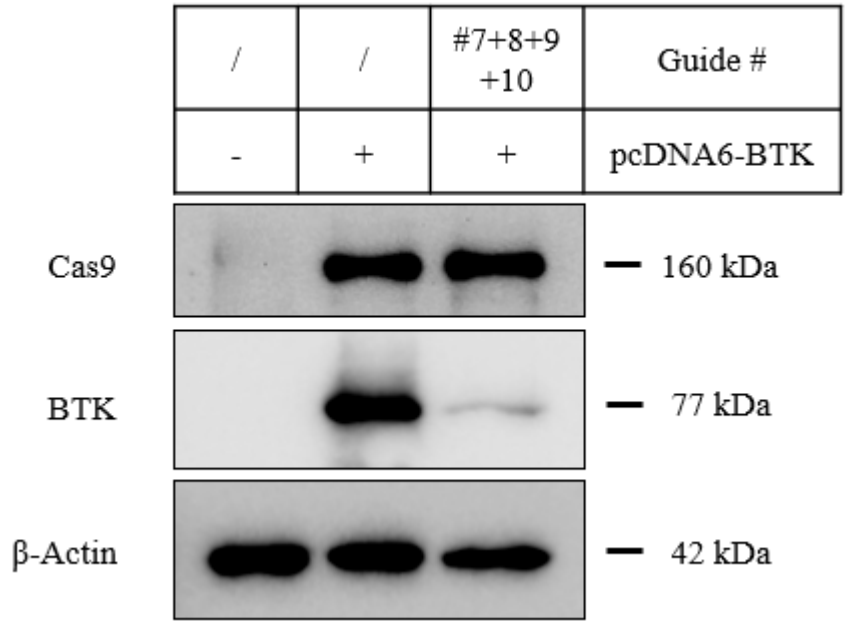

Figure 3.19 Validating BTK knock-down efficiency via Western blot

Cells were transfected with 4 guides targeting exon 2 and 3 (2 guides targeting each exon) and a BTK expressing plasmid (pcDNA6-BTK). Proteins were isolated 48 h post transfection and Cas9, BTK and β-Actin protein expression was determined by Western blot.

3.4 Discussion

The aim of this chapter was to establish and validate a CRISPR-based knock-out and knock-in strategy in HEK-293T cells targeting BTK. As the efficacy of the CRISPR/Cas system is influenced by several factors we aimed to address a few of those factors such as guide design, different Cas nucleases and delivery systems to establish a well working strategy that could be applied to other cell lines. HEK-293T cells were chosen for validation purposes due to their high transfectability.

For the BTK^{C481S} knock-in, overall 6 guides targeting exon 15 of BTK and an HDR template containing the desired mutations that we wanted to introduce, were designed. 5 of these guides were designed for the use with SpCas9 and one of these guides was designed for the use with the smaller SaCas9. The several identified Cas9 orthologues all have their own advantages and disadvantages but their use is often limited by the required PAM site in the target gene. Whilst this is less of a problem when generating knock-outs, the requirement of a PAM in close proximity to a specific target sequence, when generating knock-ins, often rules the use of Cas nucleases with more difficult PAMs, that appear less frequent within the genome, out. Hence, only one guide could be designed for SaCas9 with its required 5' NNGRRT PAM site whilst 5 guides could be designed for SpCas9 with the frequently appearing 5' NGG PAM site. All 6 guides tested were able to target exon 15 of BTK and the C481S mutation was successfully introduced as determined by genotyping PCR (Figure 3.4 and Figure 3.8).

It was shown that editing efficiency decreases with increasing cut-to-mutation distance (Paquet et al., 2016). For homozygous introductions, designed guides should therefore be as close as possible to the intended mutation. This means that in our case SpCas9 guides # 1,2,3 and 5 are expected to be most efficient and SpCas9 guide #4 and SaCas9 guide #6 are least efficient. Guide efficiency could be tested in future experiments by selecting positively transfected cells and performing a quantitative PCR.

The HDR template used to introduce the C481S mutation in BTK was designed as a 111 bp ssODN with a 47 bp left homology arm and a 36 bp right homology arm. The 28 bp between the homology arms were modified to change the bases TGC, coding for cysteine, to AGT, coding for serine, at position 481. Additional silent mutations were added around the 481 target site to allow an initial screen for a successful introduction by PCR using mutation specific primers before performing sequencing. Adding silent mutations is also recommended to destroy the PAM site or target sequence and therefore prevent CRISPR/Cas cutting after HDR-mediated editing has occurred. The silent mutations added in our HDR template destroy the PAM site for SpCas9 guides # 1,2,3 and 5 but not for guide # 4 and SaCas9 guide # 6.

The design of the ssODN template is crucial for the knock-in efficiency and is mainly affected by homology arm length, homology arm symmetry and chemical modifications. A homology arm length between 30 and 50 nucleotides gives optimal knock-in efficiency (John A. Schiel, 2015) and using asymmetric arms for unmodified templates shows a slightly higher efficiency compared to symmetric arms (Richardson, Ray, DeWitt, Curie, & Corn, 2016) whilst the use of symmetric arms is recommended for phosphorothioate-modified DNA templates giving a higher knock-in efficiency than using unmodified templates (Renaud et al., 2016). Seeing that we used an unmodified ssODN template with asymmetric arms, knock-in efficiency could be improved with a modified template and symmetric arms.

The method of delivery of the CRISPR/Cas system is still the major problem for its use. We therefore tested different delivery systems and strategies of the Cas9 nuclease, the guide and the HDR template aiming to find the most suitable method for delivery in AML cell lines.

In general, there are three different strategies to edit genes using the CRISPR/Cas system. The first strategy is a plasmid-based CRISPR/Cas system, the second is delivery of Cas9 mRNA and sgRNA and the third is delivery of Cas9 protein and

sgRNA (C. Liu, Zhang, Liu, & Cheng, 2017). Here we only tested the plasmid-based CRISPR/Cas system using non-viral and viral plasmids as well as delivery of the sgRNA as in vitro transcribed RNA.

Our first strategy was to deliver the SpCas9 and the guide in a non-viral plasmid (pX459) and the HDR template separately as a ssODN. The major advantage of non-viral plasmids is its bio-safety but reduced pathogenicity, cheap and easy production are also advantages. Disadvantages are a low transfection efficiency and insufficient cellular uptake in some cell lines. As HEK-293T cells, in comparison to AML cell lines, are highly transfectable, this first strategy was mainly to validate the designed guides and HDR template.

Transfecting cells with in vitro transcribed sgRNA rather than plasmid expressed sgRNA has a higher efficiency in some cell lines and reduces the risk of unwanted indels due to the short life of small RNA molecules. This delivery strategy worked well as shown in Figure 3.6 but and can be improved by combining sgRNA delivery with Cas9 mRNA or Cas9 proteins to give a completely DNA free option. Synthesizing the sgRNA adds the advantage of avoiding time consuming steps like cloning, sequencing and in vitro transcription. The disadvantage of using a plasmid free delivery is the missing selection marker and is therefore not recommended for hard to transfect cells or delivery methods that have a low transfection efficiency.

Using viral plasmids gives a good transfection efficiency in most cell lines but their use can be limited due to the restrictions on their packaging capacity. Cas9 variants like the SaCas9 (~3.2 kb) used in this chapter, St1Cas9 (~ 3.4 kb) or NmCas9 (~ 3.2 kb) are smaller than SpCas9 (~ 4.2 kb) and can help to overcome this problem (Murovec, Pirc, & Yang, 2017). Furthermore, some viral vectors including lentiviral vectors, allow packaging of bigger inserts without loss of packaging efficiency and

might therefore be more suitable than for example Adeno-associated viral vectors. Additionally, inserts can be packed in multiple plasmids to avoid big constructs.

To generate BTK knock-out cells we designed guides targeting exon 2 as well as exon 3 of BTK that we wanted to try as singles as well as doubles to increase the efficiency and make screening easier. Besides using SpCas9 we also wanted to test the efficiency of the Cas9 orthologue AsCas12a as it allows easy multiplexing of guides with only one promoter needed to drive expression. Designed guides for either Cas9 worked alone as well as in doubles as determined by T7E1 mismatch assay (Figure 3.16). The two doubles that seemed to have the highest efficiency (guide #7+8 and guide # 9+10) were chosen to knock-out BTK in HEK-293T cells after transfection with a BTK expressing plasmid. Using multiple guides, targeting the same gene, compared to using a single guide can result in bigger deletions. This has the advantage that larger deletions can then easily be detected by performing a standard PCR of the targeted region, avoiding the time-consuming T7E1 assay.

Choosing the right delivery method and strategy as well as Cas9 endonuclease depends a lot on the target cell line, the target sequence and the application. We have shown in this Chapter that for the generation of the C481S mutation as well as the BTK knock-out, SpCas9 is the preferred choice over SaCas9 and AsCas12a. Whilst SaCas9 has the advantage of a smaller size, it is not suitable for targeting Exon 15 of BTK due to the distance of the PAM to the mutation site. AsCas12a has the advantage of its easy use for multiplexing guides but is not suitable to knock-out BTK due to the absence of its required PAM site in Exon 3. The designed HDR template to generate the C481S mutation will destroy the PAM site of the chosen SpCas9 guide #3 once the template has successfully been introduced, preventing further editing to occur. Using lentiviral vectors will ensure a good transduction efficiency of the AML cell lines and the use of a separate SpCas9 expressing vector will allow us to generate Cas9 expressing cells

first and then use those cells for both, the generation of the C481S mutation as well as the BTK knock-out.

Chapter 4: Generating BTK^{C481S} mutant AML cell lines

4.1 Introduction

Acute myeloid leukaemia (AML) is a haematological malignancy resulting in an accumulation of immature leukaemic cells in the blood, bone marrow and organs, leading to leucocytosis and bone marrow failure (Grove & Vassiliou, 2014). Because of the diseases heterogeneity, AML is associated with a poor prognosis in general and treatment response as well as drug resistance and disease relapse varies making personalized therapeutic regimes even more important.

Targeted genome editing using CRISPR/Cas9 can be used to study molecular pathways of normal as well as cancer cells helping us to better understand and identify dysregulated pathways and therefore contributing to drug discovery and development. One of the major challenges of CRISPR/Cas9 genome editing in AML cell lines is the delivery of the 4.2 kb SpCas9 endonuclease as well as the hard to transfect nature of these cell lines.

Lentiviral vectors have the packaging capacity to deliver large inserts and have a good transduction efficiency and specificity to target AML cell lines. A disadvantage of using lentiviral vectors as delivery tool is the stable integration and expression of the transferred factors. It has been shown, both in vitro and in vivo, that CRISPR/Cas9 can induce mutations at sites that differ from the target site (Chew et al., 2016; Fu et al., 2013; Hsu et al., 2013). The number of these off-target modifications is affected by Cas9 expression with high expression levels correlating with increased off-site cleavage (Fu et al., 2013). To avoid persistent expression of the Cas9 endonuclease, an inducible promoter like the Tet-ON promoter can be used to control expression. Recently, a self-limiting SpCas9 circuit was developed that removes the nuclease from edited cells and can therefore prevent accumulation of off-target modifications (Petris et al., 2017).

Another option is the use of Integrase-defective lentiviral vectors (IDLVs) that contain either class I mutations, that lead to specific integration deficiencies, or class II mutations, that affect several stages of the viral life cycle but are not as suitable for vector development (Wiskerchen & Muesing, 1995). Most commonly introduced mutations are in the catalytic triad of the Integrase such as residue D64 mutations and result in the inactivation of the enzyme. Other mutations affect Integrase DNA binding or multimerization and linear episome processing. The use of IDLVs compared to lentiviral vectors has demonstrated transient expression with a low capacity to induce off-target mutations (Ortinski, O'Donovan, Dong, & Kantor, 2017).

In this Chapter we aimed to generate stable and inducible expressing SpCas9 MV4-11, THP-1, OCI-AML3, HL-60 and U937 cells using a lentiviral delivery system. Furthermore, we wanted to use the pLeGO construct, generated in the previous Chapter, containing the sgRNA and HDR template to induce the BTK^{C481S} mutation in those AML cell lines using a non-integrating lentiviral vector. We next wanted to derive a clonal population of cells containing the mutation for the functional characterization of the C481S mutation in AML cell lines.

The five AML cell lines used for experiments were chosen based on the availability in the lab as well as their differential sensitivity to ibrutinib. Previous studies have shown that FLT-3 ITD positive AML cell lines are more sensitive to ibrutinib than FLT-3 ITD negative cell lines explaining the different GI_{50} (μM) values of 0.33, 2.1, 8.5, >10 observed for MV4-11, HL-60, U937 and OCI-AML3 cell lines respectively (Wu et al., 2016).

4.2 BTK expression in AML cell lines

Prior to gene editing of BTK using CRISPR/Cas9 in the AML cell lines MV4-11, THP-1, OCI-AML3, HL-60 and U937 we wanted to ensure that those cell lines express BTK at a level that is detectable via Western blot. Proteins were extracted from all 5 AML cell lines and BTK, pBTK (Tyr223), and β-Actin expression was determined (Figure 4.1).

The 5 cell lines tested express BTK at similar levels and BTK appears to be active in these cells as shown by presence of a species when using the pBTK (Tyr223) antibody. Tyr223 is the autophosphorylation site within the BTK SH3 domain.

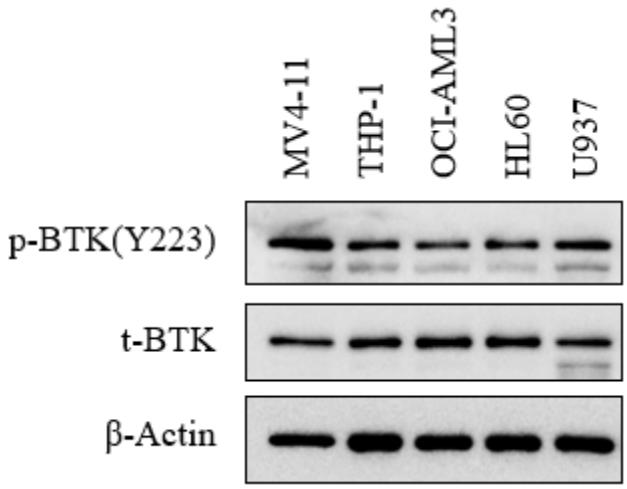

Figure 4.1 BTK expression in AML cell lines

Cell lysates from MV4-11, THP-1, OCI-AML3, HL60 and U937 cells were extracted and expression of pBTK (Tyr223), BTK and β-Actin was determined by Western blot.

As all 5 cell lines tested express the protein of interest, these cell lines are suitable to make stable and inducible SpCas9 expressing cells followed by generating the BTK^{C481S} mutation.

4.3 Generating stable and inducible SpCas9-expressing AML cell lines

4.3.1 Determination of Puromycin concentration for selection

A selectable marker is a common plasmid element that allows positive selection for cells that have taken up the plasmid which is particularly important for hard to transfect cell lines. The lentiCRISPR v2 and pCW-Cas9 plasmids both have a puromycin selection marker. We therefore needed to determine the puromycin concentration that would kill the untransfected cells ensuring that only cells that took up the plasmid survived the selection.

MV4-11, THP-1, OCI-AML3, HL-60 and U937 cells were seeded in a 6 well plate and incubated with puromycin concentrations ranging from 1-8 µg/mL. Cell viability was measured every 24 h over 4 days via flow cytometry using propidium iodide (PI) staining.

Based on the results from the puromycin kill curves (Figure 4.2) we decided to treat the cell lines MV4-11 and HL-60 with 2 µg/mL and the remaining cell lines (U937, THP-1 and OCI-AML3) with 4 µg/mL for 5 days for post transfection selection.

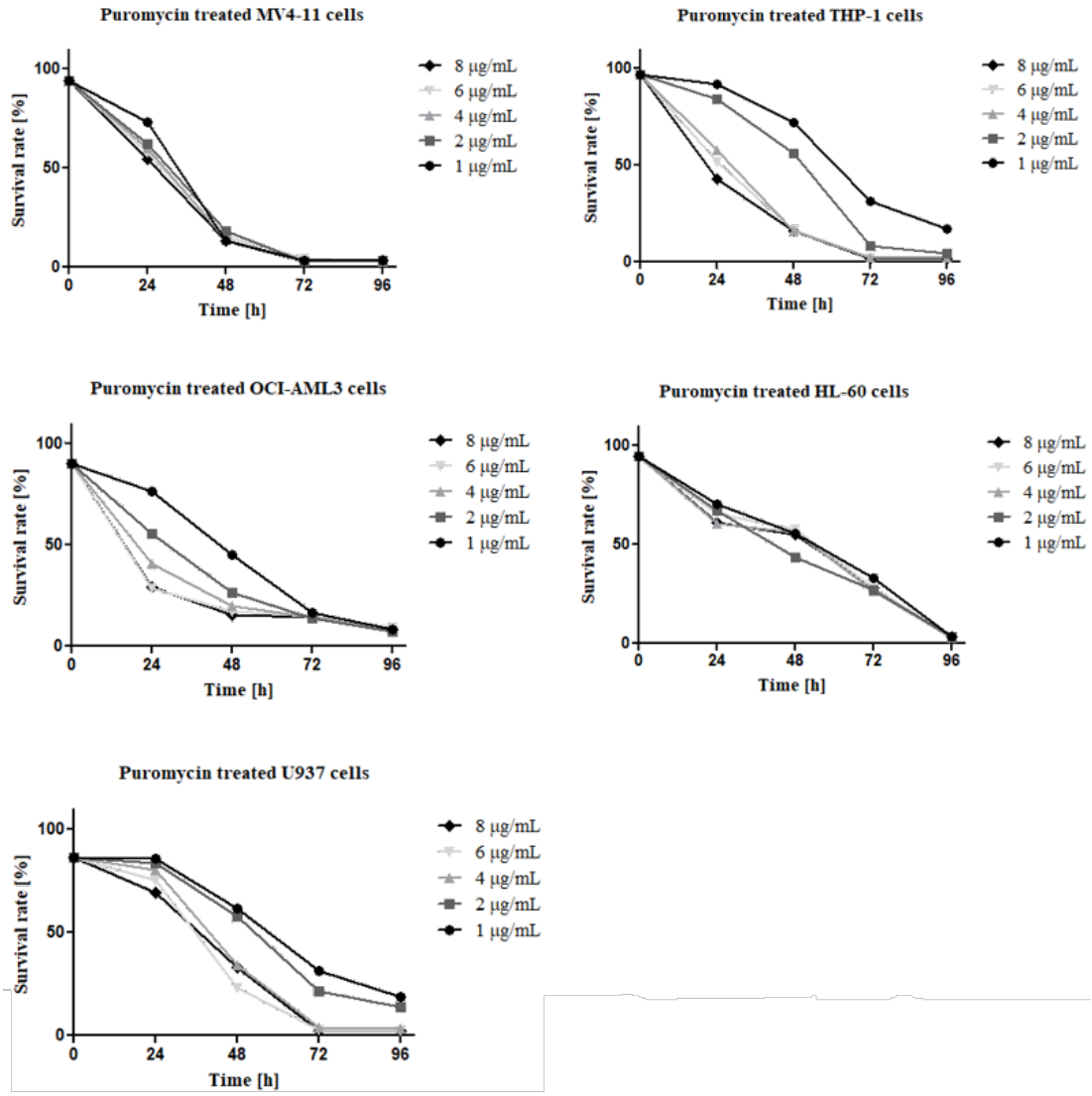

Figure 4.2 Puromycin titration in AML cell lines

MV4-11, THP-1, OCI-AML3, HL-60 and U937 cells were treated with puromycin concentrations ranging from 1 µg/mL up to 8 µg/mL. Cell viability was measured every 24 h over 4 days via flow cytometry using propidium iodide (PI) staining (n=1).

4.3.2 Stable and doxycycline inducible SpCas9 expression in AML cell lines

To generate stable and inducible SpCas9-expressing MV4-11, THP-1, OCI-AML3, HL-60 and U937 cells we used the lentiCRISPR v2 and pCW-Cas9 containing lentivirus. Cells were transduced with the lentiviral particles and positively transduced cells were selected with puromycin for 5 days using the concentrations determined previously. Cells were left to recover, post-selection, before proteins were extracted to determine Cas9 expression via Western blot.

For cells transduced with the inducible SpCas9-expressing plasmid (pCW-Cas9) we had to determine the optimal doxycycline concentration required to induce SpCas9 expression. Cells were treated for 24 h with doxycycline concentrations ranging from 2-8 μg/mL before proteins were extracted and analysed for Cas9 expression.

Western blot results showed that all AML cell lines transduced with either lentiCRISPR v2 or pCW-Cas9 containing virus express the SpCas9 protein (Figure 4.3). Weaker expression levels were seen in OCI-AML3 and HL-60 cells transduced with lentiCRISPR v2. Little difference in Cas9 expression was seen with pCW-Cas9 when using different doxycycline concentrations. Based on those results we decided to use 2 μg/mL of doxycycline to induce expression in U937 cells, 4 μg/mL for OCI-AML3 and MV4-11 cells and 6 μg/mL for HL-60 and THP-1 cells in future experiments.

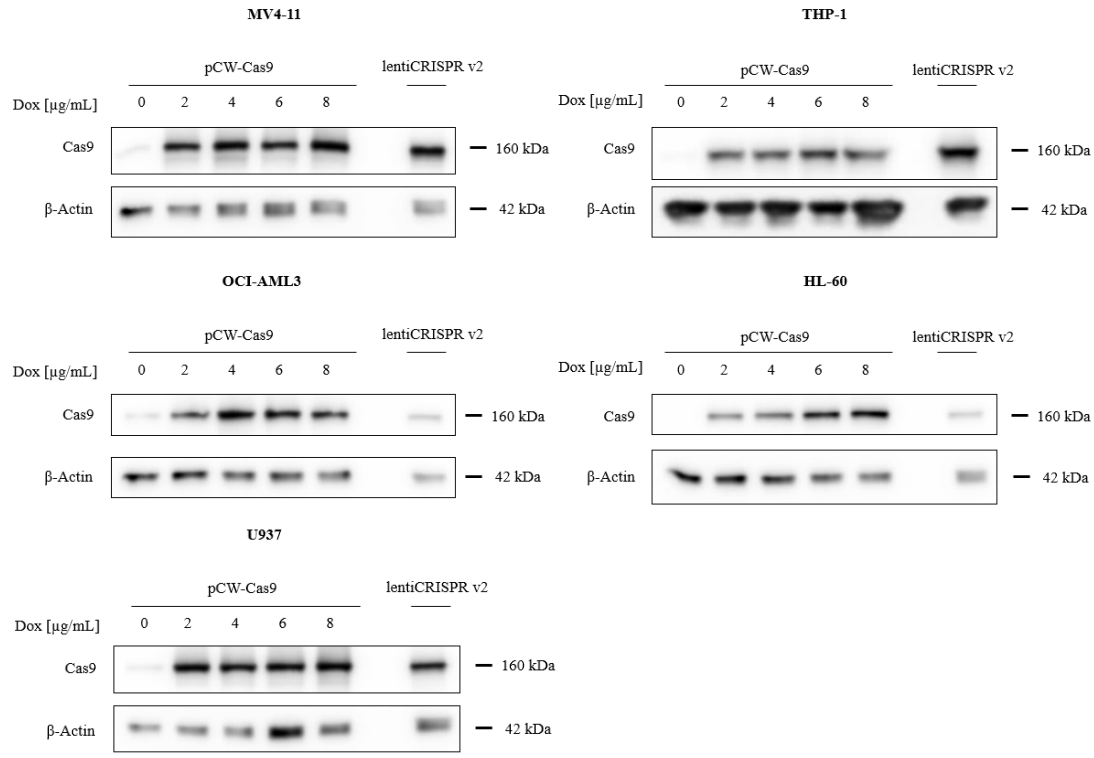

Figure 4.3 SpCas9 expression in AML cell lines

AML cells transduced with pCW-Cas9 were treated with 2-8 µg/mL doxycycline for 24 h whilst cells transduced with the stable SpCas9 expressing plasmid lentiCRISPR v2 were left untreated. Proteins were extracted and analysed for Cas9 and β-Actin expression (n=2, biological repeat).

4.4 BTK^{C481S} knock-in in AML cell lines

4.4.1 Determination of viral titre

Generating knock-ins using CRISPR/Cas9 by providing a template to repair a double strand break (DSB) through homology directed repair (HDR) is very inefficient. It is therefore very important to maximise the transduction efficiency of the cells by using high titre viral preps and a multiplicity of infection (MOI) rate that is suitable for the target cell line.

Viral titres can be distinguished by physical and functional means. Whilst physical titre assesses the amount of viral particles present in a sample, functional titre measures the expression of a gene carried by the transfer plasmid. The lentiviral plasmid we used for HDR template and guide delivery (pLeGO) carries a green fluorescent protein marker (EGFP). This allows us to measure the functional viral titre by Flow cytometry by analysing the percentage of EGFP positive cells post transduction.

HEK-293T cells were transduced with increasing amounts of the concentrated viral prep and EGFP expression was determined after 72 h (Figure 4.4).

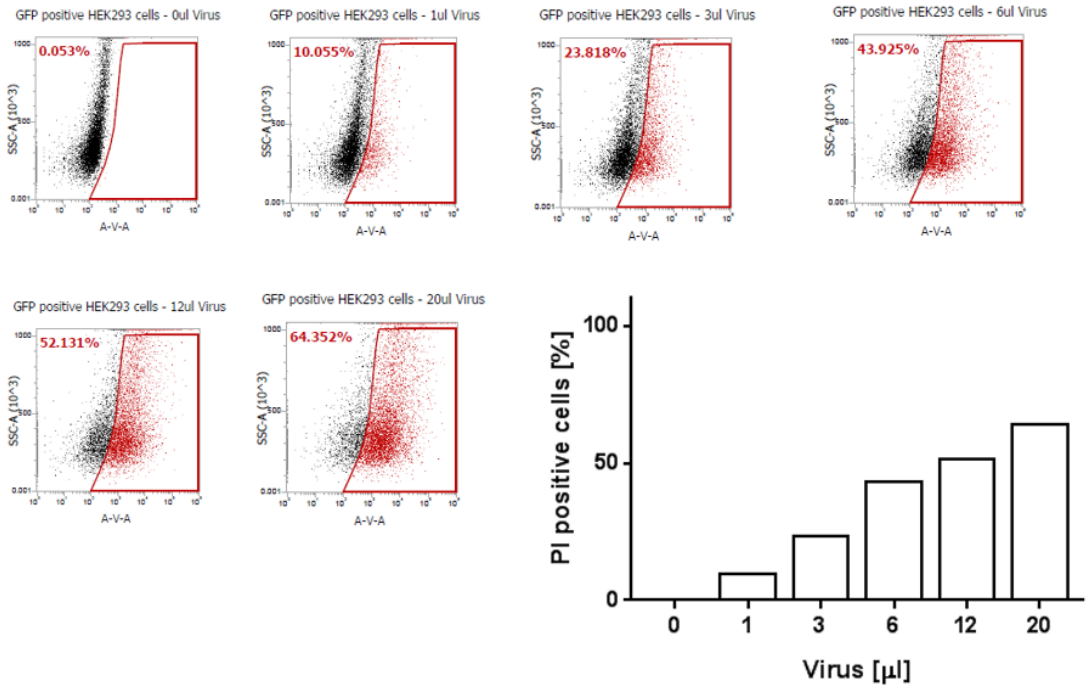

Figure 4.4 Viral titre determination in HEK-293T cells using Flow cytometry

HEK-293T cells were transduced with different amounts of concentrated viral preps ranging from 0-20 µL and subjected to flow cytometry analysis measuring the percentage of GFP positive cells indicating the percentage of positively transduced cells (n=1).

Viral titre was determined using the following formula :

$$\textbf{\textit{Viral titer}}\ [\textbf{\textit{TU/mL}}] = \frac{\textbf{\textit{number of seeded cells x GFP positive cells}}\ [\%]}{\textbf{\textit{Volume of virus}}\ [\textbf{\textit{mL}}]}$$

Volume of Virus [mL]	GFP positive cells [%]	Viral titre [TU/mL]
1 x 10^{-3}	10.055	4.022 x 10^{9}
3 x 10^{-3}	23.818	3.176 x 10^{9}
6 x 10^{-3}	43.925	2.928 x 10^{9}
12 x 10^{-3}	52.131	1.738 x 10^{9}
20 x 10^{-3}	64.352	1.287 x 10^{9}
	Mean:	**2.630 x 10^{9}**

Using a MOI of 10 and the median viral titre calculated above we calculated the amount of virus needed for transduction of AML cell lines as follows.

$$\boldsymbol{Volume\ of\ virus\ [mL] = \frac{MOI\ x\ number\ of\ seeded\ cells}{viral\ titre\ [TU/mL]}}$$

$$\boldsymbol{Volume\ of\ virus\ [mL] = \frac{10\ x\ 0.5\ x\ 10^{6}}{2.630\ x\ 10^{9}}}$$

$$\boldsymbol{Volume\ of\ virus\ [mL] = 0.0019}$$

$$\boldsymbol{Volume\ of\ virus\ [\mu L] = 1.9}$$

4.4.2 Flow-sorting of EGFP-expressing AML cells

To generate the BTK^{C481S} mutation in AML cell lines we used cells that were previously transduced with the inducible Cas9 expressing plasmid pCW-Cas9. We chose to use these cells over cells transduced with the stable Cas9 expressing plasmid lentiCRISPR v2 because two of the cell lines that were transduced with lentiCRISPR v2 only showed weak SpCas9 expression post selection. Another advantage of the inducible system is that the SpCas9 is not consistently expressed.

Cas9 expression was induced 24 h prior to transduction with the pLeGO viral preps containing the BTK^{481S} HDR template and exon 15 guide #3. Cells were transduced with the amount of viral prep calculated in 4.4.1 giving an MOI of 10 to ensure a good transduction efficiency. Cells were left to recover, post transduction, before being flow-sorted for EGFP expression. Sorting is required to select the positively transduced cells. Following sorting there was a significant enrichment of EGFP positive cells (Figure 4.5).

MV4-11 pre-sort

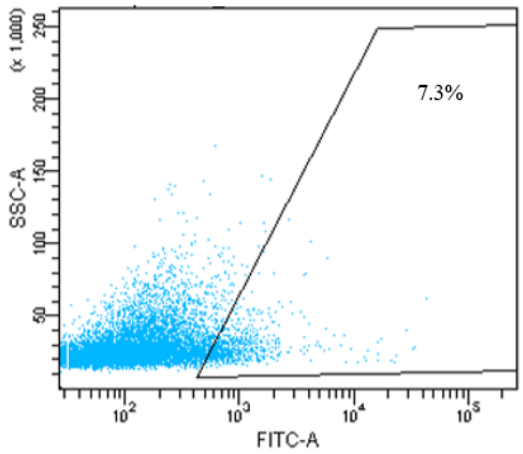

MV4-11 post-sort

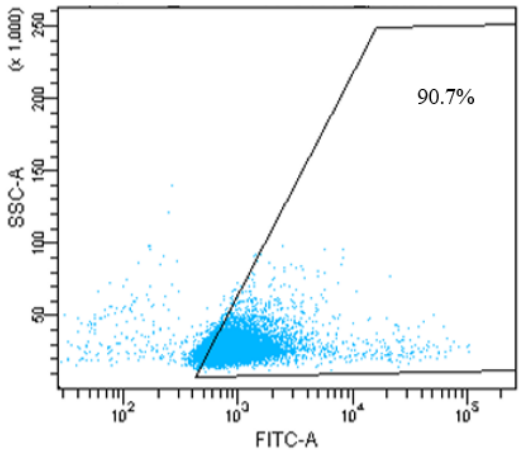

THP-1 pre-sort

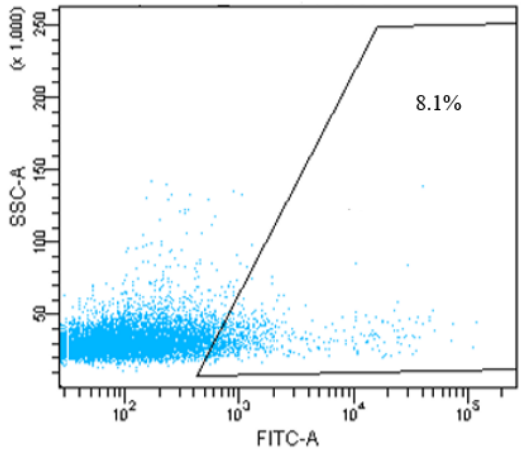

THP-1 post-sort

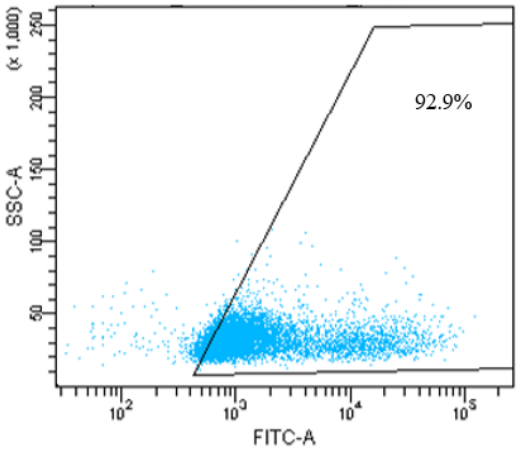

OCI-AML3 pre-sort

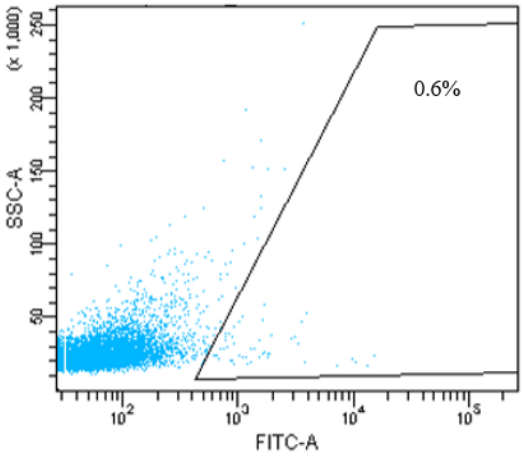

OCI-AML3 post-sort

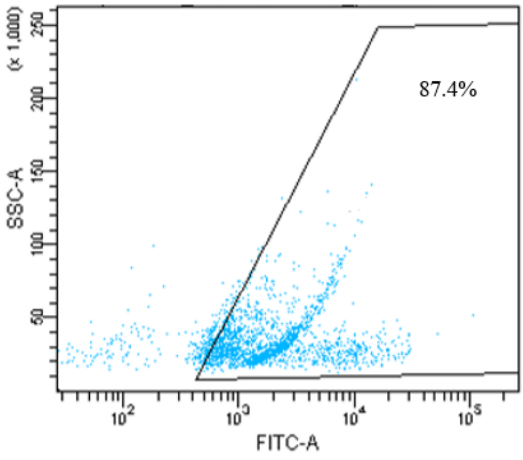

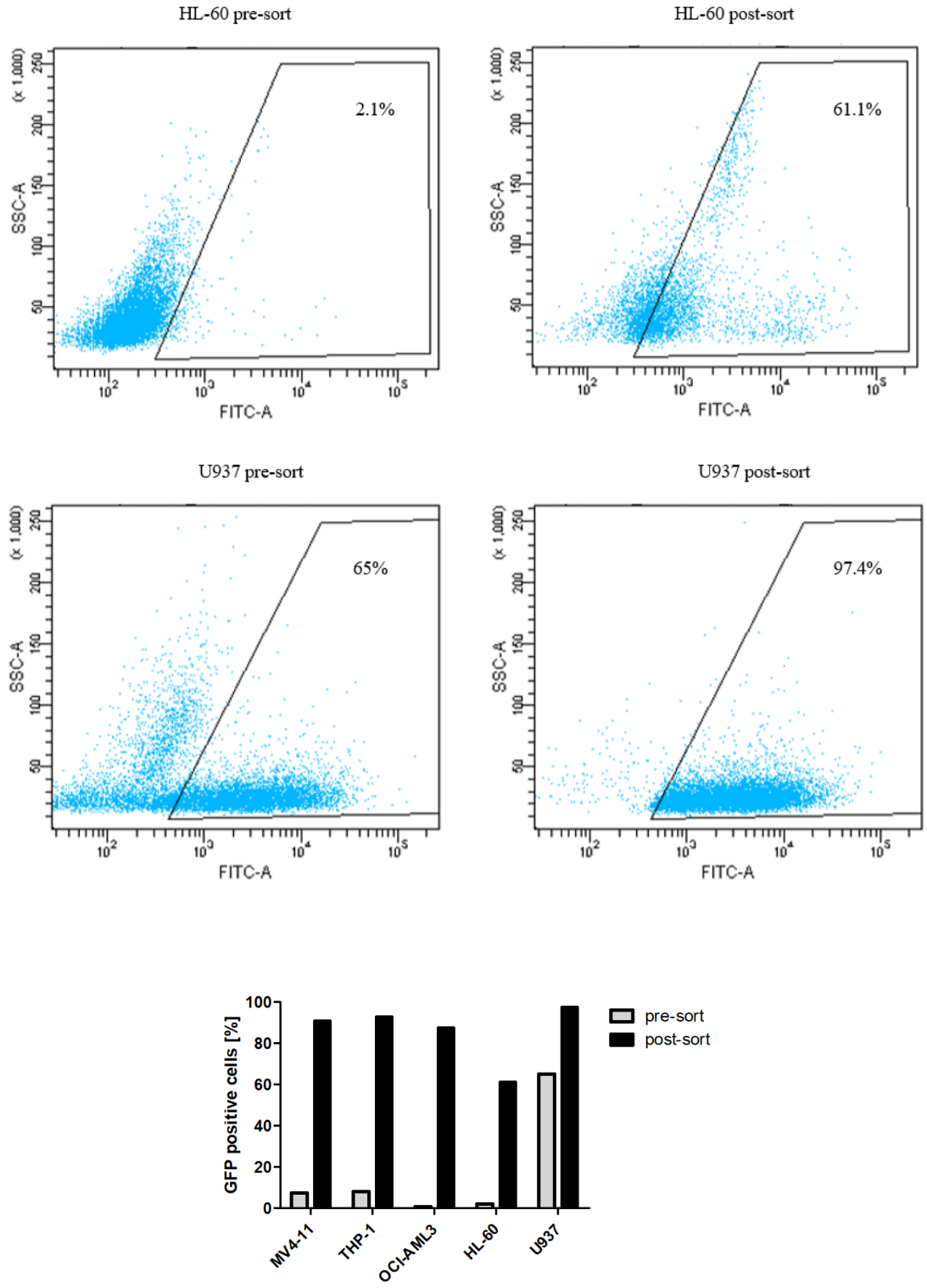

Figure 4.5 Flow sorting of EGFP-expressing AML cells

Following transduction with pLeGO containing the BTK^{481S} HDR template, exon 15 guide #3 and an EGFP selection marker, AML cell lines were flow sorted for EGFP expression. Dot plots show the percentage of GFP positive cells pre- and post-sort. The bar chart summarizes the sorting results (n=1).

HL-60 and OCI-AML3 cells had the lowest transduction efficiency and U937 the highest. The percentage of GFP positive cells post-sorting was similar between the different cell lines with HL-60 cells having the lowest percentage. Sorting only selects transduced cells, cells that have been successfully transduced with the HDR construct and EGFP selection marker, and therefore EGFP expression does not mean that these cells also contain the BTK^{C481S} mutation, but it increases the likelihood.

4.4.3 BTK^{C481S} genotyping in GFP flow-sorted cells

As shown in Figure 4.5 the sorted cell lines were not 100% pure as they still contained EGFP negative cells. As the knock-in efficiency using an HDR template is generally quite low we wanted to genotype the sorted cells to see if we were able to detect the BTK^{C481S} mutation via PCR before growing single cell clones.

Genomic DNA was isolated from AML cells pre- and post-sort and genotyping PCR was performed (Figure 4.6).

We could detect mutant-specific PCR products in THP-1, U937 and OCI-AML3 cells. Only a slight increase in the band intensity was seen in U937 cells comparing pre- and post-sort results. No mutant specific PCR products were detected in OCI-AML3 cells pre-sort, but mutant specific products were seen following sorting. We could also see an increase in the mutant specific PCR product band intensity in THP-1 cells post-sorting. No mutant specific PCR products were seen in MV4-11 cells post-sort. HL-60 cells were discarded post-sort due to a contamination and therefore only pre-sort results are shown for this cell line.

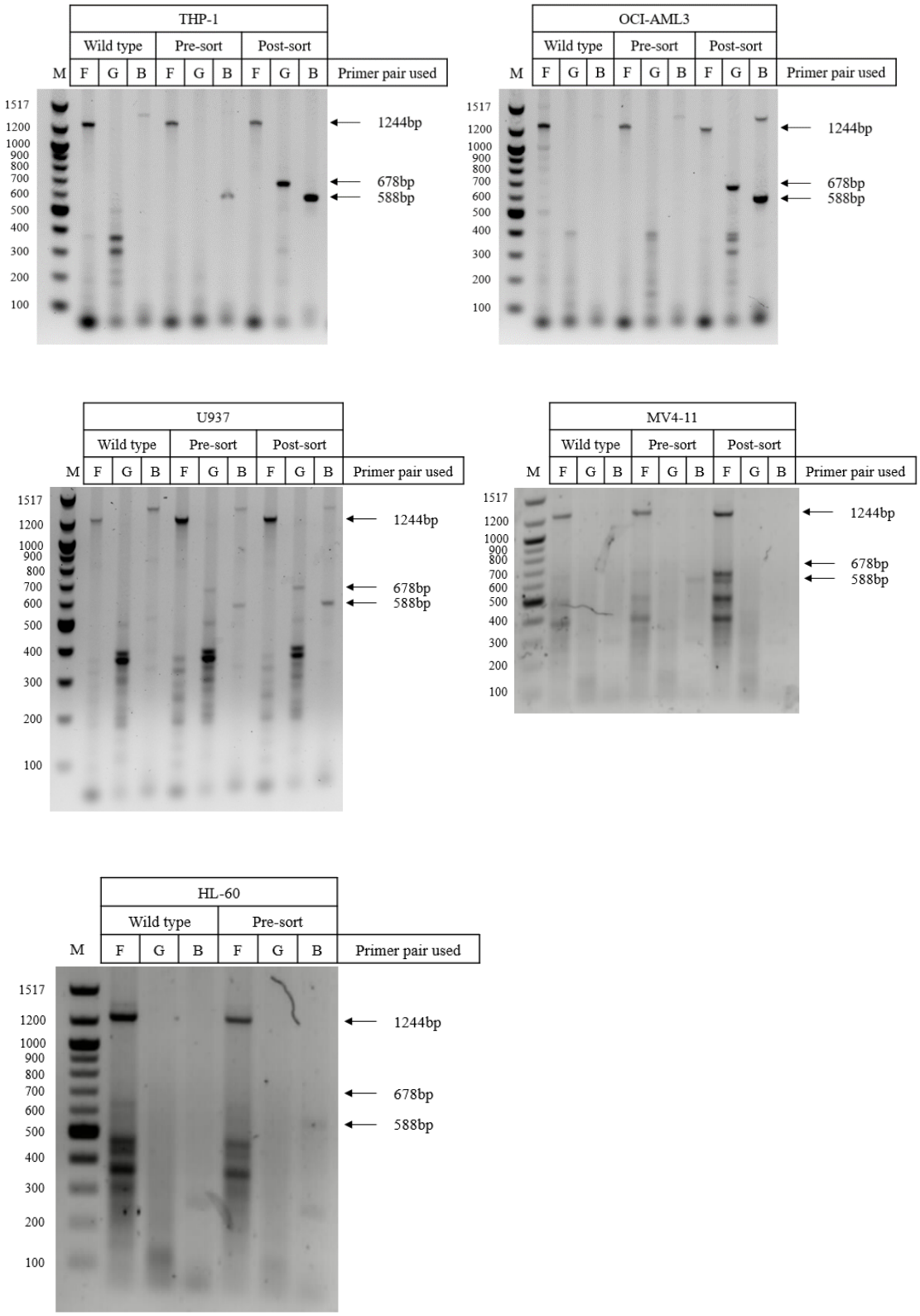

Figure 4.6 BTK^{C481S} genotyping PCR pre and post GFP flow sorting

Genomic DNA was isolated from wild type as well pLeGO transduced cells pre- and post-sort and a BTK^{C481S} genotyping PCR was performed using exon 15 spanning (F) as well as mutation specific (G and B) primers.

To ensure the HDR template was knocked-in successfully and without any further insertions or deletions we amplified exon 15 of BTK from wild type as well as sorted THP-1, U937 and OCI-AML3 cells using ex15F2 and ex15R2 primers. Following gel extraction and purification, the PCR products were subjected by Sanger sequencing.

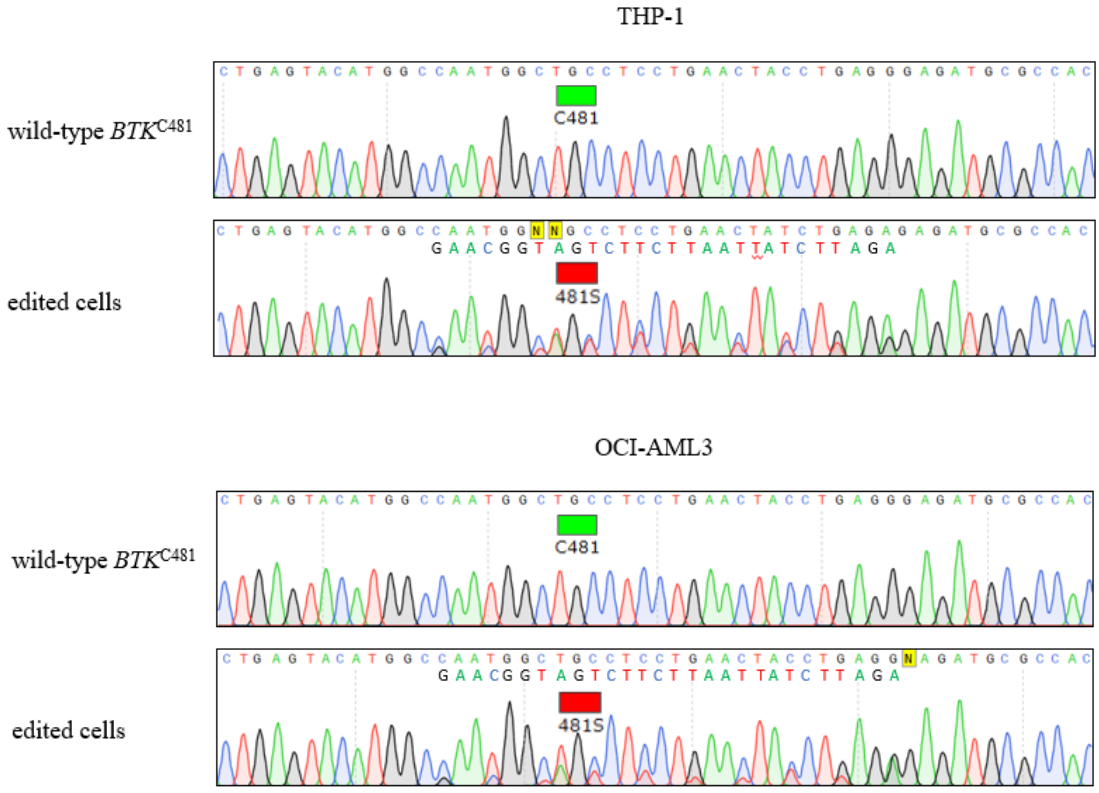

Figure 4.7 Sanger sequencing of wild type as well as sorted edited cells

Exon 15 of BTK from wild type as well as edited EGFP positive flow sorted cells was amplified by PCR and subjected to Sanger Sequencing. Shown are the sequencing results around the 481 residue for THP-1 and OCI-AML3 cells.

In both THP-1 and OCI-AML3 cells we could see double peaks around the 481 region indicating WT bases as well as bases that were knocked-in through HDR using the designed template.

No traces of a successful knock-in of the HDR template was seen in U937 cells and additional mutations were detected within exon 15. We therefore decided to only isolate single cell clones from THP-1 and OCI-AML3 cells.

4.4.4 BTK^{C481S} genotyping in isolated THP-1 and OCI-AML3 clones

To isolate single cell clones containing the BTK^{C481S} mutation, flow-sorted THP-1 and OCI-AML3 cells were seeded in 12 and 6 well plates in methylcellulose/RPMI medium as described in 2.2.3 and left to grow for 10-14 days. Colonies were transferred into a 96 well plate and expanded before genomic DNA was isolated. Isolated genomic DNA was then used for genotyping via PCR using exon 15 spanning (ex15F, ex15R2), 481 wild type specific (C481forward, C481reverse) and 481 mutation specific (mutF, mutR) primers. We used wild type-specific primers to ensure that C481S mutation positive colonies were derived from a single cell and were not a mixture of mutant positive and negative cells. PCR products were separated on a 1% agarose gel and analysed for wild type and mutation specific bands.

Overall two 96 well plates per cell line were screened using genotyping PCR. Results for wild type cells and 2 selected THP-1 and OCI-AML3 clones are shown in Figure 4.8. The genotyping PCR shows that the clones contain the C481S mutation determined by the 588 bp and 678 bp mutation specific products (primer pair G and B). No wild type specific products (primer pair K and L) were detected for the clones.

Primer pair	C481forward/ex15R 2 (**K**)	ex15F/C481reverse (**L**)	mutF/ex15R2 (**G**)	ex15F/mutR (**B**)
PCR product size	678 bp	588 bp	678 bp	588 bp

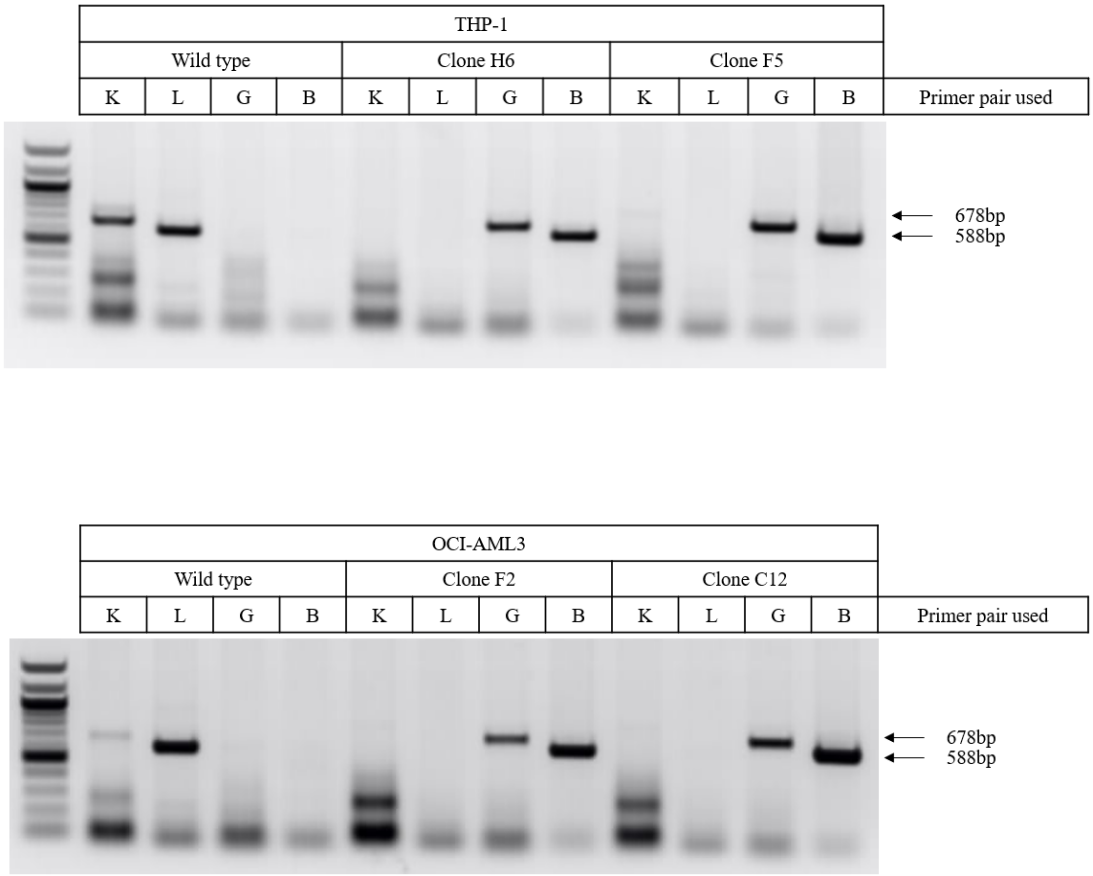

Figure 4.8 BTK^{C481S} genotyping in THP-1 and OCI-AML3 clones

Genomic DNA was isolated from wild type THP-1 and OCI-AML3 cells as well as from two BTK^{C481S} mutant clones for each cell line. Genotyping PCR using C481 wild type primer pairs (K and L) as well as a 481S mutant primer pairs (G and B) was performed using the isolated genomic DNA as a template. The table shows the expected PCR product size for each primer combination and agarose gels show the result of the separated PCR products.

To confirm a successful HDR template knock-in in the positive clones, exon 15 was amplified by PCR followed by gel extraction, purification and sequencing. Overall 5 clones per cell line were sequenced and results for OCI-AML3 clones F2 and C12 and THP-1 clones H6 and F5 are shown in Figure 4.9.

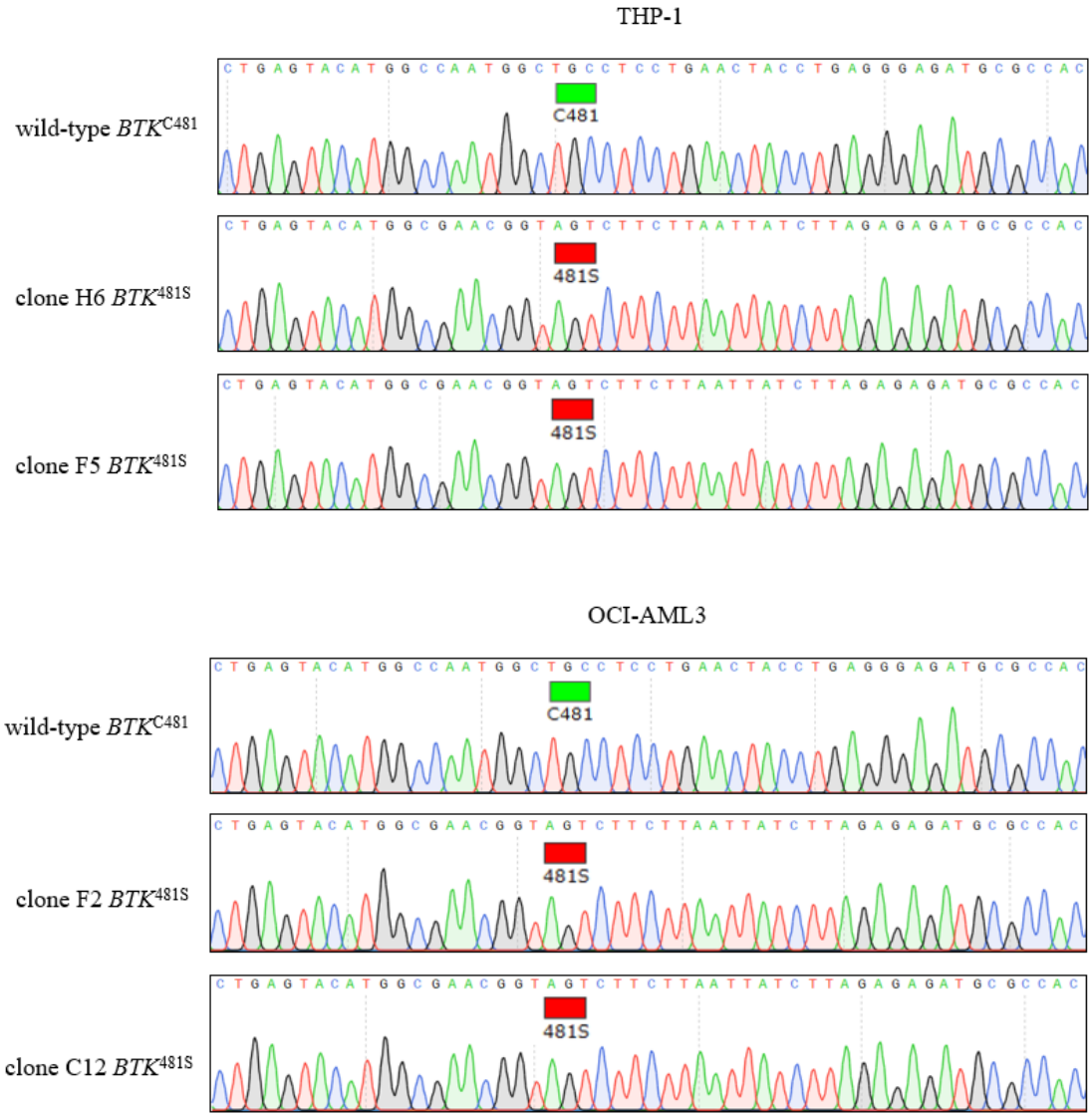

Figure 4.9 Sanger Sequencing of wild type as well as BTK^{481S} THP-1 and OCI-AML3 clones

Exon 15 of BTK from wild type as well as 481S mutant positive THP-1 and OCI-AML3 clones was amplified by PCR and subjected to Sanger Sequencing. Shown are the sequencing results around the 481 residue.

4.5 Discussion

The aim of this Chapter was to generate stable and doxycycline inducible SpCas9-expressing AML cell lines using lentivirus as a delivery system. This would be followed by the introduction of the BTK^{C481S} mutation in exon 15 using a non-integrating lentiviral vector in order to generate a BTK 481S expressing clonal cell population.

After we had confirmed that the five AML cell lines we wanted to use for further experiments had detectable BTK and p-BTK (Y223) expression levels, we used two different systems, a stable and an inducible expression plasmid, to generate the SpCas9-expressing cell lines.

Inducible gene expression plasmids allow quantitative and temporal control of the gene expression but depending on the expression system can be limited by the potential toxicity of the inducing agent, low induction expression and high basal levels under non-induction conditions (Lee et al., 1988). The tetracycline regulated gene expression system used in this thesis to generate inducible SpCas9-expressing cell lines is a very sensitive and a commonly used system in mammalian cell culture, mice and other species (Howe, Skryabin, Belcher, Zerillo, & Schmauss, 1995). Whilst stable gene expression systems are more useful when long-term gene expression is required for example for pharmacological studies, gene regulation mechanisms and gene therapy, those systems cannot be used if the expression or activation of the protein is toxic to the cells.

While Cas9 expression does not appear to be toxic to the cells, constitutive or high expression levels have been shown to correlate with increased off-target modifications (Fu et al., 2013). An inducible promoter for Cas9 expression is therefore advantageous. Only weak Cas9 expression was detected under non-induction conditions for three out of the five transduced AML cell lines (MV4-11, OCI-AML3 and U937).

The lowest doxycycline concentration (2 µg/mL) used, was sufficient at inducing Cas9 expression and no toxic/detrimental effects were seen for all concentrations tested (Figure 4.3).

Delivering the guide targeting exon 15 of BTK as well as the HDR template in a separate plasmid to that expressing the Cas9 meant that we required a second selection marker. A selection marker is not required in cases when an introduced gene changes the phenotype of the cells allowing to isolate the subpopulation of cells that have incorporated the gene via flow cytometry. As this is not the case for the introduction of the BTK^{C481S} mutation we decided to use GFP as a selection marker as this allows for easy determination of the viral titre via flow cytometry, easy monitoring of the transduction efficiency and sorting for positive transduced cells.

The transduction efficiency was relatively low (< 10%) for all AML cell lines except U937 (Figure 4.5). Therefore, a range should be tested to determine the optimal MOI to achieve a higher transduction efficiency. Whilst this is not necessary as we subsequently sorted positively transduced cells, which leads to an enrichment of the transduced subpopulation, it does help to achieve a higher purity of the sorted population. Smaller subpopulations also require a lower sorting rate meaning that the sorting process is time consuming which increases the stress on the cells and therefore affects cell viability. It also increases post-sort recovery time resulting in a higher chance of contamination. For HL-60 cells the post-sort population only contained ~60% GFP positive cells and cells had to be discarded due to a contamination. A purer post-sort population was achieved for the other AML cell lines with ~90% GFP positive cells. Genotyping of sorted cells confirmed successful introduction of the BTK^{C481S} mutation in U937, THP-1 and OCI-AML3 cells but not MV4-11 cells. Whilst sorting does enrich the successfully transduced subpopulation the post-sort population still contained ~10% untransduced cells. Knock-in efficiency via the CRISPR/HDR pathway is reported to be only in the range of 0.5-20% (B. Wang et al.,

2015) meaning that only a small percentage of the transduced cells contains the BTK^{C481S} mutation and this may explain why the genotyping for MV4-11 cells was negative.

Enhancing HDR by suppressing the NHEJ key molecules KU70, KU80 or DNA Ligase IV via gene silencing or small-molecule inhibition has been attempted in a number of studies. For example, inhibition of KU70 and DNA Ligase IV can increase HDR efficiency 4-5 fold (Chu et al., 2015). Another strategy is to exogenously express the protein Rad52, a protein involved in Homologous recombination. The combination of Rad52 overexpression and DNA Ligase IV inhibition using the small-molecule inhibitor Scr7 can improve HDR efficiency up to 40% (Shao et al., 2017). The efficacy of using these strategies has been mixed and so far, only small inserts and a few loci have been tested. It is not clear whether these strategies would enhance the BTK^{C481S} knock-in and it is important to keep in mind that NHEJ inhibition alone may cause mutagenesis or toxicity.

To ensure that cells used for further experiments do contain the BTK^{C481S} mutation and have a homogenous genetic background, clonal cell populations had to be derived from the post-sort population. This can be achieved in a number of methods all of which have their own advantages and disadvantages. The limiting dilution method, a method for which increasing dilutions of the parent cell culture are set up, has the advantage of preserving cell viability but is a very time consuming process that relies on statistical probabilities for monoclonality and varies with changes to the protocol (Nakamura & Omasa, 2015). To increase the probability of obtaining a clonal population, cells could be seeded straight into a 96 well plate at a concentration of 1 cell/well during the sorting process. Growing a single cell in RPMI medium or conditioned medium has proven to be difficult for the AML cell lines used in this thesis. To overcome this problem, cells were seeded in a methylcellulose-based semi-solid medium. The viscosity of the medium keeps secreted metabolites, growth factors

and matrix proteins in close proximity to the clones which is fundamental for cell growth (Caron et al., 2009). The viscosity also minimizes cell migration resulting in the formation of colonies that can be easily isolated and expanded.

The AML cell lines used in this thesis except the HL-60 cell line are derived from male patients, meaning they only carry one copy of the BTK gene, which makes the generation of BTK^{C481S} mutant positive cells easier. A homogenous BTK^{C481S} background of expanded clones was confirmed via sequencing and genotyping using wild type as well as mutant-specific primers (Figure 4.8 and Figure 4.9). Because additional mutations surrounding the exon 15 target site were detected in U937 cells the whole BTK gene should be sequenced in selected THP-1 and OCI-AML3 clones to ensure that clones that have been used for functional analysis do not contain additional mutations within the BTK gene. Any additional mutations could potentially change the protein conformation, its activity and expression profile. To study CRISPR off-target modifications, whole genome sequencing would need to be performed.

In this Chapter we presented a strategy to introduce the BTK^{C481S} mutation in five different inducible Cas9 expressing AML cell lines. A clonal population containing the BTK^{C481S} mutation was only isolated for two out of the five cell lines due to technical issues, methods used that affected cell viability and low CRISPR/HDR-mediated knock-in efficiency in those cell lines.

A large number of efforts have been made to address these issues but there is still a long way to go to optimize the techniques and strategies for CRISPR/Cas9 to be used in humans.

Chapter 5: Functional characterization of the AML cells containing the BTK^{C481S} mutation

5.1 Introduction

Even though advances in targeted therapy have helped to sustain therapeutic control of some cancer types, acquired drug resistance is still a huge problem in chemotherapy. Knowing about and understanding the mechanisms that cause drug resistance can help to counter this phenomenon. Mechanisms of acquired resistance to kinase inhibitors can be divided into 3 main categories: target reactivation (e.g. through a secondary mutation), activation of upstream and downstream effectors and activation of a bypass oncoprotein (Garraway & Janne, 2012). One of the most common drug resistance mechanism involves mutations in the targeted gene and are detected in a wide variety of cancer types that have been treated with kinase inhibitors. These mutations often exist before drug treatment and expand with the pressure of the drug (Michor et al., 2005; Shah et al., 2002).

Ibrutinib is a first in class BTK inhibitor that binds covalently and irreversibly to the Cysteine 481 residue in the ATP binding site. Despite good clinical efficacy in a range of B-cell malignancies, acquired resistance has developed in some of the patients treated with the drug. Mutations at the ibrutinib binding residue C481 are most common but other mutations such as T474I/S have also been reported. To overcome the ibrutinib resistance, more selective inhibitors that are efficient against these mutated BTK forms are needed. Recent studies have shown that while other covalent BTK inhibitors also display reduced potency to BTK C481 mutant forms, noncovalent, more selective BTK inhibitors are unaffected (Johnson et al., 2016). GDC-0853 is the most selective BTK inhibitor to date and does not interact with the C481 residue or the gatekeeper residue T474 but rather binds in an orthogonal orientation compared to the orientation of covalent inhibitors. GDC-0853 therefore has the potential to overcome acquired ibrutinib resistance and is currently being tested in a phase I clinical study in patients with relapsed or refractory B-cell NHL or CLL that had relapsed on ibrutinib (Crawford et al., 2018).

The aim of this Chapter was to characterize the BTK^{C481S} mutation in AML cell clones derived from CRISPR/Cas9 edited THP-1 and OCI-AML3 cell lines and study the effects of ibrutinib in BTK^{WT} and BTK^{C481S} cells. We also wanted to compare ibrutinib with GDC-0853 regarding differences in the drugs binding mechanisms and their efficacy to inhibit BTK activity. Phosphoproteomics as well as a kinase binding assay were performed to assess differences in the expression and activation profile of BTK^{WT} and BTK^{C481S} cells treated with ibrutinib.

5.2 Pharmacological inhibition of BTK in BTK^{WT} and BTK^{C481S} AML cell lines

5.2.1 BTK^{C481S} mutation reduces the binding affinity between ibrutinib and BTK

To study the functional consequences of the BTK^{C481S} mutation in the generated THP-1 and OCI-AML3 mutant clones we treated cells with increasing concentrations of the BTK inhibitor ibrutinib. Ibrutinib is an irreversible inhibitor that binds covalently to Cys481 blocking autophosphorylation at Tyr223 which was used as a parameter for BTKs enzymatic activity.

One clone of each cell line was chosen at random (THP-1 clone H6 and OCI-AML3 clone F2) and BTK mutant as well as wild type cells were treated for 2.5 h with ibrutinib concentrations ranging from 1 – 1000 nM. Protein lysates were extracted and p-BTK (Tyr223), BTK, p-PLCγ2 (Tyr1217), PLCγ2, p-AKT (Ser473), AKT, p-p42/44 (Thr202/Tyr204), p42/44 and β-Actin expression levels were determined by Western blot.

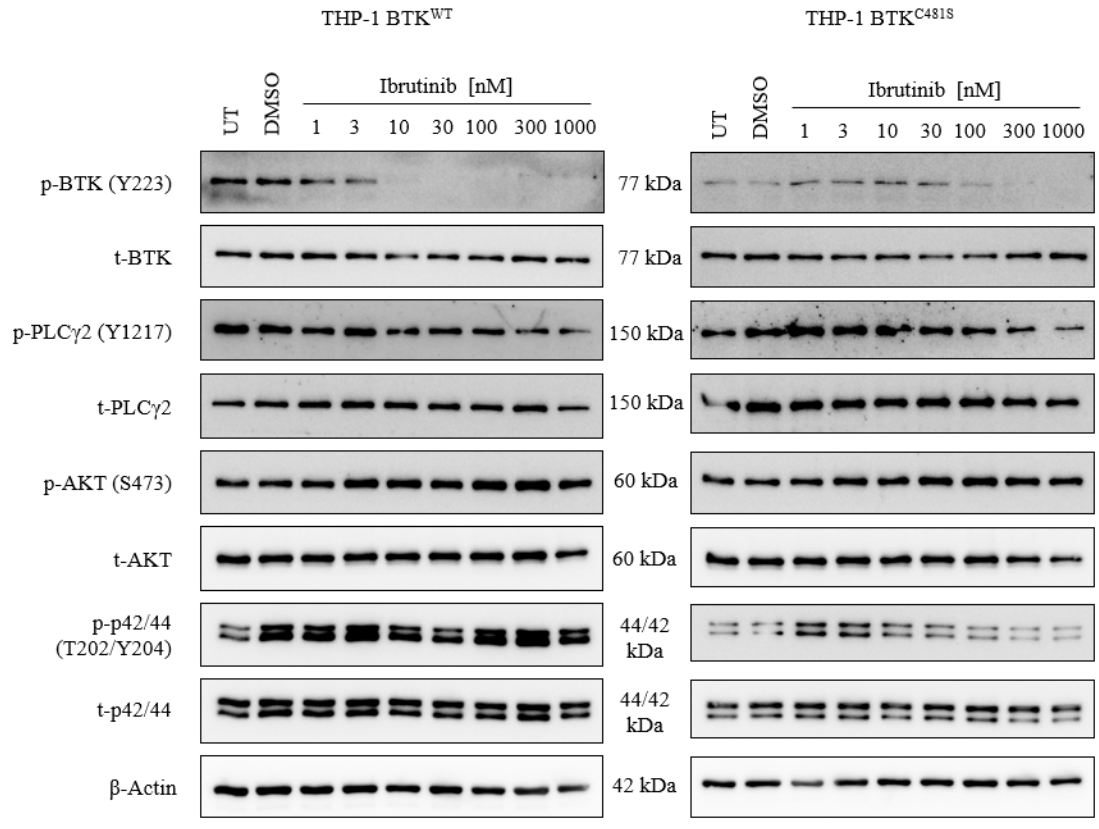

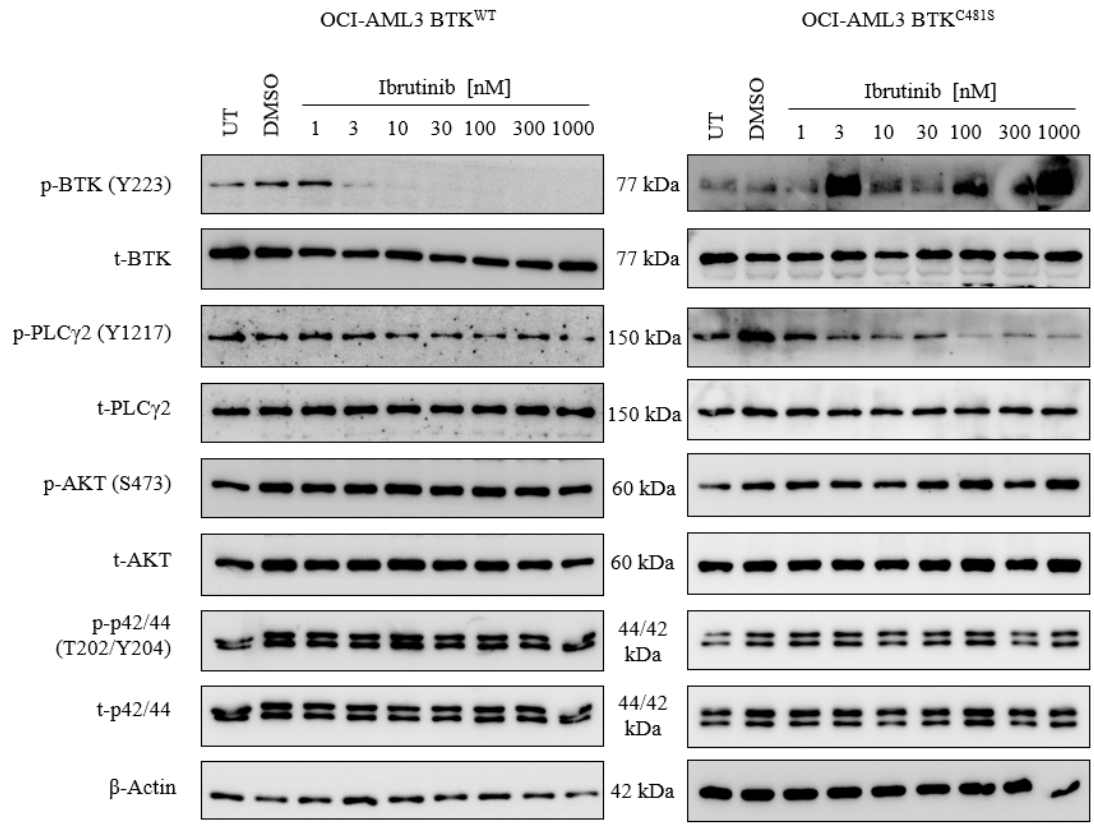

Figure 5.1 Effects of ibrutinib on BTK autophosphorylation and other proteins in BTK^{WT} and BTK^{C481S} cells

Cells were treated with indicated ibrutinib concentrations for 2.5 h after which cells were harvested and analysed for protein expression by Western blot. Top blots show results for THP-1 cells and bottom blots show results for OCI-AML3 cells (n=3 biological repeats).

Both cell lines exhibited constitutive phosphorylation of BTK (Y223) in untreated cells which was also present in BTK^{C481S} cells (Figure 5.1). A decrease in p-BTK(Y223) was observed with increasing ibrutinib concentrations in wild type as well as THP-1 mutant cells compared to untreated and vehicle treated cells. The effective ibrutinib concentration was 10 nM in THP-1 and OCI-AML3 wild type cells and 300 nM in THP-1 mutant cells. p-BTK (Y223) was not inhibited in OCI-AML3 mutant cells even for high ibrutinib concentrations (Figure 5.1 bottom right blot).

A non-specific band in OCI-AML3 mutant cells as well as low expression levels in the selected clone made it difficult to determine p-BTK (Y223) expression levels and we decided to not use this clone for further experiments due to having issues reproducing the data. The Western blot results from THP-1 and OCI-AML3 wild type as well as THP-1 mutant cells indicate that higher ibrutinib concentrations are required to inhibit autophosphorylation of BTK in BTK^{C481S} cells compared to BTK^{WT} cells. A slight decrease in p-PLCγ2(1217) expression levels was also seen in all cell lines for ibrutinib concentrations > 100 nM (> 30 nM in OCI-$AML3^{C481S}$ cells). No changes in p-AKT(S473) and p-p42/44(T202/Y204) were seen in ibrutinib treated wild type or mutant cells.

5.2.2 BTK^{C481S} mutation leads to reversible ibrutinib inhibition of BTK

Ibrutinib binds covalently to BTK Cys481 and it is expected that mutations of this residue should result in ibrutinib becoming a reversible inhibitor.

To study whether the BTK^{C481S} mutation affects the covalent and irreversible binding of ibrutinib we performed a wash out experiment. Cells were treated with ibrutinib concentrations ranging from 1 – 1000 nM for 2 h, washed with PBS 3 times and then left for another hour before cells were lysed and p-BTK (Tyr223), BTK, p-PLCγ2 (Tyr1217) and PLCγ2 expression levels were determined by Western blot.

A dose-dependent decrease in p-BTK(Y223) and p-PLCγ2(1217) expression levels was seen in all cells treated with ibrutinib (Figure 5.2). Whilst the wash out did not reverse inhibition of autophosphorylation of BTK at Y223 in wild type cells, the effects of ibrutinib seem to be reversible in BTK^{C481S} cells as shown by detectable p-BTK(Y223) expression levels even at high concentrations.

In THP-1 BTK^{WT} cells, 3 nM was effective in blocking BTK Y223 autophosphorylation and concentrations > 3 nM were effective in decreasing p-PLCγ2(1217) expression levels (Figure 5.2 top left blot).

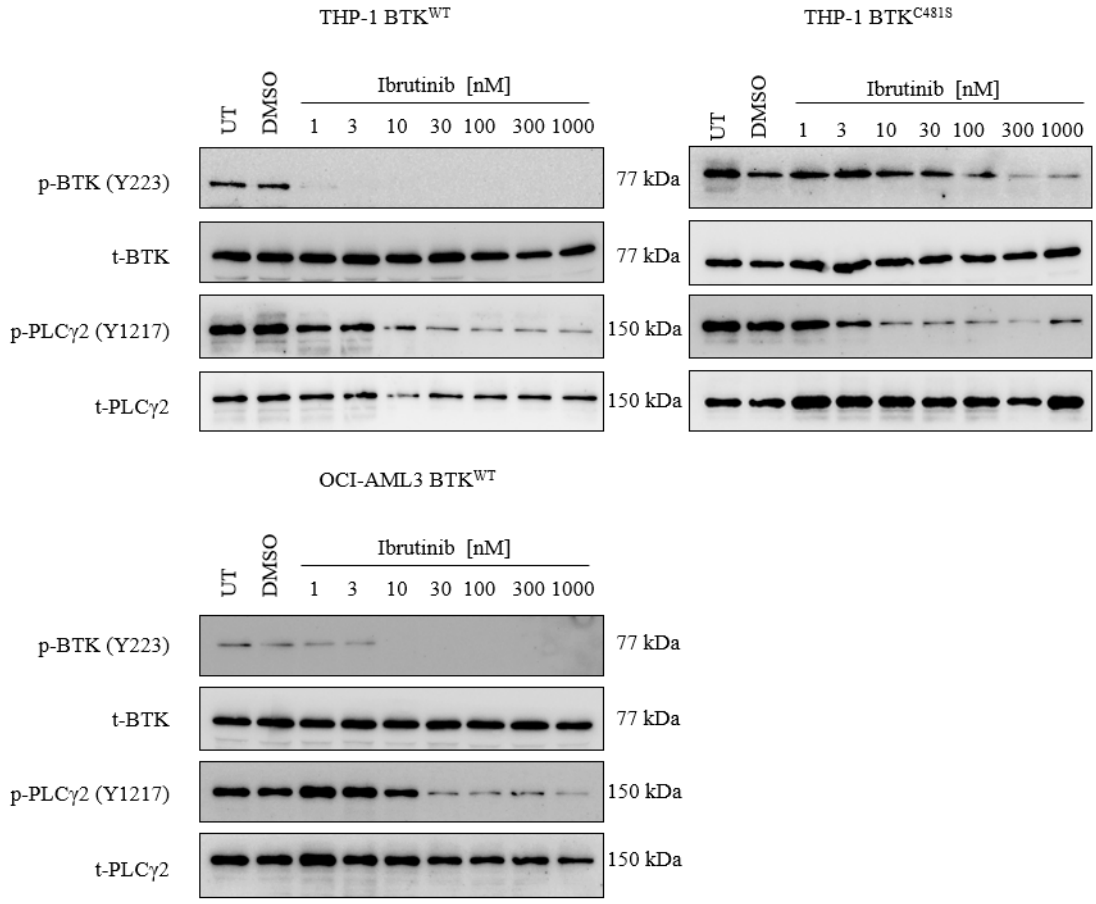

Figure 5.2 Ibrutinib wash out experiment

Cells were treated with indicated ibrutinib concentrations for 2 h followed by drug wash out and a 1 h incubation in the absence of the drug before cells were lysed and analysed for protein expression by Western blot (n=3, biological repeats).

In THP-1 BTK^{C481S} cells a slight decrease of p-BTK(Y223) was seen for ibrutinib concentrations > 30 nM and p-PLCγ2(Y1217) expression levels were decreased for ibrutinib concentrations > 3 nM compared to untreated and vehicle treated cells (Figure 5.2 top right blot). In OCI-AML3 BTK^{WT} cells 10 nM was effective in blocking BTK Y223 autophosphorylation and concentrations > 10 nM were effective in decreasing p-PLCγ2(Y1217) expression levels (Figure 5.2 bottom blot).

Comparing the Western blot results from the wash out experiment with results from cells treated continuously with ibrutinib for 2.5 h, it seems that the p-BTK(Y223) expression levels in BTK^{C481S} cells increase. This data suggests the binding of ibrutinib to BTK is reversible in BTK^{C481S} cells compared to irreversible in BTK^{WT} cells but a control for the wash-out is needed to confirm those results.

5.2.3 Inhibition of BTK using GDC-0853

Unlike ibrutinib, GDC-0853 is a non-covalent, reversible BTK inhibitor that does not interact with the C481 residue and is the most selective BTK inhibitor reported to date. We wanted to compare p-BTK (Tyr223), BTK, p-PLCγ2 (Tyr1217) and PLCγ2 expression levels in GDC-0853 treated cells with results from ibrutinib treated cells to see if we can overcome ibrutinib resistance in BTK^{C481S} cells but also to confirm the suggested reversible binding mechanism in BTK^{C481S} mutant cells by comparing results from ibrutinib and GDC-0853 wash out experiments.

THP-1 and OCI-AML3 BTK^{WT} and THP-1 BTK^{C481S} cells were treated either continuously for 2.5 h with increasing concentrations of GDC-0853 ranging from 1 – 1000 nM or were treated for 2 h, washed in PBS three times and incubated for another hour, followed by protein extraction and determination of p-BTK (Tyr223), BTK, p-PLCγ2 (Tyr1217) and PLCγ2 expression levels by Western blot.

Western blot results from cells treated with GDC-0853 continuously showed a dose-dependent decrease in p-BTK (Y223) and p-PLCγ2 (Y1217) expression levels (Figure 5.3). While GDC-0853 was similarly effective to ibrutinib in THP-1 BTK^{C481S} cells it was less effective in THP-1 and OCI-AML3 BTK^{WT} cells and even high concentrations (1000 nM) did not completely inhibit BTK autophosphorylation.

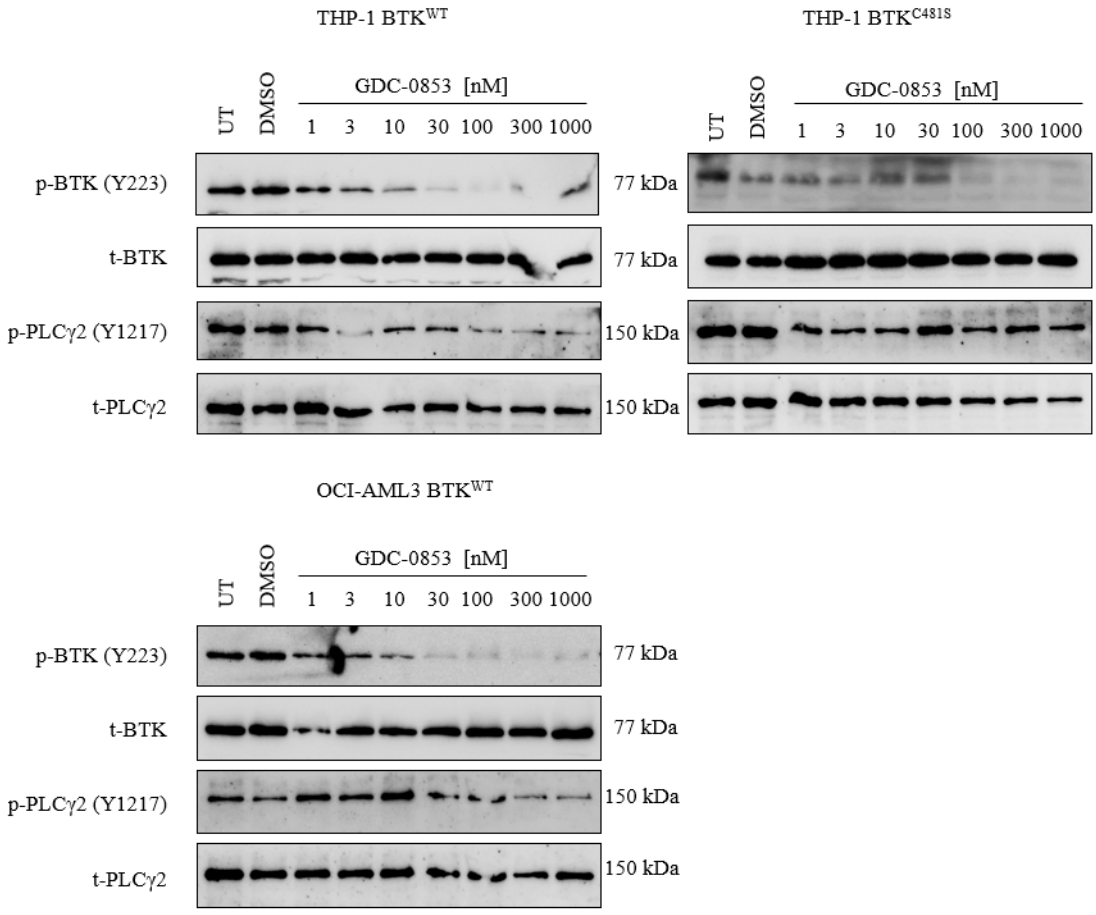

Figure 5.3 Effects of GDC-0853 on BTK autophosphorylation and p-PLCγ2(Y1217)
Cells were treated with indicated GDC-0853 concentrations for 2.5 h after which cells were harvested and analysed for protein expression by Western blot. Top blots show results for THP-1 BTK^{WT} and BTK^{C481S} cells and bottom blot shows the result for OCI-AML3 cells (n=3, biological repeats).

The wash out experiment showed that inhibition of BTK autophosphorylation at Y223 can be reversed in BTK^{WT} and BTK^{C481S} cells as shown by higher p-BTK(Y223) expression levels compared to cells treated continuously with GDC-0853 (Figure 5.4). This data confirms the non-covalent reversible binding of GDC-0853 to BTK.

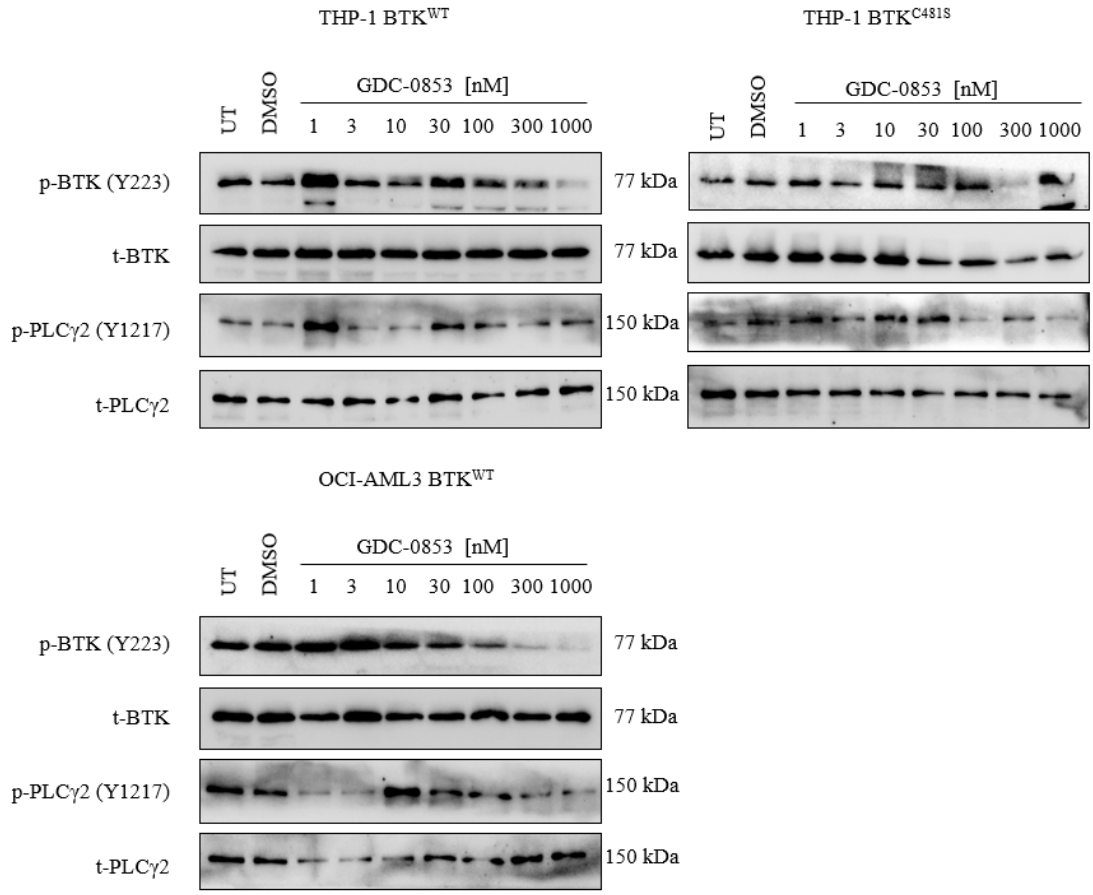

Figure 5.4 GDC-0853 wash out experiment

Cells were treated with indicated GDC-0853 concentrations for 2 h followed by drug wash out and a 1 h incubation in the absence of the drug before cells were lysed and analysed for protein expression by Western blot (n=3, biological repeats).

5.2.4 Ibrutinib does not effect cell viability and proliferation in THP-1 BTK^{WT} or BTK^{C481S} mutant cells

To study whether ibrutinib has any effects on cell viability and proliferation in THP-1 BTK^{WT} and BTK^{C481S} cells, cells were treated with ibrutinib concentrations ranging from 10 – 1000 nM for 7 days. New drug was added every 48 h, cell proliferation was measured using the CellTiter-Glo Luminescent assay and cell viability was analysed by flow cytometry and AnnexinV/PI staining.

No decrease in cell viability was observed over the 7 days in untreated and ibrutinib treated BTK^{WT} or BTK^{C481S} cells even for the highest concentration of 1000 nM (Figure 5.5). This is consistent with a previous study showing that THP-1 cell viability is not effected by ibrutinib concentrations up to 10 µM after 72 h (Rushworth et al., 2014).

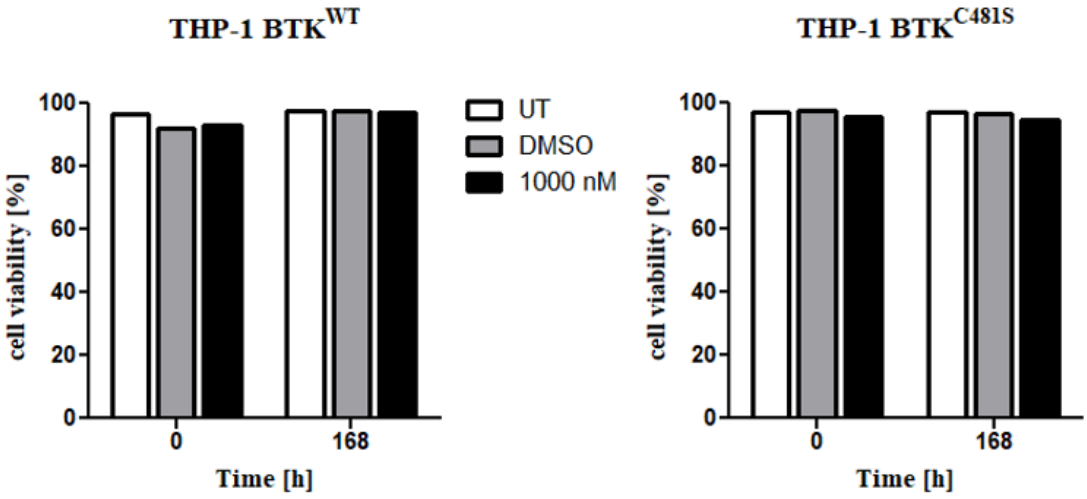

Figure 5.5 Effects of ibrutinib on cell viability

THP-1 BTK^{WT} and BTK^{C481S} cells were treated with ibrutinib concentrations ranging from 10 – 1000 nM for 7 days and cell viability was measured by flow cytometry every 48 h. Shown above are only the results for the highest ibrutinib concentration at timepoint 0 and on day 7 (n=1).

Cell proliferation was not negatively affected by ibrutinib in BTK^{WT} and BTK^{C481S} cells as shown by the increase in the relative luminescence over time which correlates with the amount of ATP which in turn is proportional to the number of cells (Figure 5.6). Cell proliferation seemed to slow down/stop after 96 h and cell density reached a plateau.

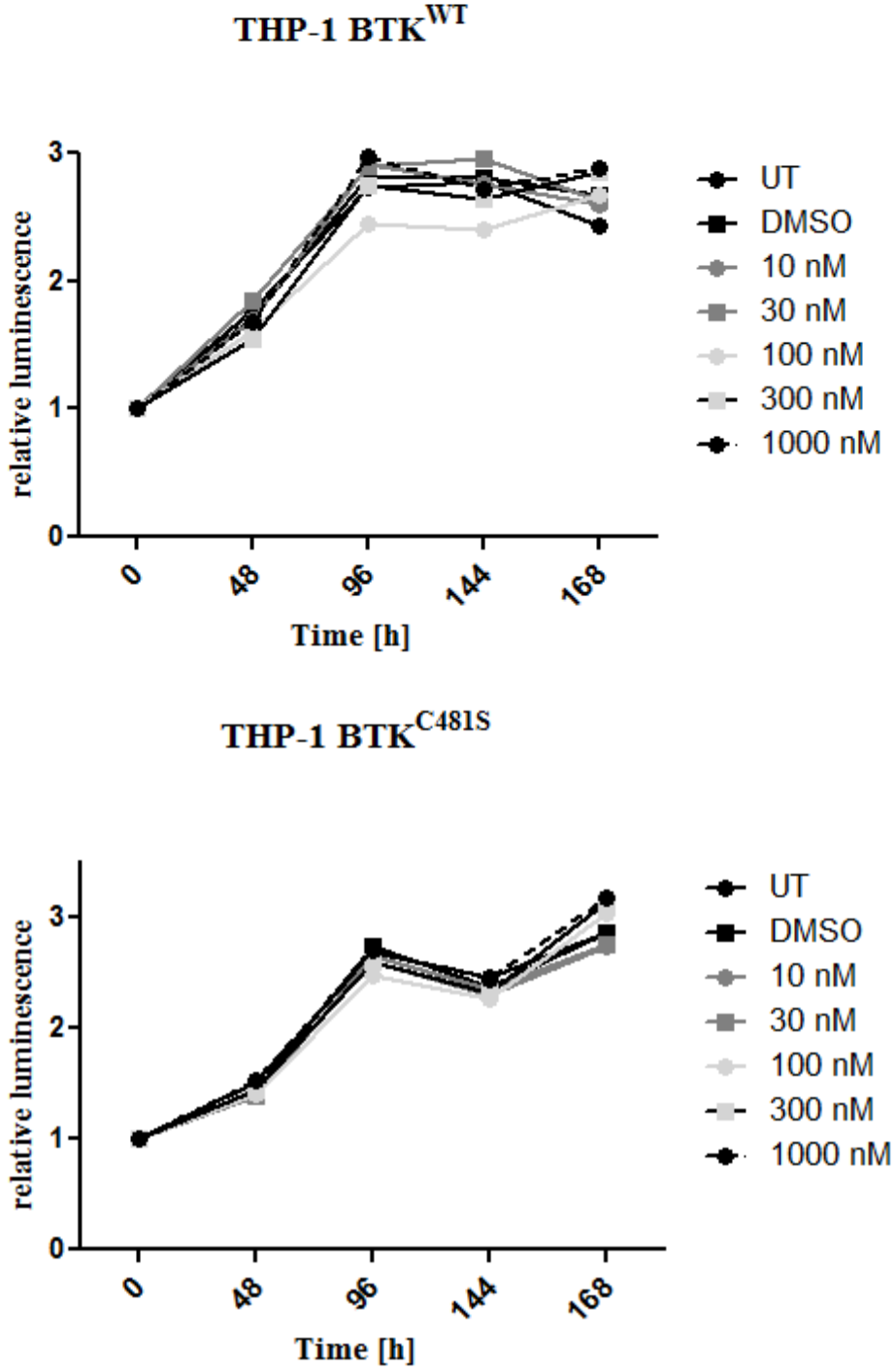

Figure 5.6 Effects of ibrutinib on cell proliferation

THP-1 BTK^{WT} and BTK^{C481S} cells were treated with ibrutinib concentrations ranging from 10 – 1000 nM for 7 days and cell proliferation was measured every 48 h using the CellTiter-Glo luminescent assay (n=1).

5.2.6 Phosphoproteomics analysis of THP-1 BTK^{WT} and BTK^{C481S} cells

As can be seen from the data above, the BTK^{C481S} mutation does not make BTK refractory to inhibition by ibrutinib but rather results in reversible binding. Higher concentrations of the drug are therefore required to achieve maximal inhibition. We wanted to assess if the BTK^{C481S} mutation only causes a change in inhibitor effectiveness or leads to more profound changes in kinase pathway activation.

To study differences in kinase activation in untreated and 30 nM ibrutinib treated THP-1 BTK^{WT} and BTK^{C481S} cells, proteins were isolated and prepared as described in 2.7.1. For the first analysis we used conventional phosphoproteomics which identifies potential kinase substrates by analysing differentially phosphorylated peptide sequences. A computational approach, kinase-substrate enrichment analysis (KSEA,) was then used to infer kinase pathway activation from phosphoproteomics data (Cascado et al., 2013). KSEA estimates changes in a kinase's activity based on the change in phosphorylation state of its substrates as identified from phosphosite-specific kinase-substrate databases.

Analysis of the ibrutinib treated THP-1 BTK^{WT} cells showed a decrease in the abundance of the NEK2 substrate group and an increase in the abundances of CDK3, CDK5, RPS6KA2 RPS6KA4 and TTBK1 substrate groups compared to untreated cells (Figure 5.7 left panel). Analysis of ibrutinib treated THP-1 BTK^{C481S} cells showed a decrease in the abundances of ABL1, PLK1, LRRK1, NEK2, PHKG1, PKM, AKT2, CDK5 and PRKDC substrate groups and an increase in the abundances of CSNK1E, PRKCD, RPS6KA1, RPS6KA3 and RPS6KB1 substrate groups compared to untreated cells (Figure 5.7 right panel). Comparing the KSEA results from THP-1 BTK^{WT} and BTK^{C481S} cells a decrease in NEK2 activity as well as an activity increase in kinases belonging to the RSK family can be seen in ibrutinib treated BTK^{WT} and BTK^{C481S} cells. Several other kinase subsets also seem to be differently regulated in BTK^{C481S} cells upon ibrutinib treatment.

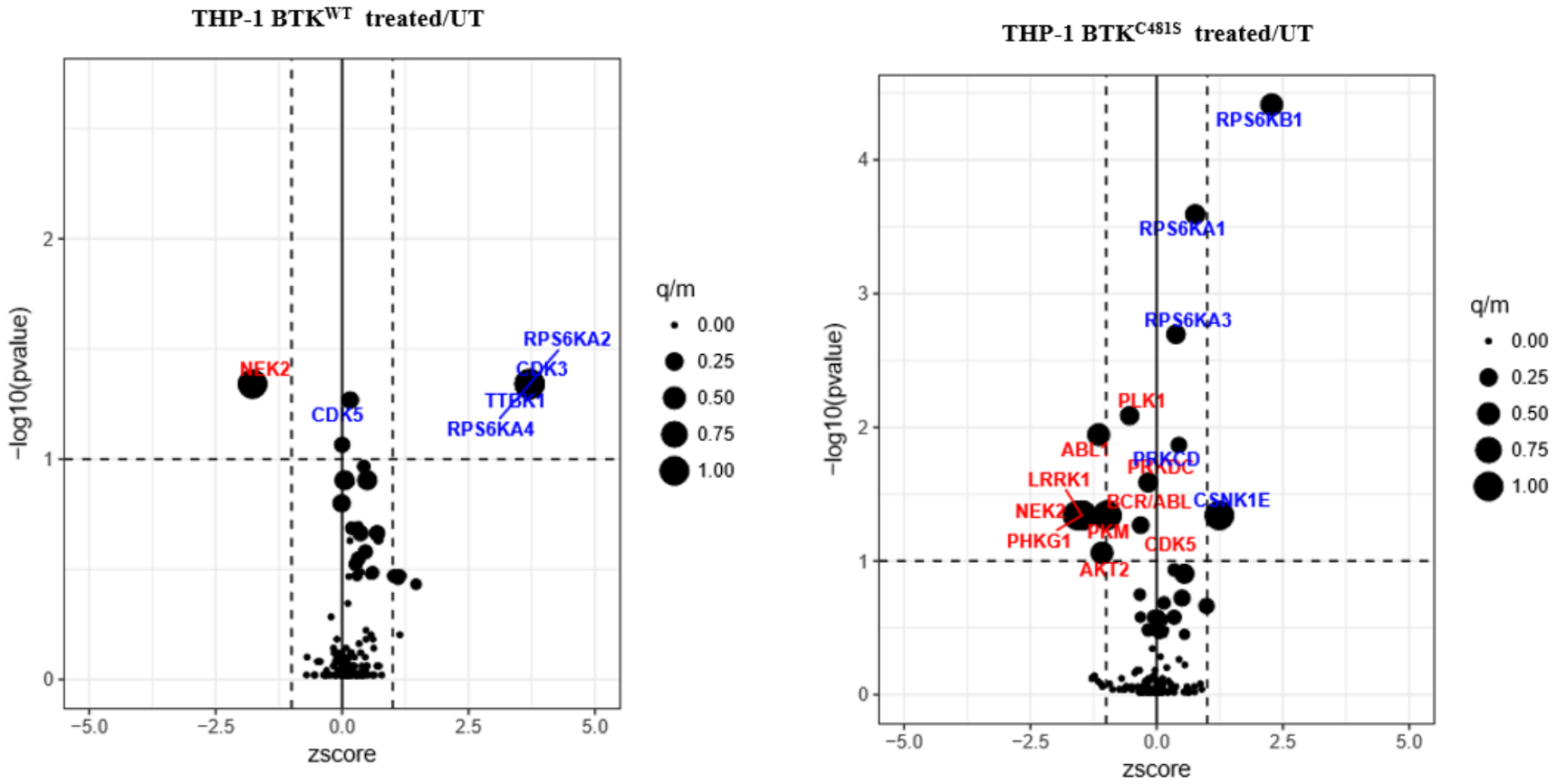

Figure 5.7 Kinase substrate enrichment analysis (KSEA) of ibrutinib treated THP-1 BTK^{WT} and BTK^{C481S} cells

Cells were treated with 30 nM ibrutinib for 2 h, after which proteins were isolated and samples analysed using Mass spectrometry. Changes in kinase pathway activation were obtained from phosphoproteomics data using KSEA (n=1, biological repeats; n=2, technical repeats).

5.2.7 Kinome inhibitor bead profiling of THP-1 BTK^{WT} and BTK^{C481S} cells

To study changes in kinase activity upon ibrutinib treatment, we used a modified version of a kinase capture method called multiplexed kinase inhibitor bead assay (Duncan et al., 2012). This is an affinity chromatography method using kinase inhibitors covalently linked to Sepharose beads coupled with LC-MS to detect the bound kinases. Both active and inactive kinases can potentially bind to the beads, allowing to measure kinase activation and expression. The modification of the assay refers to the inhibitor used. Rather than using a spectrum of kinase inhibitors the novel bis-anilino pyrimidine, CTx-0294885, was used. This inhibitor binds over 200 protein kinases therefore covering nearly 50% of the kinome (Zhang et al., 2013).

THP-1 BTK^{WT} and BTK^{C481S} cells were treated with 30 nM ibrutinib for 2 h and kinase abundance was compared to the untreated control. Table 5.1 shows the values obtained from MaxQuant analysis representing the intensity/amount of each detected kinase. 0 values were changed into the value of 1 to be included in the $\log_2$ calculations. A value of 0 means either that the kinase abundance was below the set threshold intensity or a kinase was not detected at all. Results are shown for one selected run.

Table 5.1 Kinase intensities in THP-1 cells obtained from MaxQuant analysis

Gene names	BTK^{WT} untreated	BTK^{WT} treated	BTK^{C481S} untreated	BTK^{C481S} treated
AAK1	1	2776200	1	53426000
ATM	5496700	2457500	1	1149700
BMP2K	1	1	1	9741800
BTK	1	1	1	1000200
CAMK2D	612900000	494710000	348090000	763240000
CAMK2G	43734000	32595000	21045000	67040000
CDK3	36722000	31611000	29293000	66747000
CSNK2A1	1	1	1	3441800
CSNK2A2	1	1	1	8198900
EPHB1	1	1	1	1586200
FES	2938400	2954500	1	16279000
FGR	24353000	14253000	12572000	42522000
FYN	1	1	2380500	4234300
GAK	2948000	2599400	7512400	82588000
GSK3B	1	1772000	1	1
HCK	103560000	77898000	153280000	260640000
INSR	19645000	8021900	10961000	36241000
IRAK3	15047000	17338000	5173300	18976000
LYN	220080000	228690000	177170000	420240000
MAP4K1	1560900	1	1	29853000
MAPK1	362980000	146530000	71834000	126460000
MAPK10	1	1	1	2221800
MAPK3	68626000	29738000	16118000	31845000
NEK9	14651000	3972000	3423100	35490000
PHKG2	55045000	16581000	34151000	59533000
PKMYT1	15613000	10799000	9609200	23426000
PKN1	15834000	7352500	3053100	37087000
PKN2	1	1	1	5000600
PRKAA1	9674700	3558300	6885400	21006000
PRKACB	11334000	5700900	2323700	17376000

PRKCA	9203200	1	12790000	13975000
PRKCB	26296000	2391900	1050400	6056700
PRKDC	900850000	1160500000	356280000	1344900000
PTK2B	1	1	1	5432000
PTK2B	4806600	9319500	1	88975000
RET	643410	1	4492500	54366000
RPS6KA1	3552000	13557000	4818700	85741000
RPS6KA3	1	1	1	2282100
RPS6KA4	1	1	1	1925900
SRC	48046000	55230000	39620000	159680000
STK38	1	1	1	4389100
TAOK3	1	1	2261500	10028000
TBK1	25420000	28602000	11086000	95186000
TGFBR1	12224000	11048000	26895000	79738000
TYK2	1	1	1	4736800
ULK3	6843600	4162600	2603500	22299000
YES1	2083300	1	1994600	3608300

The heatmap shows the $\log_2$ values for treated/untreated THP-1 BTK^{WT} and BTK^{C481S} cells calculated using the values from table 5.1. Red represents a decrease, green an increase in kinase abundance and grey represents ratios based on no data for at least one of the conditions (Figure 5.8). Figure 5.9 shows the same $\log_2$ values as seen in the heatmap but kinases with a value of 0 for one of the conditions were not considered. The Figure legend only shows the kinases that had an abundance difference of 2.0 or higher comparing BTK^{WT} and BTK^{C481S} cells. Figure 5.8 and 5.9 show that the abundance for the majority of detected kinases decreases upon ibrutinib treatment in THP-1 BTK^{WT} cells but increases in BTK^{C481S} cells.

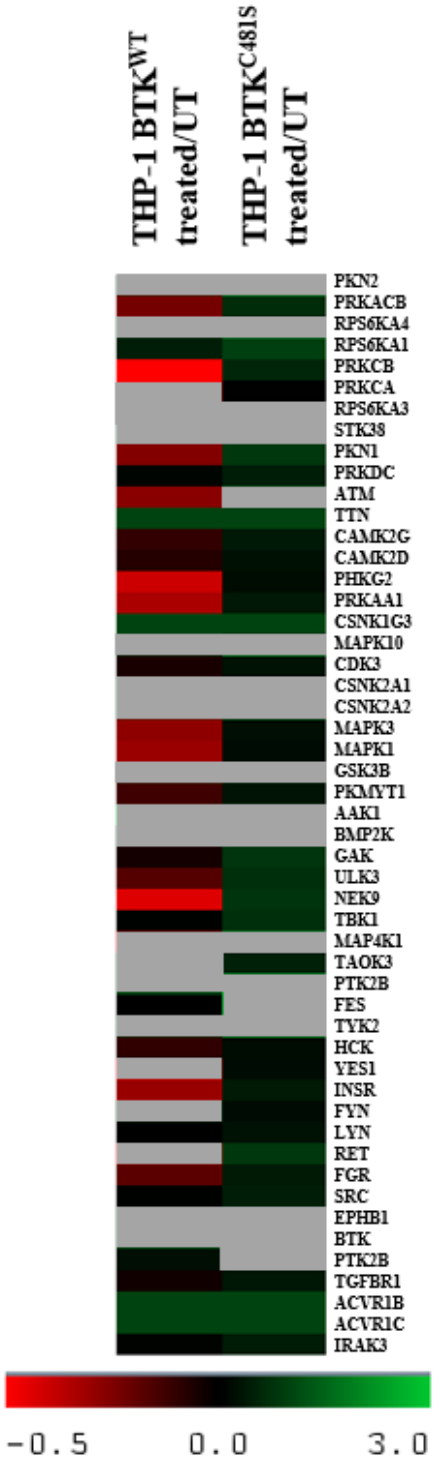

Figure 5.8 Heatmap depicting changes in kinase abundances

THP-1 BTK^{WT} and BTK^{C481S} cells were treated with 30 nM ibrutinib for 2 h, after which cells were lysed and kinases isolated using inhibitor bead analysis by mass spectrometry. The heatmap represents the change in $\log_2$ values of treated versus untreated cells with red indicating a decrease, green indicating an increase in kinase abundance and grey representing ratios based on no data for at least one of the conditions (n=2, biological repeats).

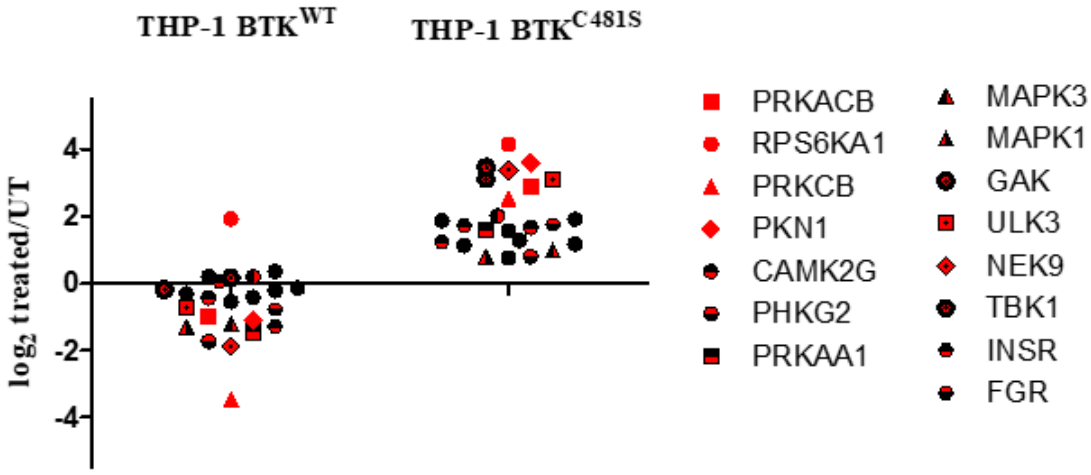

Figure 5.9 Dot plot representing changes in kinase abundances

The dot plot represents the change in $\log_2$ values of treated versus untreated cells with negative values indicating a decrease and positive values indicating an increase in kinase abundances (n=2, biological repeats).

5.3 Discussion

The aim of this Chapter was to characterize the BTK^{C481S} mutation in THP-1 and OCI-AML3 clones derived from CRISPR/Cas9 edited cells and study the effects of ibrutinib.

One clone of both cell lines was selected at random and used for further experiments. Insertion of the BTK^{C481S} mutation was confirmed by PCR and Sanger sequencing in the previous chapter but as only part of the gene was sequenced, we needed to ensure that the cells still express functional BTK. Protein lysates were extracted from untreated as well as ibrutinib treated (1 – 1000 nM) BTK^{WT} and BTK^{C481S} cells and p-BTK (Tyr223), BTK, p-PLCγ2 (Tyr1217), PLCγ2, p-AKT (Ser473), AKT, p-p42/44 (Thr202/Tyr204), p42/44 and β-Actin expression levels were determined by Western blot. PLCγ2, AKT and p42/44 are known downstream targets of BTK in B-cells and we wanted to assess whether pharmacological inhibition of BTK affects these downstream targets in AML cells also. Results showed a decrease in p-BTK (Y223) for BTK^{WT} and BTK^{C481S} cells treated with increasing ibrutinib concentrations but higher concentrations were required to achieve a p-BTK(Y223) inhibition in BTK^{C481S} cells (Figure 5.1). These results are in agreement with previously published data showing that ibrutinib is less effective against BTK^{C481S} mutant. In this study ibrutinib showed an IC_{50} of 0.72 nM against purified BTK^{WT} and an IC_{50} of 4.6 nM against purified BTK^{C481S} (Johnson et al., 2016). Another study showed that in a cellular model using HEK-293T cells ibrutinib's half maximal effective concentration was higher in BTK^{C481S} mutant cells than BTK^{WT} cells (Woyach et al., 2014). In our cell culture model ibrutinib was 10-30 fold less potent against BTK^{C481S} compared to BTK^{WT} showing a greater difference between BTK^{WT} and BTK^{C481S} than observed with purified proteins.

The role BTK plays in AML cells is currently unclear, however a slight decrease in p-PLCγ2 (Tyr1217) was seen for higher ibrutinib concentrations (>30 nM) in BTK^{WT}

and BTK^{C481S} cells suggesting it may be a downstream target of BTK in AML (Figure 5.1). No effects of ibrutinib treatment in THP-1 and OCI-AML3 BTK^{WT} or BTK^{C481S} cells were seen with p-AKT (Ser473) and p-p42/44 (Thr202/Tyr204). This is in agreement with previous studies showing that ibrutinib does not affect expression of p-AKT and p-p42/44 in OCI-AML3 and TF-1 cell lines but interestingly phosphorylation of these proteins is affected by ibrutinib in U937, MV4-11 cells and some primary AML blasts (Pillinger et al., 2015; Rushworth, Murray, Zaitseva, Bowles, & MacEwan, 2014). The heterogenous background of the disease could explain the differences seen in cell lines and patient samples and suggests a role of BTK upstream of PI3K/AKT and ERK signalling at least in some AML cell lines/blasts. Other proteins found to be regulated by BTK in AML include STAT5, RAC1, p65 (NF-κB subunit), MYC and NF-κB with FLT3-ITD and TLR9 being placed upstream of BTK (Nimmagadda et al., 2018; Oellerich et al., 2015). Recently, mutated granulocyte-colony stimulation factor receptors (G-CSFR) were implicated in upregulation of BTK in BaF3, murine 32D and c-Kit^{+} cells and human $CD\text{-}34^{+}$ cells (Dwivedi et al., 2018). Further findings supported the suggested hypothesis that cells expressing mutant receptor are dependent on BTK activation and ibrutinib can therefore suppress these cells. Such mutations have been found in AML patients and it would be of interest to see the effects of ibrutinib in AML cell lines carrying mutations in G-CSFR and BTK.

As ibrutinib failed to inhibit p-AKT and p-p42/44 in THP-1 and OCI-AML3 BTK^{WT} or BTK^{C481S} cells the results for the proliferation as well as cell viability assay were as expected. For both assays THP-1 cells were treated with ibrutinib concentrations ranging from 10 – 1000 nM for up to 168 h and cell proliferation was measured every 48 h using CellTiter-Glo assay with cell viability being analysed by flow cytometry and Annexin-V/PI staining. No effects were seen on cell proliferation or viability (Figure 5.5 and Figure 5.6). Pharmacological inhibition of BTK as well as BTK knockdown using shRNAs can affect cell proliferation and induce apoptosis in some

AML cell lines (MV4-11, MOLM-13, KG-1 and NB4) and patient-derived AML cultures (Oellerich et al., 2015).

Two FLT3-dependent mechanisms have been described so far. In FLT3-ITD negative cells, TLR9 is an activator of BTK and NF-κB and STAT5 are activated downstream of BTK whilst in FLT3-ITD positive cells MYC and STAT5 are activated downstream of BTK.
Because THP-1 and OCI-AML-3 cells are FLT3-ITD negative it would be interesting to see whether TLR9 activates BTK in these cells or not. Downstream targets are likely to be different seeing that no effects on proliferation and viability were observed in these two cell lines.

To study ibrutinib's binding mechanism in BTK^{WT} and BTK^{C481S} cells we performed a drug wash-out experiment. Cells were incubated for 2 h with various ibrutinib concentrations, the drug was washed out using PBS and the cells were incubated for another hour in the absence of the drug before proteins were extracted. Because no effects on p-AKT and p-p42/44 were seen in the previous experiment under continuous drug exposure we only assessed effects on p-BTK and p-PLCγ2. As described before, we did see a decrease in p-PLCγ2 in both THP-1 and OCI-AML3 BTK^{WT} and BTK^{C481S} cells for ibrutinib concentrations > 3 nM (Figure 5.2). Ibrutinib's binding to BTK^{WT} is irreversible and covalent by nature explaining why p-BTK is still inhibited after washing out the drug. Interestingly in THP-1 BTK^{C481S} cells p-BTK expression levels return to almost basal levels one hour after washing out the drug suggesting a reversible binding of ibrutinib to BTK^{C481S} which was previously shown in DT40 ($BTK^{-/-}$) chicken B-cells transfected with exogenous BTK^{C481S} (Woyach et al., 2014).

Several second generation BTK inhibitors have been developed to reduce off target effects as well as to overcome the resistance caused by the BTK^{C481S} mutation. Among these inhibitors is GDC-0853 which is the most selective BTK inhibitor to date.

Unlike ibrutinib, GDC-0853 does not bind to EGFR or ITK which are two targets of ibrutinib that are likely to be responsible for adverse events seen in ibrutinib treated patients. To study the potential of GDC-0853 to inhibit BTK^{WT} and BTK^{C481S} in AML cells we treated THP-1 and OCI-AML3 BTK^{WT} and BTK^{C481S} cells either continuously for 2.5 h with different drug concentrations ranging from 1 – 1000 nM or the drug was washed out with PBS after 2 h and cells were incubated in the absence of the drug for another hour before proteins were isolated. The wash-out experiment was performed to confirm the noncovalent binding of the drug to BTK. Results showed that GDC-0853 was efficient in decreasing p-BTK(Y223) expression levels but higher drug concentrations are needed compared to ibrutinib in BTK^{WT} cells. In THP-1 BTK^{C481S} cells GDC-0853 showed a similar efficiency (Figure 5.3). As with ibrutinib, higher GDC-0853 concentrations are needed to inhibit p-BTK(Y223) in BTK^{C481S} cells than BTK^{WT} cells meaning that both drugs are equally efficient in our cell culture model using the generated THP-1 BTK^{C481S} cells. These results are surprising as GDC-0853 has been reported to be highly potent in isolated primary human B-cells, inhibiting BTK autophosphorylation (Y223) with an IC_{50} of 3.1 nM and human whole blood with an IC_{50} of 11 nM (Crawford et al., 2018). In this same study GDC-0853 successfully inhibited p-BTK(Y223) autophosphorylation at 1000 nM in HEK-293 cells transfected with BTK^{WT} and BTK^{C481S} whilst ibrutinib failed to do so in BTK^{C481S} cells which is also not in agreement with our results.

A slight decrease in p-PLCγ2 (Y1217) was observed in GDC-0853 treated cells confirming it as a downstream target of BTK in the AML cell lines. The wash out experiment confirmed noncovalent binding as the inhibition was reversed and p-BTK expression levels returned to nearly basal levels after 1 h (Figure 5.4). While GDC-0853 showed a similar efficacy at inhibiting BTK in BTK^{WT} and BTK^{C481S} cells its efficiency was lower in BTK^{WT} cells compared to ibrutinib. As GDC-0853 is more selective than ibrutinib with reduced off-target binding and side effects, it is still a good alternative to ibrutinib and could be used especially in relapsed patients.

Not much is known about the role of BTK in AML and some of the known downstream targets are not affected by BTK inhibition in the cell lines we used. In order to identify additional substrates, we performed phosphoproteomics as well as a kinome inhibitor pulldown assay in THP-1 BTK^{WT} and BTK^{C481S} cells.

The high throughput and quality of MS-based techniques to measure phosphorylation has replaced the traditional method using immunochemical techniques. The high data output of phosphoproteomics data however poses an analysis challenge. Publications using the kinase substrate enrichment analysis (KSEA) are few and the depth by which KSEA can derive information about kinase activation is limited by the available databases of kinase substrate relationships (Casado et al., 2013). Whilst these databases contain experimentally verified interactions, computational approaches such as NetworKIN have been developed to help us understand and predict kinase substrates from motif analysis and functional context derived from STRING (von Mering et al., 2003).

The second MS-based approach we performed was a quantitative proteomics approach using inhibitor beads as a method of affinity enrichment and is a useful tool when kinases are only present at low abundances. The downside of using beads is that the elution step is often inefficient resulting in a low recovery. The elution method we used (SDS wash) requires additional purification steps to remove the detergent and using SDS leaves residual enzymatic activity which can affect the measurement (Bischoff, Shi and Kennelly, 1998; Duncan et al., 2012). On-column trypsin digestion has recently been described as an elution method which improves protein yield and could be used alternatively in the future (Toth et al., 2017).

The inhibitor used for kinase enrichment, CTx-0294885, is modified from the FAK inhibitor TAE-226. CTx-0294885 alone identified 235 kinases in a large scale kinome profiling experiment in MDA-MB-231 cells and a total of 261 kinases were identified

using the inhibitor in combination with 3 other inhibitors (Purvalanol B, SU6668, and VI16832) revealing 72 kinases that are unique to CTx-0294885 (Zhang et al., 2013). Even though a cross-screen profiling against 131 kinases using the chemically related inhibitor CTx-0294857 at a concentration of 1 μM displayed high potency against BTK, we were only able to identify BTK in ibrutinib treated THP-1 BTK^{C481S} cells but not untreated or THP-1 BTK^{WT} cells. Overall only 47 kinases were identified in our studies with only 23 kinases being identified in BTK^{WT} and BTK^{C481S} cells for both conditions therefore showing very inconsistent results between the different samples.

Taken together the limited results from the KSEA and inhibitor bead assay we saw an increase in kinases belonging to the RSK family in both THP-1 BTK^{WT} and BTK^{C481S} cells and an increase in abundance of PKC family members in the BTK^{C481S} cells. Kinase substrate enrichment analysis showed a decrease in NEK2 activity in THP-1 BTK^{WT} and BTK^{C481S} cells. Only discussed here are kinases for which both assays showed similar results or for which similar changes were seen in wild type as well as mutant cells within the same assay. RPS6 has previously been shown to be activated in FLT3-mutated AML cells and to mediate its antiapoptotic function through phosphorylation of the BH3-only protein BAD (Chen et al., 2010; Yang et al., 2005). RPS6KA1 was also identified as one of the top 10 kinases and a strong candidate as a target from drug response data from AML primary cells using AML 2.1 network properties and the KIEN analysis (Ong et al., 2015). The classical PKC family members are involved in pro-survival signalling and chemoresistance in leukaemia cells (Redig and Platanias, 2007, 2008). Elevated PKC β expression levels have been found in AML cell lines and blasts and inhibition of the kinase using enzastaurin was found to induce apoptosis but the mechanism of cell death does likely not involve PKC β (Ruvolo et al., 2011). NEK2 is a mitotic kinase involved in the regulation of cell cycle progression. NEK 2 has been found to be overexpressed in a variety of human cancers including leukaemia but the role of NEK2 in AML has not been studied yet.

Unfortunately, time restrictions only allowed us to perform these limited experiments. Additionally, the lack of an internal control is making it difficult to identify what effects observed are based on natural variation between experiments such as loading and sample processing and what changes in expression levels are actually down to the treatment and the mutational status. Experiments should therefore be repeated using one sample as a control for all runs allowing to normalize across the different experiments.

Conformation of target proteins should be performed by Western blot analysis. Western blot analysis of the elution samples from the beads could be performed to confirm successful pull down of BTK before performing mass spectrometry analysis. The affinity assay would also benefit from using multiple inhibitors as in the original studies (Duncan et al., 2012).

Chapter 6: Perspectives and future work

CRISPR – Does one size fit all?

The discovery of the CRISPR/Cas9 system as a gene editing tool is revolutionizing many areas of biomedical research including gene therapy, model cell line development, disease target identification and genomic screening. Its simplicity and flexibility to target nearly any location within the genome explains its popularity and widespread use. While other genome editing tools such as ZFNs and TALENs, have their own advantages, they lack the versatility of CRISPR and require more complex molecular biology expertise. The CRISPR/Cas9 system has its own drawbacks and there are several factors affecting its efficacy that still need to be addressed. Among these factors are target site selection, guide design, off- and on-target cleavage, HDR and NHEJ efficiency and how to deliver the required components. Even though the CRISPR technology has been used to create gene knock-out and knock-ins in human cell lines, animal models and nonviable human embryos, these issues preclude it from being used therapeutically.

The work described in this thesis can be used as an example for some of the issues. Even though the same strategy was used, differing knock-in efficiencies were observed between the five AML cell lines used. We successfully generated THP-1 BTK^{C481S} cells but the knock-in efficiency was too low in for example MV4-11 cells to isolate a mutation positive clone. Besides a low knock-in efficiency we also detected additional mutations in U937 cells in the BTK gene close to the target site showing the importance of sequencing the whole gene before and after targeting. If, and when, CRISPR is used for gene therapy the differences between patient DNA needs to be taken into account and therapy has to be individualized for safe and efficient usage.

For in vitro applications we, and others, have demonstrated that CRISPR is indeed a very powerful tool to precisely change the DNA sequence at a target location or prevent gene expression by generating knock-outs. Generating knock-outs using

CRISPR/Cas9 is advantageous over for example using shRNAs as it is permanent and guarantees a 100% knock-out efficiency by selecting a single cell clone containing the desired changes whereas the knock-down efficiency using shRNAs varies. Delivery of the CRISPR components is still the greatest obstacle even though several methods are available. We show here that by selecting the right delivery and selection strategy even hard to transfect cells can be edited using CRISPR allowing the study of proteins and drug resistance-related mutations by modifying gene expression levels and generating loss- or gain-of-function mutations. As the CRISPR field is developing so rapidly the outlook is certainly positive and current limitations are being addressed.

Is BTK a Potential Therapeutic Target in AML?

A phase 2 clinical trial into the effectiveness of ibrutinib in AML patients was undertaken following our group's unveiling of a role of BTK in AML (Cortes et al., 2015), however the trial was closed as there was no discernible improvement of AML patients with ibrutinib therapy either alone or in combination with standard therapy. There may be a role for BTK in AML in future, and indeed there are companies developing dual BTK/FLT3 inhibitors for the treatment of AML (Aptose Biosciences). Furthermore, information gained about BTK mutation-induced adaptations, will serve in lymphoid leukaemia drug-resistance mechanisms too.

The mutational landscape of AML is often complex and BTK is only one of the many kinases that has been found to show abnormal activity in AML. BTK is a protein of interest and our experiments in THP-1 and OCI-AML3 cell lines contribute to understanding the role BTK plays in those cell lines but more studies are required to investigate whether it has potential as a therapeutic target in the future or not. AML, being a disease with a heterogenous background, it makes it more difficult to interpret results as they do differ between different cell lines and between patient samples. If BTK is considered as a therapeutic target it will most likely be for a specific

cytogenetic/molecular abnormalities profile and as a combination therapy rather than a single agent.

Targeting BTK in AML appears most promising in FLT3-mutated AML and, as recently reported, in AML with G-CSFR mutations (Dwivedi et al., 2018). Even though the BTK^{C481S} mutation that we generated in AML cell lines using CRISPR/Cas9 does currently not appear in AML it still gives us the opportunity to study the drug resistance mechanism. Using CRISPR/Cas9 to generate mutations involved in drug resistance allows us to study those mutations and related effects to understand and overcome resistance mechanisms and find alternative therapeutic approaches.

Future work

In this thesis we successfully established a CRISPR/Cas9-based strategy to knock-out and generate a specific point mutation in the BTK gene, known as BTK^{C481S}. The strategy was established and validated in HEK-293T cells before being used in AML cell lines. Due to time constraints and technical issues only BTK^{C481S} mutant AML cells but not BTK knock-out cells were generated. This should be done in future experiments as it allows us to use these cells and the 'kinomics' approaches to compare the effects of knock-out with pharmacological inhibition of BTK. As BTKs role in AML is unclear it would help us to identify which effects are caused by CRISPR off-target effects, drug off-target binding or suppression of BTK expression itself.

Additional mutations close to the target site were detected in the BTK gene in U937 cells. Low BTK expression levels and additional Western blot bands when using p-BTK (Y223) and BTK antibodies in OCI-AML3 BTK^{C481S} cells were also observed. Whether this was caused by on-/off target effects or can be explained by clonal diversity would need to be analysed in further experiments. Whilst it is not realistic to do whole genome sequencing for every cell line that has been edited, targeted genes

should be fully sequenced to rule out any additional mutations that could affect protein expression, activity and conformation.

To provide the correct parental control for any experiments performed a single clonal cell should be selected and used for gene editing rather than editing a heterogenous population of cells. Although this would be time consuming with two rounds of clonal selection, it would help to reduce the 'noise' seen in kinome analysis.

Phosphoproteomics as well as the kinase assay were only performed once due to time constraints and should therefore be repeated as well potential substrates validated by Western blot. Cell proliferation and viability assays were also only performed a limited number of times and should be repeated. Fresh ibrutinib could be added to the cells every 24 h instead of every 48 h.

To better understand the role of BTK in AML and its potential as a therapeutic target more experiments need to be performed. Generating AML BTK knock-out cells as well as generating the BTK^{C481S} mutation in other cell lines is a good starting point. Especially MV4-11 cells that contain a FLT3-ITD mutation are of interest seeing that inhibition of BTK does affect cell proliferation and induces apoptosis in these cells (Oellerich et al., 2015). Some kinases that could be potential targets in AML were identified in Mass spectrometry analysis and should be studied further to explore their potential for combination therapy.

Appendix

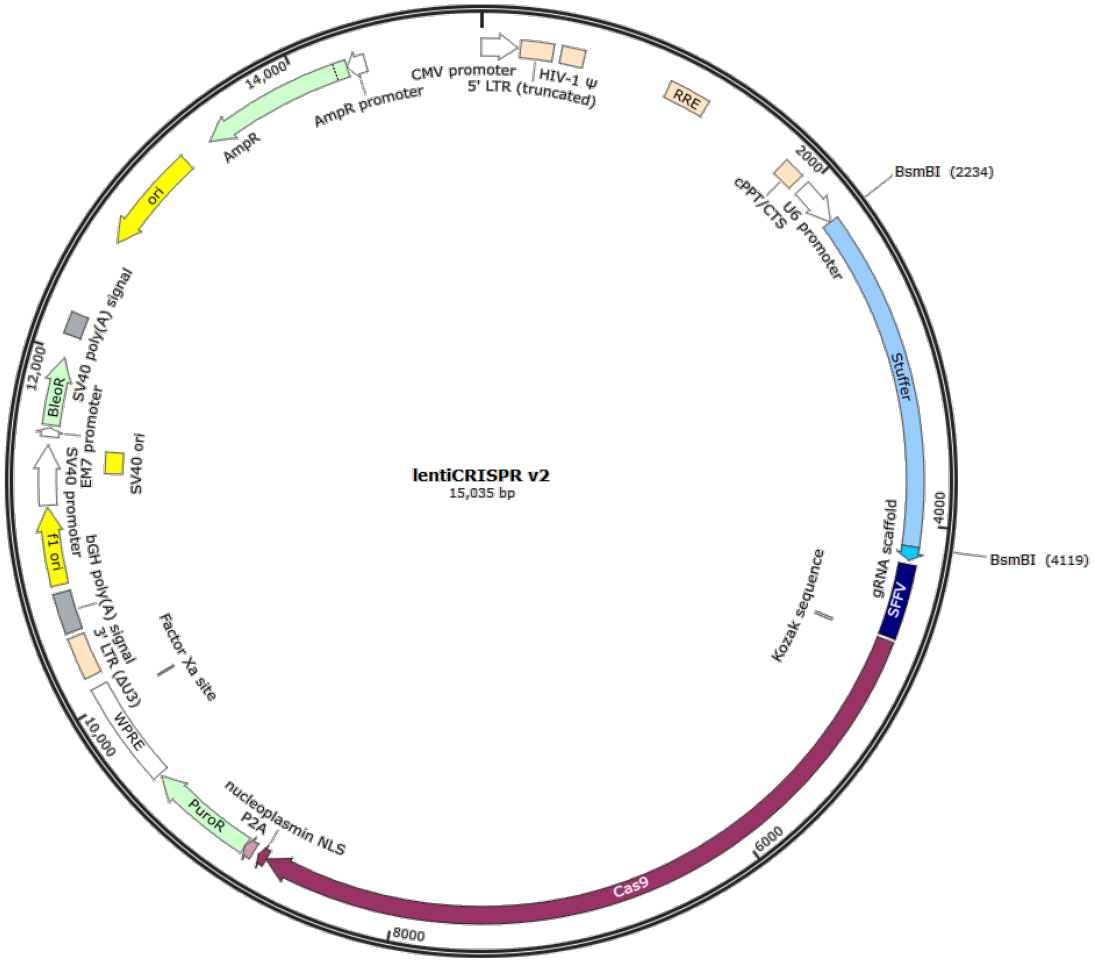

Figure A1 LentiCRISPR v2 plasmid

LentiCRISPR v2 plasmid is a lentiviral SpCas9-expressing plasmid purchased from Addgene (#52961). The original EF-1α core promoter was replaced with a SFFV promoter. For guide cloning, the plasmid was digested with BsmBI to remove the stuffer region and annealed, guide oligos were ligated into the plasmid.

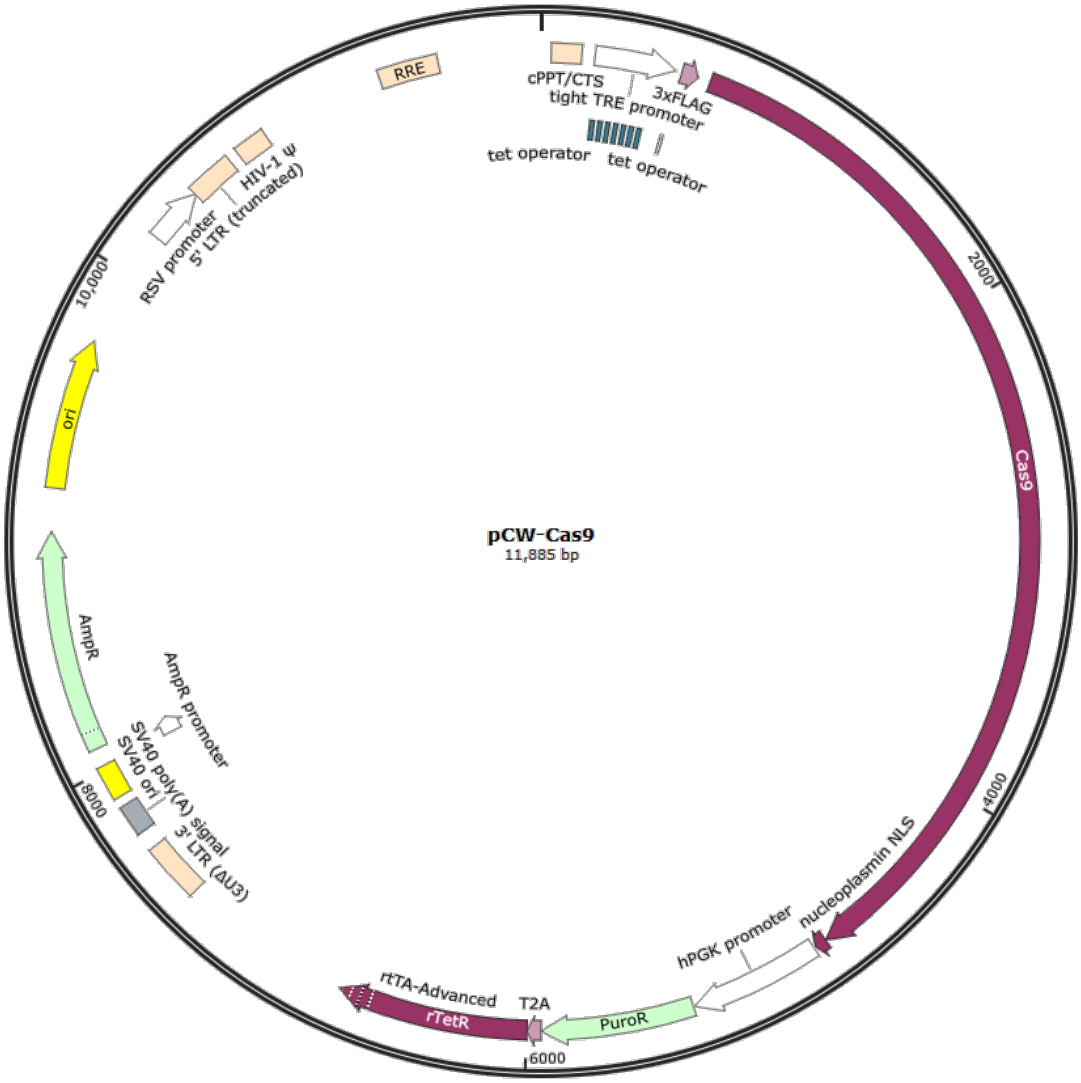

Figure A2 pCW-Cas9 plasmid

pCW-Cas9 plasmid is a doxycycline-inducible lentiviral SpCas9 expressing plasmid purchased from Addgene (#50661). Cas9 expression is under the control of a Tet-ON promoter.

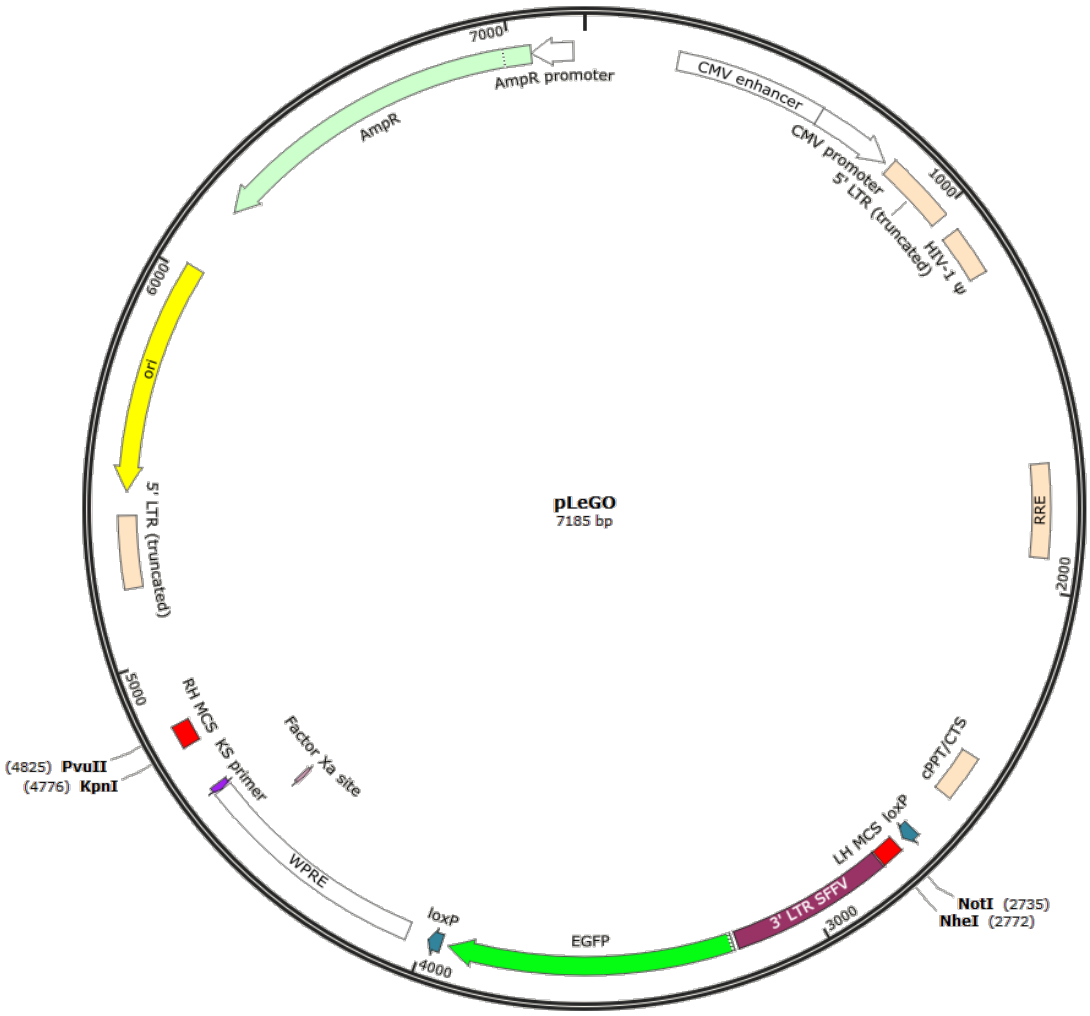

Figure A3 pLeGO plasmid

pLeGO is a lentiviral plasmid purchased from Addgene (#27341) that expresses EGFP under the control of a SFFV promoter. This plasmid was modified by adding two multiple cloning sites (LH and RH MCS depicted in red) flanking the EGFP selection cassette. The additional restriction sites allowed us to clone guide#3 and the HDR template in the LH MCS using NheI and NotI. This plasmid was also used to clone guides #7,8,9 and 10 including U6 promoters and the gRNA scaffolds. 2 guides were cloned into the LH MCS using NheI and NotI and the other two guides were cloned into the RH MCS using KpnI and PvuII.

Figure A4 pX459 plasmid

pX459 is a SpCas9-expressing plasmid under the control of a Cbh promoter purchased from Addgene (#62988). Guides were cloned into the plasmid digested with BbsI adjacent to the gRNA scaffold sequence.

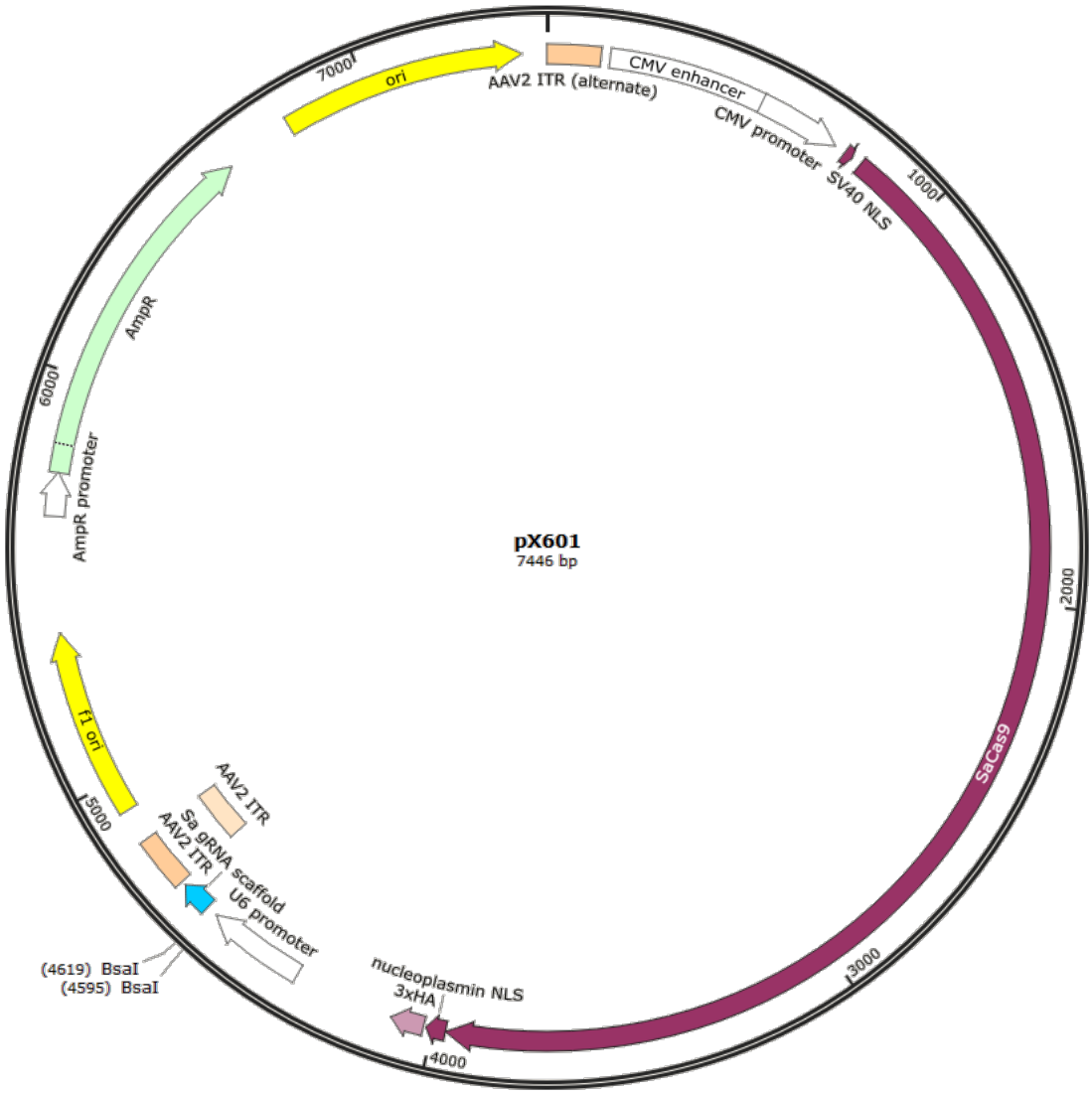

Figure A5 pX601 plasmid

pX601 is an Adeno-associated viral plasmid that expresses SaCas9 under the control of a CMV promoter. pX601 was purchased from Addgene (#61591) and guide#6 was cloned into the plasmid digested with BsaI.

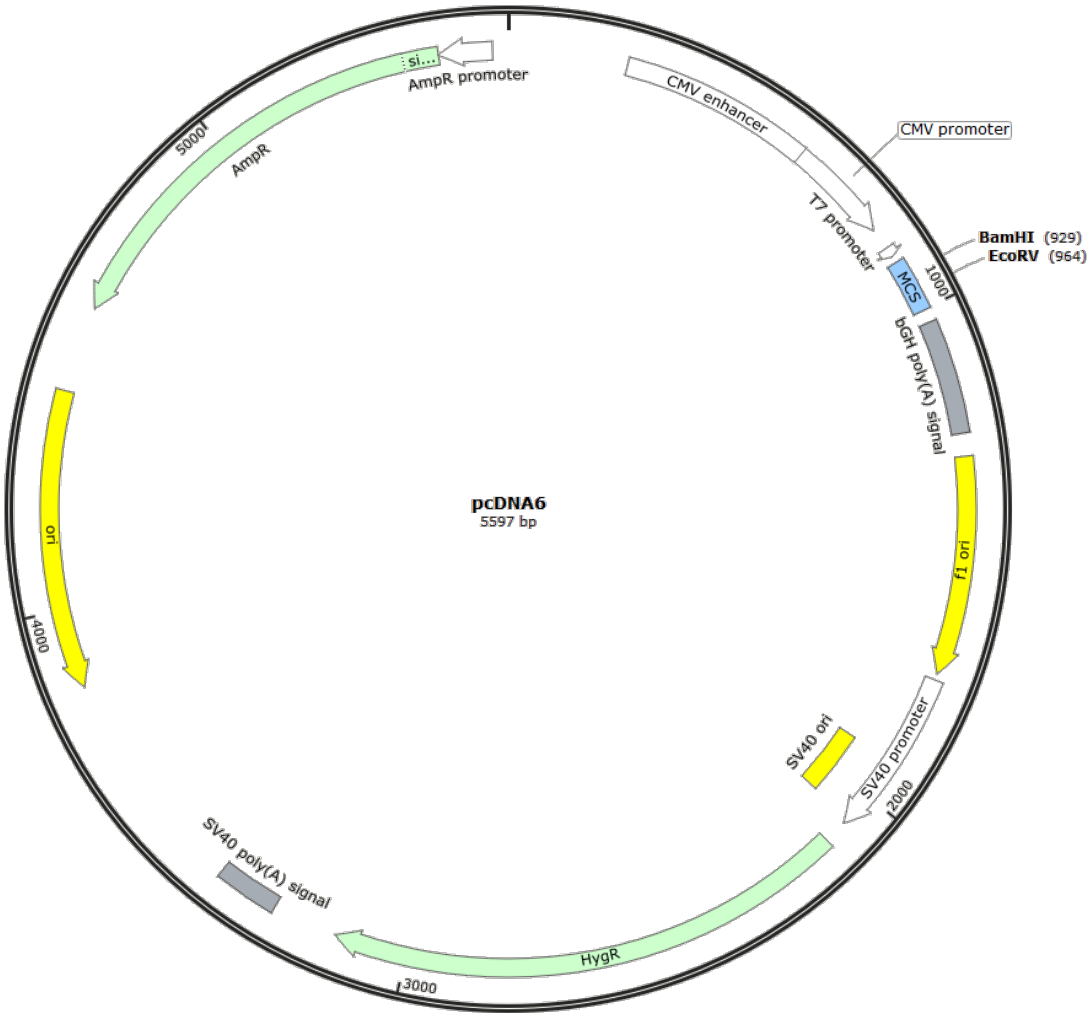

Figure A6 pcDNA6 plasmid

The pcDNA6 plasmid was a kind gift from Dr. Nicholas Harper. The BTK gene was amplified from a spleen cDNA library adding restrictions sites for cloning into the plasmid digested with BamHI and EcoRV.

References

Abdel-Wahab, O., & Levine, R. L. (2013). Mutations in epigenetic modifiers in the pathogenesis and therapy of acute myeloid leukemia. *Blood, 121*(18), 3563-3572. doi:10.1182/blood-2013-01-451781

Alcolea, M. P., Casado, P., Rodriguez-Prados, J. C., Vanhaesebroeck, B., & Cutillas, P. R. (2012). Phosphoproteomic analysis of leukemia cells under basal and drug-treated conditions identifies markers of kinase pathway activation and mechanisms of resistance. *Mol Cell Proteomics, 11*(8), 453-466. doi:10.1074/mcp.M112.017483

Almeida, A. M., & Ramos, F. (2016). Acute myeloid leukemia in the older adults. *Leuk Res Rep, 6*, 1-7. doi:10.1016/j.lrr.2016.06.001

Arber, D. A., Orazi, A., Hasserjian, R., Thiele, J., Borowitz, M. J., Le Beau, M. M., Vardiman, J. W. (2016). The 2016 revision to the World Health Organization classification of myeloid neoplasms and acute leukemia. Blood, 127(20), 2391-2405. doi:10.1182/blood-2016-03-643544

Bennett, J. M., Catovsky, D., Daniel, M. T., Flandrin, G., Galton, D. A., Gralnick, H. R., & Sultan, C. (1976). Proposals for the classification of the acute leukaemias. French-American-British (FAB) co-operative group. Br J Haematol, 33(4), 451-458.

Bhullar, K. S., Lagaron, N. O., McGowan, E. M., Parmar, I., Jha, A., Hubbard, B. P., & Rupasinghe, H. P. V. (2018). Kinase-targeted cancer therapies: progress, challenges and future directions. Mol Cancer, 17(1), 48. doi:10.1186/s12943-018-0804-2

Bibikova, M., Carroll, D., Segal, D. J., Trautman, J. K., Smith, J., Kim, Y. G., & Chandrasegaran, S. (2001). Stimulation of homologous recombination through targeted cleavage by chimeric nucleases. *Molecular and Cellular Biology, 21*(1), 289-297. doi:Doi 10.1128/Mcb.21.1.289-297.2001

Bischoff, K. M., Shi, L., & Kennelly, P. J. (1998). The detection of enzyme activity following sodium dodecyl sulfate-polyacrylamide gel electrophoresis. *Anal Biochem, 260*(1), 1-17. doi:10.1006/abio.1998.2680

Blume-Jensen, P., & Hunter, T. (2001). Oncogenic kinase signalling. *Nature, 411*(6835), 355-365. doi:10.1038/35077225

Boch, J., & Bonas, U. (2010). Xanthomonas AvrBs3 family-type III effectors: discovery and function. *Annu Rev Phytopathol, 48*, 419-436. doi:10.1146/annurev-phyto-080508-081936

Boch, J., Scholze, H., Schornack, S., Landgraf, A., Hahn, S., Kay, S.,Bonas, U. (2009). Breaking the code of DNA binding specificity of TAL-type III effectors. *Science, 326*(5959), 1509-1512. doi:10.1126/science.1178811

Bose, P., Gandhi, V. V., & Keating, M. J. (2016). Pharmacokinetic and pharmacodynamic evaluation of ibrutinib for the treatment of chronic lymphocytic leukemia: rationale for lower doses. *Expert Opin Drug Metab Toxicol, 12*(11), 1381-1392. doi:10.1080/17425255.2016.1239717

Brunet, E., Simsek, D., Tomishima, M., DeKelver, R., Choi, V. M., Gregory, P., . . . Jasin, M. (2009). Chromosomal translocations induced at specified loci in human stem cells. *Proc Natl Acad Sci U S A, 106*(26), 10620-10625. doi:10.1073/pnas.0902076106

Byrd, J. C., Brown, J. R., O'Brien, S., Barrientos, J. C., Kay, N. E., Reddy, N. M., . . . Investigators, R. (2014). Ibrutinib versus ofatumumab in previously treated chronic lymphoid leukemia. *N Engl J Med, 371*(3), 213-223. doi:10.1056/NEJMoa1400376

Byrd, J. C., Furman, R. R., Coutre, S. E., Burger, J. A., Blum, K. A., Coleman, M.O'Brien, S. (2015). Three-year follow-up of treatment-naive and previously treated patients with CLL and SLL receiving single-agent ibrutinib. *Blood, 125*(16), 2497-2506. doi:10.1182/blood-2014-10-606038

Byrd, J. C., Harrington, B., O'Brien, S., Jones, J. A., Schuh, A., Devereux, S.Furman, R. R. (2016). Acalabrutinib (ACP-196) in Relapsed Chronic Lymphocytic Leukemia. *N Engl J Med, 374*(4), 323-332. doi:10.1056/NEJMoa1509981

Caldeira, D., Alves, D., Costa, J., Ferreira, J. J., & Pinto, F. J. (2019). Ibrutinib increases the risk of hypertension and atrial fibrillation: Systematic review and meta-analysis. *Plos One, 14*(2), e0211228. doi:10.1371/journal.pone.0211228

Campbell, R., Chong, G., & Hawkes, E. A. (2018). Novel Indications for Bruton's Tyrosine Kinase Inhibitors, beyond Hematological Malignancies. *J Clin Med, 7*(4). doi:10.3390/jcm7040062

Cancer Genome Atlas Research, N., Ley, T. J., Miller, C., Ding, L., Raphael, B. J., Mungall, A. J.Eley, G. (2013). Genomic and epigenomic landscapes of adult de novo acute myeloid leukemia. *N Engl J Med, 368*(22), 2059-2074. doi:10.1056/NEJMoa1301689

Capecchi, M. R. (1989). Altering the genome by homologous recombination. *Science, 244*(4910), 1288-1292.

Capecchi, M. R. (2005). Gene targeting in mice: functional analysis of the mammalian genome for the twenty-first century. *Nat Rev Genet, 6*(6), 507-512. doi:10.1038/nrg1619

Caron, A. W., Nicolas, C., Gaillet, B., Ba, I., Pinard, M., Garnier, A.Gilbert, R. (2009). Fluorescent labeling in semi-solid medium for selection of mammalian cells secreting high-levels of recombinant proteins. *BMC Biotechnol, 9*, 42. doi:10.1186/1472-6750-9-42

Carroll, D. (2011). Genome engineering with zinc-finger nucleases. *Genetics, 188*(4), 773-782. doi:10.1534/genetics.111.131433

Casado, P., Rodriguez-Prados, J. C., Cosulich, S. C., Guichard, S., Vanhaesebroeck, B., Joel, S., & Cutillas, P. R. (2013). Kinase-substrate enrichment analysis provides insights into the heterogeneity of signaling pathway activation in leukemia cells. *Sci Signal, 6*(268), rs6. doi:10.1126/scisignal.2003573

Chen, J., Kinoshita, T., Sukbuntherng, J., Chang, B. Y., & Elias, L. (2016). Ibrutinib Inhibits ERBB Receptor Tyrosine Kinases and HER2-Amplified Breast Cancer Cell Growth. *Mol Cancer Ther, 15*(12), 2835-2844. doi:10.1158/1535-7163.MCT-15-0923

Chen, W. N., Drakos, E., Grammatikakis, I., Schlette, E. J., Li, J. A., Leventaki, V.Rassidakis, G. Z. (2010). mTOR signaling is activated by FLT3 kinase and promotes survival of FLT3-mutated acute myeloid leukemia cells. *Molecular Cancer, 9*. doi:Artn 29210.1186/1476-4598-9-292

Cebrian-Serrano, A., & Davies, B. (2017). CRISPR-Cas orthologues and variants: optimizing the repertoire, specificity and delivery of genome engineering tools. *Mamm Genome, 28*(7-8), 247-261. doi:10.1007/s00335-017-9697-4

Cheng, S., Guo, A., Lu, P., Ma, J., Coleman, M., & Wang, Y. L. (2015). Functional characterization of BTK(C481S) mutation that confers ibrutinib resistance: exploration of alternative kinase inhibitors. *Leukemia, 29*(4), 895-900. doi:10.1038/leu.2014.263

Chew, W. L., Tabebordbar, M., Cheng, J. K., Mali, P., Wu, E. Y., Ng, A. H.Church, G. M. (2016). A multifunctional AAV-CRISPR-Cas9 and its host response. *Nat Methods, 13*(10), 868-874. doi:10.1038/nmeth.3993

Chiron, D., Di Liberto, M., Martin, P., Huang, X., Sharman, J., Blecua, P.Chen-Kiang, S. (2014). Cell-cycle reprogramming for PI3K inhibition overrides a relapse-specific C481S BTK mutation revealed by longitudinal functional genomics in mantle cell lymphoma. *Cancer Discov, 4*(9), 1022-1035. doi:10.1158/2159-8290.CD-14-0098

Cho, S. W., Kim, S., Kim, J. M., & Kim, J. S. (2013). Targeted genome engineering in human cells with the Cas9 RNA-guided endonuclease. *Nature Biotechnology, 31*(3), 230-232. doi:10.1038/nbt.2507

Chou, S. T., Leng, Q., & Mixson, A. J. (2012). Zinc Finger Nucleases: Tailor-made for Gene Therapy. *Drugs Future, 37*(3), 183-196.

Chu, V. T., Weber, T., Wefers, B., Wurst, W., Sander, S., Rajewsky, K., & Kuhn, R. (2015). Increasing the efficiency of homology-directed repair for CRISPR-Cas9-induced precise gene editing in mammalian cells. *Nat Biotechnol, 33*(5), 543-548. doi:10.1038/nbt.3198

Cong, L., Ran, F. A., Cox, D., Lin, S., Barretto, R., Habib, N.Zhang, F. (2013). Multiplex genome engineering using CRISPR/Cas systems. *Science, 339*(6121), 819-823. doi:10.1126/science.1231143

Cortes, J. E., Estey, E., Stein, A. S., Graef, T., Cavazos, N., Kinoshita, T., . . . Tawashi, A. (2015). A multicenter, open-label phase 2a study of ibrutinib with or without cytarabine in patients with acute myeloid leukemia (PCYC-1131). *33*(15_suppl), TPS7096-TPS7096. doi:10.1200/jco.2015.33.15_suppl.tps7096

Crawford, J. J., Johnson, A. R., Misner, D. L., Belmont, L. D., Castanedo, G., Choy, R.Young, W. B. (2018). Discovery of GDC-0853: A Potent, Selective, and Noncovalent Bruton's Tyrosine Kinase Inhibitor in Early Clinical Development. *J Med Chem, 61*(6), 2227-2245. doi:10.1021/acs.jmedchem.7b01712

D'Cruz, O. J., & Uckun, F. M. (2013). Novel Bruton's tyrosine kinase inhibitors currently in development. *Onco Targets Ther, 6*, 161-176. doi:10.2147/OTT.S33732

De Kouchkovsky, I., & Abdul-Hay, M. (2016). 'Acute myeloid leukemia: a comprehensive review and 2016 update'. *Blood Cancer J, 6*(7), e441. doi:10.1038/bcj.2016.50

Deltcheva, E., Chylinski, K., Sharma, C. M., Gonzales, K., Chao, Y., Pirzada, Z. A.Charpentier, E. (2011). CRISPR RNA maturation by trans-encoded small RNA and host factor RNase III. *Nature, 471*(7340), 602-607. doi:10.1038/nature09886

Deng, D., Yan, C., Pan, X., Mahfouz, M., Wang, J., Zhu, J. K.Yan, N. (2012). Structural basis for sequence-specific recognition of DNA by TAL effectors. *Science, 335*(6069), 720-723. doi:10.1126/science.1215670

Dohner, H., Estey, E. H., Amadori, S., Appelbaum, F. R., Buchner, T., Burnett, A. K.European, L. (2010). Diagnosis and management of acute myeloid leukemia in adults: recommendations from an international expert panel, on behalf of the European LeukemiaNet. *Blood, 115*(3), 453-474. doi:10.1182/blood-2009-07-235358

Drake, J. M., Lee, J. K., & Witte, O. N. (2014). Clinical targeting of mutated and wild-type protein tyrosine kinases in cancer. *Molecular and Cellular Biology, 34*(10), 1722-1732. doi:10.1128/MCB.01592-13

Dreyling, M., Jurczak, W., Jerkeman, M., Silva, R. S., Rusconi, C., Trneny, M., . . . Rule, S. (2016). Ibrutinib versus temsirolimus in patients with relapsed or refractory mantle-cell lymphoma: an international, randomised, open-label, phase 3 study. *Lancet, 387*(10020), 770-778. doi:10.1016/S0140-6736(15)00667-4

Dull, T., Zufferey, R., Kelly, M., Mandel, R. J., Nguyen, M., Trono, D., & Naldini, L. (1998). A third-generation lentivirus vector with a conditional packaging system. *J Virol, 72*(11), 8463-8471.

Duncan, J. S., Whittle, M. C., Nakamura, K., Abell, A. N., Midland, A. A., Zawistowski, J. S.Johnson, G. L. (2012). Dynamic reprogramming of the kinome in response to targeted MEK inhibition in triple-negative breast cancer. *Cell, 149*(2), 307-321. doi:10.1016/j.cell.2012.02.053

Dwivedi, P., Muench, D. E., Wagner, M., Azam, M., Grimes, H. L., & Greis, K. D. (2018). Time resolved quantitative phospho-tyrosine analysis reveals Bruton's Tyrosine kinase mediated signaling downstream of the mutated granulocyte-colony stimulating factor receptors. *Leukemia*. doi:10.1038/s41375-018-0188-8

Eckhart, W., Hutchinson, M. A., & Hunter, T. (1979). An activity phosphorylating tyrosine in polyoma T antigen immunoprecipitates. *Cell, 18*(4), 925-933.

Faderl, S., Talpaz, M., Estrov, Z., O'Brien, S., Kurzrock, R., & Kantarjian, H. M. (1999). The biology of chronic myeloid leukemia. *N Engl J Med, 341*(3), 164-172. doi:10.1056/NEJM199907153410306

Fiedler, K., Sindrilaru, A., Terszowski, G., Kokai, E., Feyerabend, T. B., Bullinger, L.Brunner, C. (2011). Neutrophil development and function critically depend on Bruton tyrosine kinase in a mouse model of X-linked agammaglobulinemia. *Blood, 117*(4), 1329-1339. doi:10.1182/blood-2010-04-281170

Fluckiger, A. C., Li, Z., Kato, R. M., Wahl, M. I., Ochs, H. D., Longnecker, R.Rawlings, D. J. (1998). Btk/Tec kinases regulate sustained increases in intracellular Ca2+ following B-cell receptor activation. *EMBO J, 17*(7), 1973-1985. doi:10.1093/emboj/17.7.1973

Fonfara, I., Richter, H., Bratovic, M., Le Rhun, A., & Charpentier, E. (2016). The CRISPR-associated DNA-cleaving enzyme Cpf1 also processes precursor CRISPR RNA. *Nature, 532*(7600), 517-+. doi:10.1038/nature17945

Fu, Y., Foden, J. A., Khayter, C., Maeder, M. L., Reyon, D., Joung, J. K., & Sander, J. D. (2013). High-frequency off-target mutagenesis induced by CRISPR-Cas nucleases in human cells. *Nat Biotechnol, 31*(9), 822-826. doi:10.1038/nbt.2623

Furman, R. R., Cheng, S., Lu, P., Setty, M., Perez, A. R., Guo, A.Wang, Y. L. (2014). Ibrutinib resistance in chronic lymphocytic leukemia. *N Engl J Med, 370*(24), 2352-2354. doi:10.1056/NEJMc1402716

Galloway, J. L., & Zon, L. I. (2003). Ontogeny of hematopoiesis: examining the emergence of hematopoietic cells in the vertebrate embryo. *Curr Top Dev Biol, 53*, 139-158.

Garraway, L. A., & Janne, P. A. (2012). Circumventing cancer drug resistance in the era of personalized medicine. *Cancer Discov, 2*(3), 214-226. doi:10.1158/2159-8290.CD-12-0012

Gayko, U., Fung, M., Clow, F., Sun, S., Faust, E., Price, S.Zhuang, S. H. (2015). Development of the Bruton's tyrosine kinase inhibitor ibrutinib for B cell malignancies. *Ann N Y Acad Sci, 1358*, 82-94. doi:10.1111/nyas.12878

Gilbert, L. A., Horlbeck, M. A., Adamson, B., Villalta, J. E., Chen, Y., Whitehead, E. H., . . . Weissman, J. S. (2014). Genome-Scale CRISPR-Mediated Control of Gene Repression and Activation. *Cell, 159*(3), 647-661. doi:10.1016/j.cell.2014.09.029

Gilbert, L. A., Larson, M. H., Morsut, L., Liu, Z., Brar, G. A., Torres, S. E., . . . Qi, L. S. (2013). CRISPR-mediated modular RNA-guided regulation of transcription in eukaryotes. *Cell, 154*(2), 442-451. doi:10.1016/j.cell.2013.06.044

Gilliland, D. G., & Griffin, J. D. (2002). The roles of FLT3 in hematopoiesis and leukemia. *Blood, 100*(5), 1532-1542. doi:10.1182/blood-2002-02-0492

Gocek, E., Moulas, A. N., & Studzinski, G. P. (2014). Non-receptor protein tyrosine kinases signaling pathways in normal and cancer cells. *Crit Rev Clin Lab Sci, 51*(3), 125-137. doi:10.3109/10408363.2013.874403

Graham, D. B., & Root, D. E. (2015). Resources for the design of CRISPR gene editing experiments. *Genome Biol, 16*, 260. doi:10.1186/s13059-015-0823-x

Grove, C. S., & Vassiliou, G. S. (2014). Acute myeloid leukaemia: a paradigm for the clonal evolution of cancer? *Dis Model Mech, 7*(8), 941-951. doi:10.1242/dmm.015974

Gustafsson, M. O., Hussain, A., Mohammad, D. K., Mohamed, A. J., Nguyen, V., Metalnikov, P.Nore, B. F. (2012). Regulation of Nucleocytoplasmic Shuttling of Bruton's Tyrosine Kinase (Btk) through a Novel SH3-Dependent Interaction with Ankyrin Repeat Domain 54 (ANKRD54). *Molecular and Cellular Biology, 32*(13), 2440-2453. doi:10.1128/Mcb.06620-11

Hendriks, R. W., Yuvaraj, S., & Kil, L. P. (2014). Targeting Bruton's tyrosine kinase in B cell malignancies. *Nat Rev Cancer, 14*(4), 219-232. doi:10.1038/nrc3702

Hilton, I. B., D'Ippolito, A. M., Vockley, C. M., Thakore, P. I., Crawford, G. E., Reddy, T. E., & Gersbach, C. A. (2015). Epigenome editing by a CRISPR-Cas9-based acetyltransferase activates genes from promoters and enhancers. *Nature Biotechnology, 33*(5), 510-517. doi:10.1038/nbt.3199

Horwood, N. J., Page, T. H., McDaid, J. P., Palmer, C. D., Campbell, J., Mahon, T.Foxwell, B. M. (2006). Bruton's tyrosine kinase is required for TLR2 and TLR4-induced TNF, but not IL-6, production. *J Immunol, 176*(6), 3635-3641

Howe, J. R., Skryabin, B. V., Belcher, S. M., Zerillo, C. A., & Schmauss, C. (1995). The responsiveness of a tetracycline-sensitive expression system differs in different cell lines. *J Biol Chem, 270*(23), 14168-14174.

Hsu, P. D., Scott, D. A., Weinstein, J. A., Ran, F. A., Konermann, S., Agarwala, V.Zhang, F. (2013). DNA targeting specificity of RNA-guided Cas9 nucleases. *Nat Biotechnol, 31*(9), 827-832. doi:10.1038/nbt.2647

Hubbard, S. R., & Till, J. H. (2000). Protein tyrosine kinase structure and function. *Annu Rev Biochem, 69*, 373-398. doi:10.1146/annurev.biochem.69.1.373

Hussain, A., Yu, L., Faryal, R., Mohammad, D. K., Mohamed, A. J., & Smith, C. I. (2011). TEC family kinases in health and disease--loss-of-function of BTK and ITK and the gain-of-function fusions ITK-SYK and BTK-SYK. *Febs j, 278*(12), 2001-2010. doi:10.1111/j.1742-4658.2011.08134.x

Hyvonen, M., & Saraste, M. (1997). Structure of the PH domain and Btk motif from Bruton's tyrosine kinase: molecular explanations for X-linked agammaglobulinaemia. *EMBO J, 16*(12), 3396-3404. doi:10.1093/emboj/16.12.3396

Jagannathan-Bogdan, M., & Zon, L. I. (2013). Hematopoiesis. *Development, 140*(12), 2463-2467. doi:10.1242/dev.083147

JanssenMD® Retrieved from https://www.janssenmd.com/pdf/imbruvica/imbruvica_pi.pdf

Jeon, Y., Choi, Y. H., Jang, Y., Yu, J., Goo, J., Lee, G.Bae, S. (2018). Direct observation of DNA target searching and cleavage by CRISPR-Cas12a. *Nat Commun, 9*(1), 2777. doi:10.1038/s41467-018-05245-x

Jinek, M., Chylinski, K., Fonfara, I., Hauer, M., Doudna, J. A., & Charpentier, E. (2012). A programmable dual-RNA-guided DNA endonuclease in adaptive bacterial immunity. *Science, 337*(6096), 816-821. doi:10.1126/science.1225829

Jinek, M., East, A., Cheng, A., Lin, S., Ma, E., & Doudna, J. (2013). RNA-programmed genome editing in human cells. *Elife, 2*, e00471. doi:10.7554/eLife.00471

John A. Schiel, E. C., Maren Mayer, Emily M. Anderson, and Anja van Brabant Smith (2015). Homology-directed repair with Dharmacon™ Edit-R™ CRISPR-Cas9 reagents and single-stranded DNA oligos. *Dharmacon*.

Johnson, A. R., Kohli, P. B., Katewa, A., Gogol, E., Belmont, L. D., Choy, R., . . . Young, W. B. (2016). Battling Btk Mutants With Noncovalent Inhibitors That Overcome Cys481 and Thr474 Mutations. *ACS Chem Biol, 11*(10), 2897-2907. doi:10.1021/acschembio.6b00480

Joung, J. K., & Sander, J. D. (2013). TALENs: a widely applicable technology for targeted genome editing. *Nat Rev Mol Cell Biol, 14*(1), 49-55. doi:10.1038/nrm3486

Kakarougkas, A., & Jeggo, P. A. (2014). DNA DSB repair pathway choice: an orchestrated handover mechanism. *Br J Radiol, 87*(1035), 20130685. doi:10.1259/bjr.20130685

Kannan, R., & Ventura, A. (2015). The CRISPR revolution and its impact on cancer research. *Swiss Med Wkly, 145*, w14230. doi:10.4414/smw.2015.14230

Kantarjian, H., O'Brien, S., Cortes, J., Giles, F., Faderl, S., Jabbour, E., . . . Estey, E. (2006). Results of intensive chemotherapy in 998 patients age 65 years or older with acute myeloid leukemia or high-risk myelodysplastic syndrome: predictive prognostic models for outcome. *Cancer, 106*(5), 1090-1098. doi:10.1002/cncr.21723

Kantarjian, H., O'Brien, S., Jabbour, E., Garcia-Manero, G., Quintas-Cardama, A., Shan, J., . . . Cortes, J. (2012). Improved survival in chronic myeloid leukemia since the introduction of imatinib therapy: a single-institution historical experience. *Blood, 119*(9), 1981-1987. doi:10.1182/blood-2011-08-358135

Kawakami, Y., Inagaki, N., Salek-Ardakani, S., Kitaura, J., Tanaka, H., Nagao, K., . . . Kawakami, T. (2006). Regulation of dendritic cell maturation and function by Bruton's tyrosine kinase via IL-10 and Stat3. *Proc Natl Acad Sci U S A, 103*(1), 153-158. doi:10.1073/pnas.0509784103

Kelly, L. M., & Gilliland, D. G. (2002). Genetics of myeloid leukemias. *Annu Rev Genomics Hum Genet, 3*, 179-198. doi:10.1146/annurev.genom.3.032802.115046

Kim, H., & Kim, J. S. (2014). A guide to genome engineering with programmable nucleases. *Nat Rev Genet, 15*(5), 321-334. doi:10.1038/nrg3686

Kim, J. S. (2016). Genome editing comes of age. *Nat Protoc, 11*(9), 1573-1578. doi:10.1038/nprot.2016.104

Kim, Y. G., Cha, J., & Chandrasegaran, S. (1996). Hybrid restriction enzymes: zinc finger fusions to Fok I cleavage domain. *Proc Natl Acad Sci U S A, 93*(3), 1156-1160.

Kobayashi, J., Antoccia, A., Tauchi, H., Matsuura, S., & Komatsu, K. (2004). NBS1 and its functional role in the DNA damage response. *DNA Repair (Amst), 3*(8-9), 855-861. doi:10.1016/j.dnarep.2004.03.023

Komarova, N. L., Burger, J. A., & Wodarz, D. (2014). Evolution of ibrutinib resistance in chronic lymphocytic leukemia (CLL). *Proc Natl Acad Sci U S A, 111*(38), 13906-13911. doi:10.1073/pnas.1409362111

Komor, A. C., Badran, A. H., & Liu, D. R. (2017). CRISPR-Based Technologies for the Manipulation of Eukaryotic Genomes. *Cell, 168*(1-2), 20-36. doi:10.1016/j.cell.2016.10.044

Kondo, M., Wagers, A. J., Manz, M. G., Prohaska, S. S., Scherer, D. C., Beilhack, G. F.Weissman, I. L. (2003). Biology of hematopoietic stem cells and progenitors: implications for clinical application. *Annu Rev Immunol, 21*, 759-806. doi:10.1146/annurev.immunol.21.120601.141007

Koonin, E. V., Makarova, K. S., & Zhang, F. (2017). Diversity, classification and evolution of CRISPR-Cas systems. *Curr Opin Microbiol, 37*, 67-78. doi:10.1016/j.mib.2017.05.008

Krause, D. S., & Van Etten, R. A. (2005). Tyrosine kinases as targets for cancer therapy. *New England Journal of Medicine, 353*(2), 172-187. doi:DOI 10.1056/NEJMra044389

Kumar, C. C. (2011). Genetic abnormalities and challenges in the treatment of acute myeloid leukemia. *Genes Cancer, 2*(2), 95-107. doi:10.1177/1947601911408076

Larsen, M. R., Thingholm, T. E., Jensen, O. N., Roepstorff, P., & Jorgensen, T. J. (2005). Highly selective enrichment of phosphorylated peptides from peptide mixtures using titanium dioxide microcolumns. *Mol Cell Proteomics, 4*(7), 873-886. doi:10.1074/mcp.T500007-MCP200

Lee, H. J., Kim, E., & Kim, J. S. (2010). Targeted chromosomal deletions in human cells using zinc finger nucleases. *Genome Res, 20*(1), 81-89. doi:10.1101/gr.099747.109

Lee, H. J., Kweon, J., Kim, E., Kim, S., & Kim, J. S. (2012). Targeted chromosomal duplications and inversions in the human genome using zinc finger nucleases. *Genome Res, 22*(3), 539-548. doi:10.1101/gr.129635.111

Lee, S. W., Tsou, A. P., Chan, H., Thomas, J., Petrie, K., Eugui, E. M., & Allison, A. C. (1988). Glucocorticoids selectively inhibit the transcription of the interleukin 1 beta gene and decrease the stability of interleukin 1 beta mRNA. *Proc Natl Acad Sci U S A, 85*(4), 1204-1208.

Lin, J., & Weiss, A. (2001). T cell receptor signalling. *J Cell Sci, 114*(Pt 2), 243-244.

Lindvall, J. M., Blomberg, K. E., Valiaho, J., Vargas, L., Heinonen, J. E., Berglof, A.Smith, C. I. (2005). Bruton's tyrosine kinase: cell biology, sequence

conservation, mutation spectrum, siRNA modifications, and expression profiling. *Immunol Rev, 203*, 200-215. doi:10.1111/j.0105-2896.2005.00225.x

Liu, C., Zhang, L., Liu, H., & Cheng, K. (2017). Delivery strategies of the CRISPR-Cas9 gene-editing system for therapeutic applications. *J Control Release, 266*, 17-26. doi:10.1016/j.jconrel.2017.09.012

Liu, T. M., Woyach, J. A., Zhong, Y., Lozanski, A., Lozanski, G., Dong, S., . . . Johnson, A. J. (2015). Hypermorphic mutation of phospholipase C, gamma2 acquired in ibrutinib-resistant CLL confers BTK independency upon B-cell receptor activation. *Blood, 126*(1), 61-68. doi:10.1182/blood-2015-02-626846

Maddalo, D., Manchado, E., Concepcion, C. P., Bonetti, C., Vidigal, J. A., Han, Y. C.Ventura, A. (2014). In vivo engineering of oncogenic chromosomal rearrangements with the CRISPR/Cas9 system. *Nature, 516*(7531), 423-427. doi:10.1038/nature13902

Maddocks, K. J., Ruppert, A. S., Lozanski, G., Heerema, N. A., Zhao, W., Abruzzo, L.Woyach, J. A. (2015). Etiology of Ibrutinib Therapy Discontinuation and Outcomes in Patients With Chronic Lymphocytic Leukemia. *Jama Oncology, 1*(1), 80-87. doi:10.1001/jamaoncol.2014.218

Mahaney, B. L., Meek, K., & Lees-Miller, S. P. (2009). Repair of ionizing radiation-induced DNA double-strand breaks by non-homologous end-joining. *Biochem J, 417*(3), 639-650. doi:10.1042/BJ20080413

Mali, P., Yang, L., Esvelt, K. M., Aach, J., Guell, M., DiCarlo, J. E., . . . Church, G. M. (2013). RNA-guided human genome engineering via Cas9. *Science, 339*(6121), 823-826. doi:10.1126/science.1232033

Manning, G., Plowman, G. D., Hunter, T., & Sudarsanam, S. (2002). Evolution of protein kinase signaling from yeast to man. *Trends Biochem Sci, 27*(10), 514-520.

Manning, G., Whyte, D. B., Martinez, R., Hunter, T., & Sudarsanam, S. (2002). The protein kinase complement of the human genome. *Science, 298*(5600), 1912-1934. doi:10.1126/science.1075762

Michor, F., Hughes, T. P., Iwasa, Y., Branford, S., Shah, N. P., Sawyers, C. L., & Nowak, M. A. (2005). Dynamics of chronic myeloid leukaemia. *Nature, 435*(7046), 1267-1270. doi:10.1038/nature03669

Miller, J. C., Tan, S., Qiao, G., Barlow, K. A., Wang, J., Xia, D. F., . . . Rebar, E. J. (2011). A TALE nuclease architecture for efficient genome editing. *Nature Biotechnology, 29*(2), 143-148. doi:10.1038/nbt.1755

Mohamed, A. J., Nore, B. F., Christensson, B., & Smith, C. I. (1999). Signalling of Bruton's tyrosine kinase, Btk. *Scand J Immunol, 49*(2), 113-118.

Moscou, M. J., & Bogdanove, A. J. (2009). A simple cipher governs DNA recognition by TAL effectors. *Science, 326*(5959), 1501. doi:10.1126/science.1178817

Mrozek, K., Marcucci, G., Nicolet, D., Maharry, K. S., Becker, H., Whitman, S. P.Bloomfield, C. D. (2012). Prognostic significance of the European LeukemiaNet standardized system for reporting cytogenetic and molecular alterations in adults with acute myeloid leukemia. *J Clin Oncol, 30*(36), 4515-4523. doi:10.1200/JCO.2012.43.4738

Murovec, J., Pirc, Z., & Yang, B. (2017). New variants of CRISPR RNA-guided genome editing enzymes. *Plant Biotechnol J, 15*(8), 917-926. doi:10.1111/pbi.12736

Nakamura, T., & Omasa, T. (2015). Optimization of cell line development in the GS-CHO expression system using a high-throughput, single cell-based clone selection system. *J Biosci Bioeng, 120*(3), 323-329. doi:10.1016/j.jbiosc.2015.01.002

Nick McElhinny, S. A., Havener, J. M., Garcia-Diaz, M., Juarez, R., Bebenek, K., Kee, B. L.Ramsden, D. A. (2005). A gradient of template dependence defines distinct biological roles for family X polymerases in nonhomologous end joining. *Mol Cell, 19*(3), 357-366. doi:10.1016/j.molcel.2005.06.012

Nimmagadda, S. C., Frey, S., Edelmann, B., Hellmich, C., Zaitseva, L., Konig, G. M.Fischer, T. (2018). Bruton's tyrosine kinase and RAC1 promote cell survival in MLL-rearranged acute myeloid leukemia. *Leukemia, 32*(3), 846-849. doi:10.1038/leu.2017.324

O'Donnell, M. R., Abboud, C. N., Altman, J., Appelbaum, F. R., Arber, D. A., Attar, E.Gregory, K. M. (2012). NCCN Clinical Practice Guidelines Acute myeloid leukemia. *J Natl Compr Canc Netw, 10*(8), 984-1021.

O'Donnell, M. R., Tallman, M. S., Abboud, C. N., Altman, J. K., Appelbaum, F. R., Arber, D. A.Ogba, N. (2017). Acute Myeloid Leukemia, Version 3.2017, NCCN Clinical Practice Guidelines in Oncology. *J Natl Compr Canc Netw, 15*(7), 926-957. doi:10.6004/jnccn.2017.0116

Oellerich, T., Mohr, S., Corso, J., Beck, J., Dobele, C., Braun, H.Serve, H. (2015). FLT3-ITD and TLR9 use Bruton tyrosine kinase to activate distinct transcriptional programs mediating AML cell survival and proliferation. *Blood, 125*(12), 1936-1947. doi:10.1182/blood-2014-06-585216

Ong, E., Szedlak, A., Kang, Y., Smith, P., Smith, N., McBride, M.Paternostro, G. (2015). A scalable method for molecular network reconstruction identifies properties of targets and mutations in acute myeloid leukemia. *J Comput Biol, 22*(4), 266-288. doi:10.1089/cmb.2014.0297

Ortinski, P. I., O'Donovan, B., Dong, X., & Kantor, B. (2017). Integrase-Deficient Lentiviral Vector as an All-in-One Platform for Highly Efficient CRISPR/Cas9-Mediated Gene Editing. *Mol Ther Methods Clin Dev, 5*, 153-164. doi:10.1016/j.omtm.2017.04.002

Palis, J. (2014). Primitive and definitive erythropoiesis in mammals. *Front Physiol, 5*, 3. doi:10.3389/fphys.2014.00003

Palis, J., & Yoder, M. C. (2001). Yolk-sac hematopoiesis: the first blood cells of mouse and man. *Exp Hematol, 29*(8), 927-936.

Pan, Z., Scheerens, H., Li, S. J., Schultz, B. E., Sprengeler, P. A., Burrill, L. C.Palmer, J. T. (2007). Discovery of selective irreversible inhibitors for Bruton's tyrosine kinase. *ChemMedChem, 2*(1), 58-61. doi:10.1002/cmdc.200600221

Paquet, D., Kwart, D., Chen, A., Sproul, A., Jacob, S., Teo, S.Tessier-Lavigne, M. (2016). Efficient introduction of specific homozygous and heterozygous mutations using CRISPR/Cas9. *Nature, 533*(7601), 125-129. doi:10.1038/nature17664

Park, H., Wahl, M. I., Afar, D. E. H., Turck, C. W., Rawlings, D. J., Tam, C.Witte, O. N. (1996). Regulation of Btk function by a major autophosphorylation site within the SH3 domain. *Immunity, 4*(5), 515-525. doi:Doi 10.1016/S1074-7613(00)80417-3

Patel, J. P., Gonen, M., Figueroa, M. E., Fernandez, H., Sun, Z., Racevskis, J.Levine, R. L. (2012). Prognostic relevance of integrated genetic profiling in acute myeloid leukemia. *N Engl J Med, 366*(12), 1079-1089. doi:10.1056/NEJMoa1112304

Pavletich, N. P., & Pabo, C. O. (1991). Zinc finger-DNA recognition: crystal structure of a Zif268-DNA complex at 2.1 A. *Science, 252*(5007), 809-817.

Pellagatti, A., Dolatshad, H., Yip, B. H., Valletta, S., & Boultwood, J. (2016). Application of genome editing technologies to the study and treatment of hematological disease. *Adv Biol Regul, 60*, 122-134. doi:10.1016/j.jbior.2015.09.005

Petris, G., Casini, A., Montagna, C., Lorenzin, F., Prandi, D., Romanel, A.Cereseto, A. (2017). Hit and go CAS9 delivered through a lentiviral based self-limiting circuit. *Nat Commun, 8*, 15334. doi:10.1038/ncomms15334

Pillinger, G., Abdul-Aziz, A., Zaitseva, L., Lawes, M., MacEwan, D. J., Bowles, K. M., & Rushworth, S. A. (2015). Targeting BTK for the treatment of FLT3-ITD mutated acute myeloid leukemia. *Sci Rep, 5*, 12949. doi:10.1038/srep12949

Platt, R. J., Chen, S. D., Zhou, Y., Yim, M. J., Swiech, L., Kempton, H. R.Zhang, F. (2014). CRISPR-Cas9 Knockin Mice for Genome Editing and Cancer Modeling. *Cell, 159*(2), 440-455. doi:10.1016/j.cell.2014.09.014

Ponader, S., & Burger, J. A. (2014). Bruton's tyrosine kinase: from X-linked agammaglobulinemia toward targeted therapy for B-cell malignancies. *J Clin Oncol, 32*(17), 1830-1839. doi:10.1200/JCO.2013.53.1046

Qi, L. S., Larson, M. H., Gilbert, L. A., Doudna, J. A., Weissman, J. S., Arkin, A. P., & Lim, W. A. (2013). Repurposing CRISPR as an RNA-guided platform for sequence-specific control of gene expression. *Cell, 152*(5), 1173-1183. doi:10.1016/j.cell.2013.02.022

Quek, L. S., Bolen, J., & Watson, S. P. (1998). A role for Bruton's tyrosine kinase (Btk) in platelet activation by collagen. *Curr Biol, 8*(20), 1137-1140.

Raje, N., & Roodman, G. D. (2011). Advances in the biology and treatment of bone disease in multiple myeloma. *Clinical Cancer Research, 17*(6), 1278-1286. doi:10.1158/1078-0432.CCR-10-1804

Rajeeve, V., Vendrell, I., Wilkes, E., Torbett, N., & Cutillas, P. R. (2014). Cross-species proteomics reveals specific modulation of signaling in cancer and stromal cells by phosphoinositide 3-kinase (PI3K) inhibitors. *Mol Cell Proteomics, 13*(6), 1457-1470. doi:10.1074/mcp.M113.035204

Ramsay, R. G., & Gonda, T. J. (2008). MYB function in normal and cancer cells. *Nat Rev Cancer, 8*(7), 523-534. doi:10.1038/nrc2439

Ran, F. A., Cong, L., Yan, W. X., Scott, D. A., Gootenberg, J. S., Kriz, A. J.Zhang, F. (2015). In vivo genome editing using Staphylococcus aureus Cas9. *Nature, 520*(7546), 186-U198. doi:10.1038/nature14299

Ran, F. A., Hsu, P. D., Wright, J., Agarwala, V., Scott, D. A., & Zhang, F. (2013). Genome engineering using the CRISPR-Cas9 system. *Nat Protoc, 8*(11), 2281-2308. doi:10.1038/nprot.2013.143

Rao, A. V., Valk, P. J., Metzeler, K. H., Acharya, C. R., Tuchman, S. A., Stevenson, M. M.Lowenberg, B. (2009). Age-specific differences in oncogenic pathway dysregulation and anthracycline sensitivity in patients with acute myeloid leukemia. *J Clin Oncol, 27*(33), 5580-5586. doi:10.1200/JCO.2009.22.2547

Rawlings, D. J., Scharenberg, A. M., Park, H., Wahl, M. I., Lin, S., Kato, R. M.Kinet, J. P. (1996). Activation of BTK by a phosphorylation mechanism initiated by SRC family kinases. *Science, 271*(5250), 822-825.

Reardon, S. (2015). Leukaemia success heralds wave of gene-editing therapies. *Nature, 527*(7577), 146-147. doi:10.1038/nature.2015.18737

Redig, A. J., & Platanias, L. C. (2007). The protein kinase C (PKC) family of proteins in cytokine signaling in hematopoiesis. *J Interferon Cytokine Res, 27*(8), 623-636. doi:10.1089/jir.2007.0007

Redig, A. J., & Platanias, L. C. (2008). Protein kinase C signalling in leukemia. *Leuk Lymphoma, 49*(7), 1255-1262. doi:10.1080/10428190802007726

Renaud, J. B., Boix, C., Charpentier, M., De Cian, A., Cochennec, J., Duvernois-Berthet,E.Giovannangeli, C. (2016). Improved Genome Editing Efficiency and Flexibility Using Modified Oligonucleotides with TALEN and CRISPR-Cas9 Nucleases. *Cell Rep, 14*(9), 2263-2272. doi:10.1016/j.celrep.2016.02.018

Richardson, C. D., Ray, G. J., DeWitt, M. A., Curie, G. L., & Corn, J. E. (2016). Enhancing homology-directed genome editing by catalytically active and inactive CRISPR-Cas9 using asymmetric donor DNA. *Nat Biotechnol, 34*(3), 339-344. doi:10.1038/nbt.3481

Ritis, K., Speletas, M., Tsironidou, V., Pardali, E., Kanariou, M., Moschese, V.Sideras, P. (1998). Absence of Bruton's tyrosine kinase (Btk) mutations in patients with acute myeloid leukaemia. *Br J Haematol, 102*(5), 1241-1248.

Rodgers, K., & McVey, M. (2016). Error-Prone Repair of DNA Double-Strand Breaks. *J Cell Physiol, 231*(1), 15-24. doi:10.1002/jcp.25053

Rouet, P., Smih, F., & Jasin, M. (1994). Introduction of Double-Strand Breaks into the Genome of Mouse Cells by Expression of a Rare-Cutting Endonuclease. *Molecular and Cellular Biology, 14*(12), 8096-8106. doi:Doi 10.1128/Mcb.14.12.8096

Rudin, N., & Haber, J. E. (1988). Efficient Repair of Ho-Induced Chromosomal Breaks in Saccharomyces-Cerevisiae by Recombination between Flanking Homologous Sequences. *Molecular and Cellular Biology, 8*(9), 3918-3928. doi:Doi 10.1128/Mcb.8.9.3918

Rushworth, S. A., Bowles, K. M., Barrera, L. N., Murray, M. Y., Zaitseva, L., & MacEwan, D. J. (2013). BTK inhibitor ibrutinib is cytotoxic to myeloma and potently enhances bortezomib and lenalidomide activities through NF-kappaB. *Cell Signal, 25*(1), 106-112. doi:10.1016/j.cellsig.2012.09.008

Rushworth, S. A., Murray, M. Y., Zaitseva, L., Bowles, K. M., & MacEwan, D. J. (2014). Identification of Bruton's tyrosine kinase as a therapeutic target in acute myeloid leukemia. *Blood, 123*(8), 1229-1238. doi:10.1182/blood-2013-06-511154

Rushworth, S. A., Zaitseva, L., Murray, M. Y., Lawes, M. J., MacEwan, D. J., & Bowles, K. M. (2014). The BTK Inhibitor Ibrutinib Blocks SDF1/CXCR4 Mediated Migration of Acute Myeloid Leukemia Cells. *Blood, 124*(21).

Ruvolo, P. P., Zhou, L., Watt, J. C., Ruvolo, V. R., Burks, J. K., Jiffar, T.Andreeff, M. (2011). Targeting PKC-mediated signal transduction pathways using enzastaurin to promote apoptosis in acute myeloid leukemia-derived cell lines and blast cells. *J Cell Biochem, 112*(6), 1696-1707. doi:10.1002/jcb.23090

Sachdeva, M., Sachdeva, N., Pal, M., Gupta, N., Khan, I. A., Majumdar, M., & Tiwari, A. (2015). CRISPR/Cas9: molecular tool for gene therapy to target genome and epigenome in the treatment of lung cancer. *Cancer Gene Ther, 22*(11), 509-517. doi:10.1038/cgt.2015.54

San Filippo, J., Sung, P., & Klein, H. (2008). Mechanism of eukaryotic homologous recombination. *Annu Rev Biochem, 77*, 229-257. doi:10.1146/annurev.biochem.77.061306.125255

Shaffer, A. L., 3rd, Young, R. M., & Staudt, L. M. (2012). Pathogenesis of human B cell lymphomas. *Annu Rev Immunol, 30*, 565-610. doi:10.1146/annurev-immunol-020711-075027

Shah, N. P., Nicoll, J. M., Nagar, B., Gorre, M. E., Paquette, R. L., Kuriyan, J., & Sawyers, C. L. (2002). Multiple BCR-ABL kinase domain mutations confer polyclonal resistance to the tyrosine kinase inhibitor imatinib (STI571) in chronic phase and blast crisis chronic myeloid leukemia. *Cancer Cell, 2*(2), 117-125.

Shao, S., Ren, C., Liu, Z., Bai, Y., Chen, Z., Wei, Z.Xu, K. (2017). Enhancing CRISPR/Cas9-mediated homology-directed repair in mammalian cells by expressing Saccharomyces cerevisiae Rad52. *Int J Biochem Cell Biol, 92*, 43-52. doi:10.1016/j.biocel.2017.09.012

Sharma, S., Galanina, N., Guo, A., Lee, J., Kadri, S., Van Slambrouck, C.Wang, Y. L. (2016). Identification of a structurally novel BTK mutation that drives ibrutinib resistance in CLL. *Oncotarget, 7*(42), 68833-68841. doi:10.18632/oncotarget.11932

Shawver, L. K., Slamon, D., & Ullrich, A. (2002). Smart drugs: tyrosine kinase inhibitors in cancer therapy. *Cancer Cell, 1*(2), 117-123.

Shih, A. H., Abdel-Wahab, O., Patel, J. P., & Levine, R. L. (2012). The role of mutations in epigenetic regulators in myeloid malignancies. *Nat Rev Cancer, 12*(9), 599-612. doi:10.1038/nrc3343

Shinohara, M., Koga, T., Okamoto, K., Sakaguchi, S., Arai, K., Yasuda, H.Takayanagi, H. (2008). Tyrosine kinases Btk and Tec regulate osteoclast differentiation by linking RANK and ITAM signals. *Cell, 132*(5), 794-806. doi:10.1016/j.cell.2007.12.037

Sill, H., Olipitz, W., Zebisch, A., Schulz, E., & Wolfler, A. (2011). Therapy-related myeloid neoplasms: pathobiology and clinical characteristics. *Br J Pharmacol, 162*(4), 792-805. doi:10.1111/j.1476-5381.2010.01100.x

Singh, J., Petter, R. C., & Kluge, A. F. (2010). Targeted covalent drugs of the kinase family. *Curr Opin Chem Biol, 14*(4), 475-480. doi:10.1016/j.cbpa.2010.06.168

Smith, C. I., Islam, T. C., Mattsson, P. T., Mohamed, A. J., Nore, B. F., & Vihinen, M. (2001). The Tec family of cytoplasmic tyrosine kinases: mammalian Btk, Bmx, Itk, Tec, Txk and homologs in other species. *Bioessays, 23*(5), 436-446. doi:10.1002/bies.1062

Smith, J., Bibikova, M., Whitby, F. G., Reddy, A. R., Chandrasegaran, S., & Carroll, D. (2000). Requirements for double-strand cleavage by chimeric restriction enzymes with zinc finger DNA-recognition domains. *Nucleic Acids Research, 28*(17), 3361-3369. doi:DOI 10.1093/nar/28.17.3361

Speck, N. A., & Gilliland, D. G. (2002). Core-binding factors in haematopoiesis and leukaemia. *Nat Rev Cancer, 2*(7), 502-513. doi:10.1038/nrc840

Sternberg, S. H., LaFrance, B., Kaplan, M., & Doudna, J. A. (2015). Conformational control of DNA target cleavage by CRISPR-Cas9. *Nature, 527*(7576), 110-113. doi:10.1038/nature15544

Sternberg, S. H., Redding, S., Jinek, M., Greene, E. C., & Doudna, J. A. (2014). DNA interrogation by the CRISPR RNA-guided endonuclease Cas9. *Nature, 507*(7490), 62-67. doi:10.1038/nature13011

Swerdlow SH, Campo E, Harris NL, et al. WHO Classification of Tumours of Haematopoietic and Lymphoid Tissues. Lyon, France: IARC; 2008.

Tai, Y.-T., Chang, B. Y., Kong, S.-Y., Fulciniti, M., Yang, G., Calle, Y.Anderson, K. C. (2012). Bruton tyrosine kinase inhibition is a novel therapeutic strategy targeting tumor in the bone marrow microenvironment in multiple myeloma. *Blood, 120*(9), 1877-1887. doi:10.1182/blood-2011-12-396853

Takahashi, S. (2011). Current findings for recurring mutations in acute myeloid leukemia. *J Hematol Oncol, 4*, 36. doi:10.1186/1756-8722-4-36

Tao, S. D., Deng, Y., He, Z. M., Chen, Y., Deng, Z. K., Li, Y. Y.Yu, L. (2013). [Expression of Btk and NFkappaB in acute myeloid leukemia cells and its significance]. *Zhongguo Shi Yan Xue Ye Xue Za Zhi, 21*(1), 25-28. doi:10.7534/j.issn.1009-2137.2013.01.006

Tempero, M. A., Coussens, L. M., Fong, L., Manges, R., Singh, P., Li, Y. F.Tabernero, J. (2016). A randomized, double-blind, placebo-controlled study of ibrutinib, a Bruton tyrosine kinase inhibitor, with nab-paclitaxel and gemcitabine in the first-line treatment of patients with metastatic pancreatic adenocarcinoma (RESOLVE). *Journal of Clinical Oncology, 34*(15). doi:10.1200/JCO.2016.34.15_suppl.TPS2601

Thakore, P. I., D'Ippolito, A. M., Song, L., Safi, A., Shivakumar, N. K., Kabadi, A. M., . . . Gersbach, C. A. (2015). Highly specific epigenome editing by CRISPR-Cas9 repressors for silencing of distal regulatory elements. *Nat Methods, 12*(12), 1143-1149. doi:10.1038/nmeth.3630

Toth, C. A., Kuklenyik, Z., Jones, J. I., Parks, B. A., Gardner, M. S., Schieltz, D. M., . . . Barr, J. R. (2017). On-column trypsin digestion coupled with LC-MS/MS for quantification of apolipoproteins. *J Proteomics, 150*, 258-267. doi:10.1016/j.jprot.2016.09.011

Treon, S. P., Tripsas, C. K., Meid, K., Warren, D., Varma, G., Green, R., . . . Advani, R. H. (2015). Ibrutinib in previously treated Waldenstrom's macroglobulinemia. *N Engl J Med, 372*(15), 1430-1440. doi:10.1056/NEJMoa1501548

Tsukada, S., Saffran, D. C., Rawlings, D. J., Parolini, O., Allen, R. C., Klisak, I.et al. (1993). Deficient expression of a B cell cytoplasmic tyrosine kinase in human X-linked agammaglobulinemia. *Cell, 72*(2), 279-290.

Urnov, F. D., Miller, J. C., Lee, Y. L., Beausejour, C. M., Rock, J. M., Augustus, S., . . . Holmes, M. C. (2005). Highly efficient endogenous human gene correction using designed zinc-finger nucleases. *Nature, 435*(7042), 646-651. doi:10.1038/nature03556

Urnov, F. D., Rebar, E. J., Holmes, M. C., Zhang, H. S., & Gregory, P. D. (2010). Genome editing with engineered zinc finger nucleases. *Nat Rev Genet, 11*(9), 636-646. doi:10.1038/nrg2842

von Mering, C., Huynen, M., Jaeggi, D., Schmidt, S., Bork, P., & Snel, B. (2003). STRING: a database of predicted functional associations between proteins. *Nucleic Acids Res, 31*(1), 258-261.

Wake, C. T., Gudewicz, T., Porter, T., White, A., & Wilson, J. H. (1984). How Damaged Is the Biologically-Active Subpopulation of Transfected DNA. *Molecular and Cellular Biology, 4*(3), 387-398. doi:Doi 10.1128/Mcb.4.3.387

Walker, J. R., Corpina, R. A., & Goldberg, J. (2001). Structure of the Ku heterodimer bound to DNA and its implications for double-strand break repair. *Nature, 412*(6847), 607-614. doi:10.1038/35088000

Walter, H. S., Rule, S. A., Dyer, M. J., Karlin, L., Jones, C., Cazin, B.Salles, G. (2016). A phase 1 clinical trial of the selective BTK inhibitor ONO/GS-4059 in relapsed and refractory mature B-cell malignancies. *Blood, 127*(4), 411-419. doi:10.1182/blood-2015-08-664086

Wang, B., Li, K., Wang, A., Reiser, M., Saunders, T., Lockey, R. F., & Wang, J. W. (2015). Highly efficient CRISPR/HDR-mediated knock-in for mouse embryonic stem cells and zygotes. *Biotechniques, 59*(4), 201-202, 204, 206-208. doi:10.2144/000114339

Wang, C. X., & Cannon, P. M. (2016). The clinical applications of genome editing in HIV. *Blood, 127*(21), 2546-2552. doi:10.1182/blood-2016-01-678144

Wang, M. L., Blum, K. A., Martin, P., Goy, A., Auer, R., Kahl, B. S.Rule, S. (2015). Long-term follow-up of MCL patients treated with single-agent ibrutinib: updated safety and efficacy results. *Blood, 126*(6), 739-745. doi:10.1182/blood-2015-03-635326

Weissman, I. L. (2000). Stem cells: units of development, units of regeneration, and units in evolution. *Cell, 100*(1), 157-168.

Weterings, E., & Chen, D. J. (2008). The endless tale of non-homologous end-joining. *Cell Res, 18*(1), 114-124. doi:10.1038/cr.2008.3

Weterings, E., Verkaik, N. S., Bruggenwirth, H. T., Hoeijmakers, J. H., & van Gent, D. C. (2003). The role of DNA dependent protein kinase in synapsis of DNA ends. *Nucleic Acids Res, 31*(24), 7238-7246.

Wiedenheft, B., Sternberg, S. H., & Doudna, J. A. (2012). RNA-guided genetic silencing systems in bacteria and archaea. *Nature, 482*(7385), 331-338. doi:10.1038/nature10886

Wilson, L. J., Linley, A., Hammond, D. E., Hood, F. E., Coulson, J. M., MacEwan, D. J., Prior, I. A. (2018). New Perspectives, Opportunities, and Challenges in Exploring the Human Protein Kinome. *Cancer Res, 78*(1), 15-29. doi:10.1158/0008-5472.CAN-17-2291

Wilson, W. H., Young, R. M., Schmitz, R., Yang, Y., Pittaluga, S., Wright, G.Staudt, L. M. (2015). Targeting B cell receptor signaling with ibrutinib in diffuse large B cell lymphoma. *Nat Med, 21*(8), 922-926. doi:10.1038/nm.3884

Wiskerchen, M., & Muesing, M. A. (1995). Human immunodeficiency virus type 1 integrase: effects of mutations on viral ability to integrate, direct viral gene expression from unintegrated viral DNA templates, and sustain viral propagation in primary cells. *J Virol, 69*(1), 376-386.

Woyach, J. A., Furman, R. R., Liu, T. M., Ozer, H. G., Zapatka, M., Ruppert, A. S., . . . Byrd, J. C. (2014). Resistance mechanisms for the Bruton's tyrosine kinase inhibitor ibrutinib. *N Engl J Med, 370*(24), 2286-2294. doi:10.1056/NEJMoa1400029

Woyach, J. A., Ruppert, A. S., Guinn, D., Lehman, A., Blachly, J. S., Lozanski, A.Byrd, J. C. (2017). BTK(C481S)-Mediated Resistance to Ibrutinib in Chronic Lymphocytic Leukemia. *J Clin Oncol, 35*(13), 1437-1443. doi:10.1200/JCO.2016.70.2282

Wu, H., Hu, C., Wang, A., Weisberg, E. L., Wang, W., Chen, C., Liu, Q. (2016). Ibrutinib selectively targets FLT3-ITD in mutant FLT3-positive AML. *Leukemia, 30*(3), 754-757. doi:10.1038/leu.2015.175

Wu, J., Liu, C., Tsui, S. T., & Liu, D. (2016). Second-generation inhibitors of Bruton tyrosine kinase. *J Hematol Oncol, 9*(1), 80. doi:10.1186/s13045-016-0313-y

Xue, W., Chen, S., Yin, H., Tammela, T., Papagiannakopoulos, T., Joshi, N. S.Jacks, T. (2014). CRISPR-mediated direct mutation of cancer genes in the mouse liver. *Nature, 514*(7522), 380-384. doi:10.1038/nature13589

Yamano, T., Nishimasu, H., Zetsche, B., Hirano, H., Slaymaker, I. M., Li, Y.Nureki, O. (2016). Crystal Structure of Cpf1 in Complex with Guide RNA and Target DNA. *Cell, 165*(4), 949-962. doi:10.1016/j.cell.2016.04.003

Yang, X., Liu, L., Sternberg, D., Tang, L., Galinsky, I., DeAngelo, D., & Stone, R. (2005). The FLT3 internal tandem duplication mutation prevents apoptosis in interleukin-3-deprived BaF3 cells due to protein kinase A and ribosomal S6 kinase 1-mediated BAD phosphorylation at serine 112. *Cancer Research, 65*(16), 7338-7347. doi:10.1158/0008-5472.CAN-04-2263

Zaboikin, M., Zaboikina, T., Freter, C., & Srinivasakumar, N. (2017). Non-Homologous End Joining and Homology Directed DNA Repair Frequency of Double-Stranded Breaks Introduced by Genome Editing Reagents. *PLoS One, 12*(1), e0169931. doi:10.1371/journal.pone.0169931

Zetsche, B., Heidenreich, M., Mohanraju, P., Fedorova, I., Kneppers, J., DeGennaro, E. M.Zhang, F. (2017). Multiplex gene editing by CRISPR-Cpf1 using a single crRNA array (vol 35, pg 31, 2017). *Nature Biotechnology, 35*(2), 178-178.

Zhang, L., Holmes, I. P., Hochgrafe, F., Walker, S. R., Ali, N. A., Humphrey, E. S.Daly, R. J. (2013). Characterization of the novel broad-spectrum kinase inhibitor CTx-0294885 as an affinity reagent for mass spectrometry-based kinome profiling. *J Proteome Res, 12*(7), 3104-3116. doi:10.1021/pr3008495

Zhou, Q., Lee, G. S., Brady, J., Datta, S., Katan, M., Sheikh, A.Aksentijevich, I. (2012). A Hypermorphic Missense Mutation in PLCG2, Encoding Phospholipase C gamma 2, Causes a Dominantly Inherited Autoinflammatory

Disease with Immunodeficiency. *American Journal of Human Genetics, 91*(4), 713-720. doi:10.1016/j.ajhg.2012.08.006